UPPSALA
UNIVERSITET

Digital Comprehensive Summaries of Uppsala Dissertations from the Faculty of Science and Technology 2180

Mechanistic Studies on Proton-Coupled Electron Transfer from Tyrosine and Tryptophan Derivatives

ASTRID NILSEN-MOE

ACTA
UNIVERSITATIS
UPSALIENSIS
UPPSALA
2022

ISSN 1651-6214
ISBN 978-91-513-1578-2
URN urn:nbn:se:uu:diva-482203

Dissertation presented at Uppsala University to be publicly examined in Heinz-Otto Kreiss, 101195, Ångström, Ångströmlaboratoriet, Lägerhyddsvägen 1, Uppsala, Friday, 7 October 2022 at 09:15 for the degree of Doctor of Philosophy. The examination will be conducted in English. Faculty examiner: Professor Pia Ädelroth (Department of Biochemistry and Biophysics, Stockholm University).

Abstract

Nilsen-Moe, A. 2022. Mechanistic Studies on Proton-Coupled Electron Transfer from Tyrosine and Tryptophan Derivatives. *Digital Comprehensive Summaries of Uppsala Dissertations from the Faculty of Science and Technology* 2180. 86 pp. Uppsala: Acta Universitatis Upsaliensis. ISBN 978-91-513-1578-2.

Proton-coupled electron transfer (PCET) from tyrosine (Y) and tryptophan (W) is vital to many redox reactions in Nature where PCET between several Ys, or Ws, or between a mix of Ys and Ws can be used to transfer electrons, or protons, or both over large distances of several Å. Studying the PCET reaction mechanisms of Y and W is important for fundamental knowledge, and can help researchers that wish to mimic redox reactions in Nature. To this end, model proteins and small model molecules can be used to investigate PCET reactions without the complexity of large enzymes.

PCET can proceed via two different types of mechanisms; the stepwise mechanism and the concerted mechanism. Detailed mechanistic studies to determine which PCET mechanism dominates are often difficult to perform on biological systems due to their size and complexity, which is why we instead study model systems. In this thesis, the PCET mechanisms and their dependence on pH and driving force for electron transfer (ET) and proton transfer (PT) are studied by determining PCET rate constants using transient absorption (TA) as a function of pH and driving force for ET and PT.

In Papers I and II, Y and a Y derivative sequestered in a model protein are studied. The results show that the PCET mechanism for Y is dependent on bulk pH, with a stepwise PCET mechanism at high pH, and a concerted or stepwise mechanism at lower pH depending on the driving force for ET and PT. Interestingly, these are all parameters that can shift depending on the protein environment, which can be finetuned in Nature to promote a certain PCET mechanism. H2O is an inherently poor proton acceptor due to its low pK_a = 0. Nevertheless, from TA kinetic and molecular dynamic simulation studies, we suggest that H_2O is the primary proton acceptor for the CEPT reaction in the model systems. These studies also indicate that the protein structure gates intrinsically better proton acceptors (such as buffer species) from coming into sufficiently close contact with the Y or Y derivative, even when the Y derivative exhibits as much as 30 to 40% exposure to the solution.

In Paper III, the PCET mechanism and primary proton acceptor for two small molecule W analogs in solution are investigated. Due to the relatively large pKa value exhibited by oxidized W (pK_a = 4.3), PCET was previously thought to not proceed via the concerted mechanism when H_2O was the primary proton acceptor. By studying these two W derivatives, we show that W oxidation can in fact proceed via the concerted mechanism when appropriate oxidants are used. Our results also show that both W analogs exhibit concerted rate constants with a weak pH dependence that currently lacks a theoretical explanation. These results have implications for solution exposed W in biological systems by showing that the concerted mechanism is viable for W PCET even with water as the primary proton acceptor.

Keywords: Proton-Coupled Electron Transfer, PCET, Tyrosine, Tryptophan, Amino Acid Radicals, Transient Absorption

Astrid Nilsen-Moe, Department of Chemistry - Ångström, Physical Chemistry, Box 523, Uppsala University, SE-75120 Uppsala, Sweden.

ISSN 1651-6214
ISBN 978-91-513-1578-2
URN urn:nbn:se:uu:diva-482203 (http://urn.kb.se/resolve?urn=urn:nbn:se:uu:diva-482203)

I... a universe of atoms, an atom in the universe.
–Richard P. Feynman

List of papers

This thesis is based on the following papers, which are referred to in the text by their Roman numerals.

I **Proton-Coupled Electron Transfer from Tyrosine in the Interior of a *de novo* Protein: Mechanisms and Primary Proton Acceptor**
Astrid Nilsen-Moe, Clorice R. Reinhardt, Starla D. Glover, Li Liang, Sharon Hammes-Schiffer, Leif Hammarström, Cecilia Tommos. **2020** Journal of the American Chemical Society, *142*, 26, 11550–11559
Contribution: I contributed to planning the study, I performed all experiments and data analysis apart from MD simulations. I contributed to the discussion and wrote the first draft of the manuscript.

II **Switching the Proton-Coupled Electron Transfer Mechanism for Phenolic Amino Acids in a *de novo* Protein**
Astrid Nilsen-Moe, Clorice R. Reinhardt, Ping Huang, Hemlata Agarwala, Rosanna Lopes, Mauricio Lasagna, Starla D. Glover, Sharon Hammes-Schiffer, Leif Hammarström, Cecilia Tommos.
In Manuscript.
Contribution: I planned and performed all transient and steady-state absorption experiments and data analysis, and was main responsible for planning the study. I was the main responsible for writing the manuscript.

III **Concerted and Stepwise Proton-Coupled Electron Transfer for Tryptophan-Derivative Oxidation with Water as the Primary Proton Acceptor: Clarifying a Controversy**
Astrid Nilsen-Moe, Andrea Rosichini, Starla D. Glover, Leif Hammarström. **2022** Journal of the American Chemical Society, *144*, 26, 7308–7319
Contribution: I contributed to the planning of the study. I performed all transient absorption experiments and data analysis on WEE. I co-supervised the student that performed the transient absorption experiments and data analysis on NAWEE. I performed all electrochemical experiments. I was the main responsible for writing the manuscript.

Contents

Abbreviations

A	alanine
α_3	three α-helices that form a bundle
CEPT	concerted electron proton transfer
E	glutamic acid
ET	electron transfer
ETPT	electron transfer followed by proton transfer
$ETPT_{pre\text{-}eq}$	pre-equilibrium electron transfer followed by proton transfer
$ETPT_{lim}$	electron transfer limited reaction followed by proton transfer
KIE	kinetic isotope effect
MP	mercaptophenol
PCET	proton-coupled electron transfer
PT	proton transfer
PTET	proton transfer followed by electron transfer
$PTET_{pre\text{-}eq}$	pre-equilibrium proton transfer followed by electron transfer
$PTET_{lim}$	proton transfer limited reaction followed by electron transfer
SASA	solvent accessible surface area
TA	transient absorption
W	tryptophan
Y	tyrosine
$^{\bullet}$	radical species

1. Introduction

Many reactions that chemists would like to perform, such as H_2 formation, water oxidation, nitrogen fixation, and CH-bond activation, often require dangerous chemicals, heavy metals, a lot of energy, and can result in greenhouse gases.[1–4] Meanwhile, these are everyday reactions in Nature and have been performed there for millions of years.[5–8] This wide array of reactions all include two elementary processes: electron transfer (ET) and proton transfer (PT). In fact, in Nature, these processes are often coupled in what is called proton-coupled electron transfer (PCET). PCET can proceed via two different mechanisms, concerted PCET, where electron and proton are transferred in one kinetic step, and step-wise PCET, where one particle is transferred after the other. Concerted PCET typically results in higher driving forces and lower activation barriers.[9–12] The examples of reactions given above typically require high activation energies, something that can be lowered by the use of a catalyst. Therefore, Nature uses enzymes, which are proteins with a catalytic function, to perform these generally difficult reactions, often by the use of PCET. All proteins, including enzymes, consist of a sequence of amino acids that fold into specific structures. Ever since the first structures and active sites of enzymes were characterized, chemists have been taking inspiration from Nature when designing new catalysts. However, the characterization of the behavior of natural proteins can be very difficult because of the sheer size and complexity of many enzymes and proteins in general. Studying models of enzymes, such as smaller proteins or designed molecules, can often be very helpful in understanding the details of how the enzyme functions.[13,14] In general, ET and PCET in enzymes are facilitated by a few cofactors (small molecules that facilitate catalytic function), metals, and amino acids. In particular, the amino acids tyrosine (Y), tryptophan (W), cysteine, and glycine have been identified to serve as high-potential one-electron cofactors.[13] Of these, the aromatic amino acids Y and W often participate in long-range ET/PCET reactions at high potentials. Studying the reactivity of Y and W is important on a fundamental level for both basic science and the future design of good catalysts.

This thesis describes detailed mechanistic studies on Y and W radical formation via PCET. The radical formation and decay are studied for Y and unnatural amino acid mimics of Y in a model protein that provides an environment sequestered from water, which is similar to the environment inside many enzymes. W radical formation is studied in water, where its reactivity has been debated.

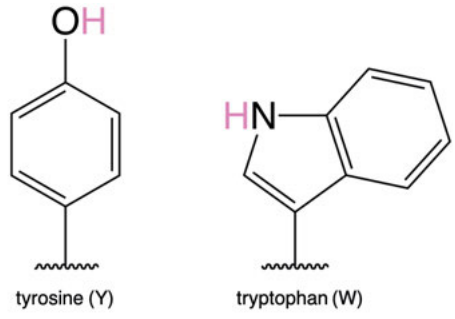

Figure 1.1. The chemical structures of tyrosine and tryptophan. The proton that is transferred upon PCET is marked in pink. The squiggly line at the bottom represents the protein backbone.

To give an introduction to Y and W, some examples of their reactions in Nature are introduced next, followed by a brief summary of some studies on protein mimics of Y and W in Nature, and a short overview of molecular mimics for Y and W reactivity.

1.1 Tyrosine and Tryptophan in Nature

It has been suggested that Y and W, Figure 1.1, were among the last of the 20 common amino acids to be widely incorporated into proteins. The wide integration of Y and W could be an effect of the great oxygenation event since these amino acids are very efficient at deactivating reactive oxygen species such as hydrogen peroxide.[15] Mitigating the damage that can be done by reactive oxygen species is only one of the many roles Y and W take in Nature. These two amino acids can move oxidizing equivalents over large distances and, when working together with a metallocofactor, catalyze complex multi-electron reactions.[11,16] Other cofactors with similar roles include iron-sulfur clusters, heme iron, and copper, but these are limited to potentials $\leq$ 800 mV, while Y and W operate at potentials at or around 1 V.[11,17,18] Upon oxidation, the pK_a value drop from 10 to below 0 for Y and from 17 to 4.3 for W in molecular form in water, making oxidized Y and W much more acidic.[19–21] The exact p$K_a$values change when the amino acids are in a protein, and can also vary with the protein environment, but the trend is the same. The fact that the pK_a of Y shifts to negative values upon oxidation means that it will deprotonate at the pH values typically found in biological systems, see Reaction 1.1. Upon oxidation, the pK_a of W stays sufficiently high such that W does not always deprotonate, see Reaction 1.3. However, if there are proton acceptors nearby such as a base or water, W has been shown to deprotonate following

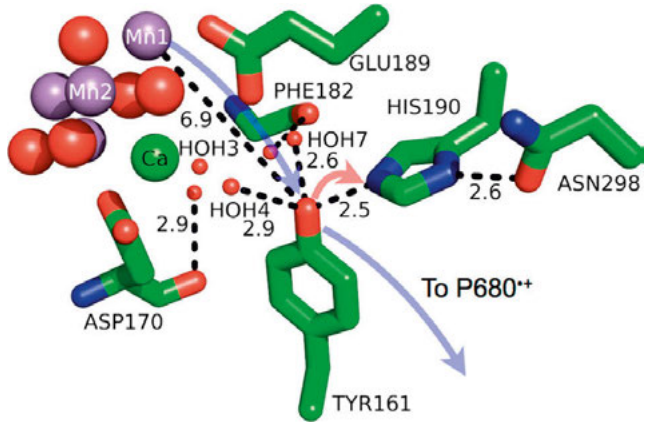

Figure 1.2. Model of the protein environment surrounding Tyr161 (Y_Z) of Photosystem II from *T vulcanus*. Distances shown (dashed lines) are in Å. Crystallographic waters are shown as small, red spheres and the oxygen-evolving complex as large spheres with Mn colored purple, oxygen red, and Ca green. The directions of ET and PT are denoted by transparent blue and red arrows, respectively. Reprinted with permission from Chem. Rev. 2014, 114, 7, 3381–3465. Copyright 2014 American Chemical Society. Published by American Chemical Society.

oxidation, see Reaction 1.2.

$$\mathrm{Y{-}OH} \xrightarrow{\mathrm{PCET}} \mathrm{Y{-}O^{\bullet}} + \mathrm{e^{-}} + \mathrm{H^{+}} \tag{1.1}$$

$$\mathrm{W{-}NH} \xrightarrow{\mathrm{PCET}} \mathrm{W{-}N^{\bullet}} + \mathrm{e^{-}} + \mathrm{H^{+}} \tag{1.2}$$

$$\mathrm{W{-}NH} \xrightarrow{\mathrm{ET}} \mathrm{W{-}N^{\bullet+}} + \mathrm{e^{-}} \tag{1.3}$$

A few examples are given below in order to highlight the common motif of having several Ys and/or Ws in charge transfer chains and that Y oxidation is proton-coupled, while W oxidation can proceed without being proton-coupled. Following these examples, a few challenges of studying PCET in biological systems are discussed.

Photosystem II

Y plays a key role in photosynthesis, which takes sunlight as its energy source when oxidizing water. In Photosystem II (PSII)a Y (known as Y_Z) is responsible for oxidizing the oxygen-evolving complex (a four-manganese metal cluster) four consecutive times, providing the cluster with sufficient oxidizing equivalents to split water into oxygen, electrons, and protons, Figure 1.2. Each oxidation event is coupled to proton transfer to a nearby histidine, yielding the neutral Y_Z radical.[6]

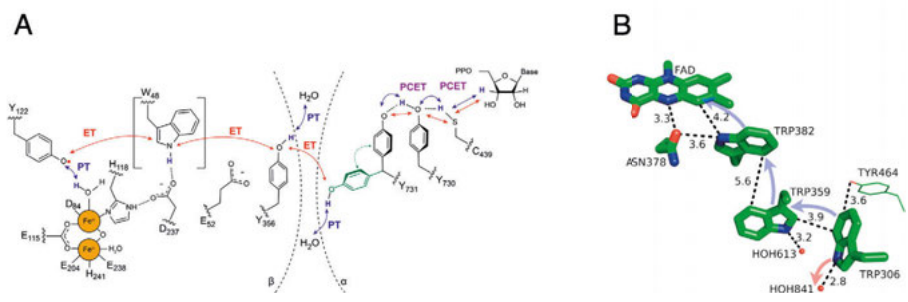

Figure 1.3. (A) The radical transfer chain in class 1a Ribonucleotide Reductase from *E. Coli*. ET is shown with red arrows and PT is shown with blue arrows. (B) The ET transfer chain in DNA photolyase from *E. Coli*. ET is shown with blue arrows, and PT is shown with red arrows. Distances shown with dashed lines are in Å. (A) Reprinted with permission from J. Am. Chem. Soc. 2020, 142, 32, 13768–13778. Copyright 2020 American Chemical Society. Published by American Chemical Society. (B) Reprinted with permission from Chem. Rev. 2014, 114, 7, 3381–3465. Copyright 2014 American Chemical Society. Published by American Chemical Society.

Ribonucleotide Reductase

Y and W are often seen as parts of amino acid chains that facilitate electron or radical transfer over several Å. Performing ET and radical transfer in multiple steps allows for rapid transfer. For example, in class 1a ribonucleotide reductase (RNR), which catalyzes the conversion of RNA to DNA. Several Ys, together with possibly a W, have been identified to form a radical transfer pathway. The radical transfer occurs over 32 Å between a cysteine radical and a Y radical stabilized by a di-iron complex, Figure 1.3 (A). In the RNR radical transfer chain, each ET between two Ys is coupled to a nearby PT in a PCET reaction. Possible proton acceptors have been identified as glutamic acid (an amino acid), Y, or water.[22,23] The PCET mechanism (i.e., if the reaction is stepwise or concerted) for each step has not yet been determined experimentally, however, molecular dynamics simulations indicate a mix of stepwise and concerted PCET.[24]

DNA Photolyase

Similarly to RNR, an ET chain instead consisting of several Ws has been identified in DNA photolyase, which catalyzes the repair of UV-induced DNA damage, Figure 1.3 (B). The ET chain connects a flavin adenine dinucleotide (FAD) with the protein exterior. Upon light absorption, FAD oxidizes the nearest W, which leads to subsequent oxidation of the other Ws in the chain at rates below 150 ps. Only the W that is both the furthest away from the FAD and closest to the protein surface is deprotonated upon oxidation in a stepwise ET followed by PT mechanism to water. This was shown by observing the formation of the different W radicals formed.[25,26]

Challenges of Studying PCET in Biological Systems

Since radical species are inherently short-lived, determining their PCET mechanisms is often very difficult. We are interested in determining if the reaction is concerted or stepwise and, for the latter, if proton or electron are transferred first. For a stepwise mechanism, a short-lived intermediate is formed. Unfortunately, this intermediate is typically so short-lived that it can be exceedingly difficult to capture or observe. Therefore, the absence of observing an intermediate is not sufficient proof that the PCET reaction is not stepwise. One way to assign the PCET mechanism is to study the reaction rate as a function of the driving force for ET and PT. This means introducing new electron and proton acceptors, which can be very difficult in large enzymes, and risks altering unwanted parameters in the process such as the protein structure and electrostatics.

1.2 Studies on Protein Model Systems for Tyrosine and Tryptophan

A model protein system can be created for various reasons. For example, it can be created to make a structurally simpler model for a particular reaction, to imitate active sites, to imitate catalytic functions, to perform detailed mechanistic studies, or to better understand Nature. When creating model protein systems that mimic biological functions, there are two approaches that are commonly used: re-engineering already existing proteins by introduction of new metals and amino acids, or designing new (*de novo*) proteins.[13,14,27,28] Detailed mechanistic studies and characterization of the reaction mechanism often result in highly cross-disciplinary collaborations between biochemists and physical chemists. A few examples are given below of model systems based on re-engineered proteins and model systems based on *de novo* design.

Model Systems Based on Re-engineered Proteins

Re-engineered azurins have been used in several studies, ranging from studying the distance-dependence of ET,[29,30] to PCET reactions between Y and W.[31] The study of an azurin containing a single W has helped characterize a neutral W radical. By applying several spectroscopic techniques such as UV resonance Raman, UV-vis absorption, and electronic paramagnetic resonance spectroscopy, the vibrational frequencies and spin distribution associated with the W radical were determined.[32] Using azurins for these studies has been in part motivated by relatively facile structural characterization using crystallography, and the fact that the proteins can be modified (e.g., insertion of Y and W at different positions, or adding different photosensitizers) without loss of structural integrity. Re-engineered proteins have also been used in order to create enzymes from proteins that do not have a catalytic function, or to change

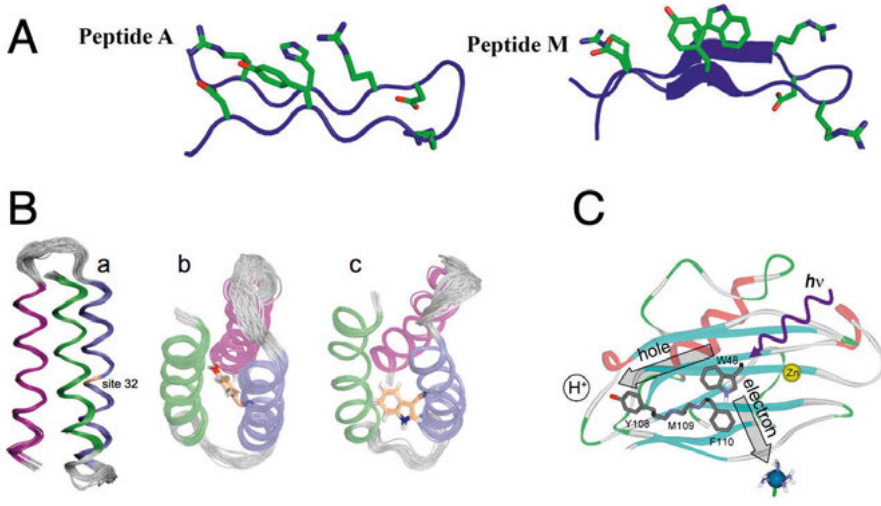

Figure 1.4. (A) NMR structures of two β-hairpin model proteins. Peptide A was designed to simulate the Y_Z-histidine interaction in Photosystem II, and Peptide M was designed to study charge transfer between Y and W. (B) a. The α_3X protein structure with site 32 highlighted where the redox active amino acid is placed, b. α_3Y, c. α_3W. (C) Zn-substituted azurin where W_{48} is directly excited followed by ET to an external quencher and subsequent ET from Y_{108} to W_{48} (shown as hole transfer in the figure) which is coupled to PT to the solution. (A) Reprinted with permission from J. Phys. Chem. B 2019, 123, 13, 2780–2791. Copyright 2019 American Chemical Society. Published by American Chemical Society. (B) Modified with permission from J. Am. Chem. Soc. 2014, 136, 40, 14039–14051. Copyright 2020 American Chemical Society. Published by American Chemical Society. (C) Modified with permission from J. Phys. Chem. B 2015, 119, 29, 9438–9449. Copyright 2015 American Chemical Society. Published by American Chemical Society.

the catalytic function of enzymes. For example, the incorporation of Ni instead of Fe into Rubredoxin results in an enzyme that can produce hydrogen.[33] These examples highlight different ways in which protein re-engineering can be used to understand and mimic Nature.

Model Systems Based on *de novo* Designed Proteins

De novo protein design is an approach for developing an experimental simplified system in order to study specific structural and functional properties. Several secondary structural motifs have been made such as β-sheets and α-helices.[34–36] *De novo*-designed peptides and small proteins have been used to study redox-active amino acids and their radicals in different environments. For example, ET between Y and W in β-hairpins has been studied.[35] By directly exciting the W, ET to a Y was observed using transient absorption spectroscopy. This ET is accelerated compared to ET between W and Y in solution. In these β-hairpins, Y and W are solvent exposed which likely leads to Y de-

protonation to water upon oxidation by W. In an attempt to mimic Y reactivity in PSII, a histidine was positioned close to the Y residue and investigated in the same β-hairpin motif.[34] The two amino acids were positioned such that there were π interactions between them, and PT between the two amino acids could be observed.

Another example of using protein design to study amino acid redox chemistry is the α_3X model protein system, which is used in this thesis. The α_3X system is a family of model proteins based on a *de novo* designed 65-residue 3-helix bundle (alpha$_3$) with a redox-active residue at position 32 (X32 = canonical or non-canonical Y and W residues).[13,37,38] A driving motivation to develop α_3X was to obtain formal (reversible) reduction potentials of Y and W residues at highly comparable protein and solution conditions. A second key motivation was to be able to perform detailed kinetic and mechanistic studies of Y and W radical formation and decay in a structurally well-defined protein environment. Spectroscopic studies on the α_3-bundle containing Y and W (named α_3Y and α_3W) have been performed prior to this thesis. They show that neutral Y and W radicals are formed via PCET that exhibit much longer lifetimes than Y and W radicals in solution, which is likely because the amino acids are occluded from the solution.[39,40] The α_3X proteins allow for a higher degree of control over the environment surrounding the amino acid compared to solution studies, making them very interesting to use as model systems for amino acid reactivity. Details regarding the structure and characterization of the α_3X proteins are found in Chapter 4.

It should be noted that a large field in *de novo*-protein design focuses on incorporating metals into different α-helical structures in order to make both single and dimetal binding sites that mimic enzyme functions, as well as heme proteins.[14] The design of metal sites is beyond the scope of this thesis, and will therefore not be discussed in further detail.

1.3 Studies on Small Molecule Models for Mimicking Tyrosine and Tryptophan PCET

Small molecules generally allow for a higher degree of freedom when designing a model system compared to proteins since they are not limited by which amino acids can be introduced. Using small molecule systems, fundamental questions about PCET can be investigated such as its dependence on proton- and electron-acceptors, bulk pH, and intra- vs intermolecular proton or electron transfer. These systems can also be used to mimic certain parts of enzymes such as an active site, or charge transfer channels. An added advantage of using small molecule mimics is that detailed mechanistic studies into the PCET mechanism can be performed using a variety of methods such as electrochemistry and laser-flash photolysis.

Determining the PCET mechanism can be difficult even in molecular systems, and is usually done by excluding mechanisms until one remains. Once the mechanism is known, the factors that govern the mechanism can be studied. For example, the driving force for ET and PT, the steric hindrance for the PT, and isotope substitution have been shown to alter the PCET mechanism.[41]

While ET can occur over several Å, PT is limited to < 1 Å. This means that the PT distance and angle can have a large influence on PCET rate constants and mechanisms. Designing internal proton acceptors, typically as hydrogen bonds, and altering the base strength can modulate the PT driving force. In the absence of a designed or added proton acceptor, water or, at high pH, OH^- acts as the primary proton acceptor in aqueous solutions. Water is a poor proton acceptor, forming hydronium ions in the PCET step. Concerted PCET from Y to water as proton acceptor is well-established and can proceed smoothly due to the low pK_a of oxidized Y.[42] On the other hand, concerted PCET from W with water as the proton acceptor has been questioned when the proton and electron transfer together, because the W pK_a value remains relatively large upon oxidation.[43]

Y Mimics

Y mimics are often used to investigate Y reactivity in, e.g., PSII and RNR. Most small molecule PSII and RNR mimics are used to study PCET from tyrosine, a tyrosine analog, or phenol and phenol derivatives. The PCET mechanisms available to phenols have been investigated both with water as the proton acceptor and with different intramolecular bases.[44–46] These investigations have shown that the concerted mechanism is available in both scenarios.[47] In one study, pyridines were used as examples of biological nitrogen bases for PCET from phenol. Also with pyridines as proton acceptors, concerted PCET could be observed. Furthermore, the role of buffers on PCET has also been investigated.[48,49]

With radicals having such short lifetimes, many use photosensitizers to form an oxidant *in situ*, which allows for mechanistic studies on fast processes. If the photosensitizer is in turn linked to the Y or phenol studied, as shown in Figure 1.5 (A),[50] then the two do not need to diffuse together, which provides a system more similar to enzymes where oxidant and Y are typically at fixed positions in the protein. Using these types of systems, the PCET mechanisms available to Y or phenol have been investigated both with[51–53] and without[54] a hydrogen bond. Having an internal hydrogen bond provides a closer mimic of Y_Z in PSII which is hydrogen bonded to a nearby histidine. The effect of the driving forces for Y PCET has been explored using similarly linked Y-photosensitizers.[10,55] These results are important for understanding the variety of PCET mechanisms available for Y and Y analogs. Using the same kind of molecule where Y and photosensitizer are linked, the distance-dependence of ET upon the PCET mechanism and rate constants has also been investigated.[56]

A model system where a phenol was covalently attached to a succession of bases was used to investigate what happens to the proton after it has been transferred to histidine from Y_Z in PSII. Upon phenol oxidation, this molecule was able to perform two PT reactions in succession. In this way, a PT channel was designed, Figure 1.5 (B).[57]

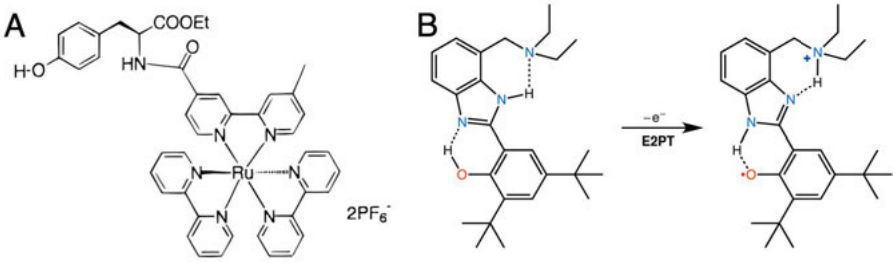

Figure 1.5. (A) Ruthenium-Y dyad used to mimic oxidation of the oxygen-evolving complex by Y_Z. (B) The bio-inspired system where one ET from phenol is coupled to two consecutive PTs. (A) Reprinted with permission from J. Am. Chem. Soc. 1997, 119, 44, 10720–10725. Copyright 1997 American Chemical Society. Published by American Chemical Society. (B) Reprinted with permission from ACS Cent. Sci. 2017, 3, 5, 372–380. Copyright 2017 American Chemical Society. Published by American Chemical Society.

In another system of molecules, intramolecular PCET with PT from a phenol to a linked pyridine base and ET from the same phenol to a linked anthracene was investigated.[58] Upon excitation of the anthracene moiety, PCET from the phenol moiety was triggered. This system was especially interesting to study because not only did charge separation follow the concerted PCET mechanism, recombination was found to be in the Marcus inverted region. This provided the first evidence of concerted PCET in the Marcus inverted region. Having charge recombination being in the Marcus inverted region means that increasing the driving force for the reaction leads to slower rate constants. It had previously been theorized that PCET charge recombination in Nature may often be in the Marcus inverted region to avoid unwanted charge recombination. This may be one of the many ways in which PCET reactions are optimized in biological systems.

W Mimics

There are not as many examples of molecular mimics for studying W reactivity, however, a few studies have been made. In one study, the focus lay on investigating if a few W analogs could undergo concerted PCET using different driving forces for ET and PT.[59] Two other studies have investigated if W analogs can undergo concerted PCET with water as the primary proton acceptor.[43,60] Studies where W has been covalently linked to photosensitizers

also exist. These have also been interested in determining if W can undergo concerted PCET with water as the primary proton acceptor.[61,62]

1.4 Contributions

This thesis contributes to our understanding of Y PCET reactivity in proteins in two ways: First, we show that the exhibited PCET mechanism for Y, when sequestered in the model protein α_3Y, depends on the bulk pH (Paper I) and on the driving force for ET and PT (Paper II). Second, we show that water can act as the primary proton acceptor for the concerted PCET mechanism from α_3Y. Water gains access to the deeply buried Y by local conformational changes of nearby amino acids (Paper I). This thesis also contributes to our understanding of W PCET reactivity in solution by showing that W can indeed proceed via the concerted PCET mechanism when water is the primary proton (Paper III). PT to W is uphill and was therefore hypothesized to not occur. These results have implications for solution-exposed Ws in proteins.

1.5 Outline

This thesis is organized as follows. A brief overview of the theory behind electron transfer, proton transfer, proton-coupled electron transfer, and how the mechanisms can be altered are presented in Chapter 2. In Chapter 3, transient absorption, the primary method used to study PCET reactions, is presented. The effect of the protein pocket on amino acid PCET reactivity is discussed in Chapter 4. The effects of altering electron transfer and proton transfer driving forces on tyrosine and similar artificial amino acids are discussed in Chapter 5. Concerted PCET for tryptophan is investigated in Chapter 6. Finally, the major findings and outlook of this thesis are summarized in Chapter 7.

2. Proton-Coupled Electron Transfer

Proton-coupled electron transfer (PCET) can follow three mechanistic pathways, outlined in Figure 2.1 for a generic PCET donor molecule (DH) where ET stands for electron transfer and PT stands for proton transfer. Along the outer edges, stepwise PCET mechanisms are shown. These are proton transfer followed by electron transfer (PTET), and electron transfer followed by proton transfer (ETPT). Along the diagonal, the concerted electron-proton transfer (CEPT) is represented in which the proton and the electron are transferred in one kinetic step. The stepwise mechanisms can be further divided depending on whether the initial step is a pre-equilibrium or if it is rate-limiting.[12]

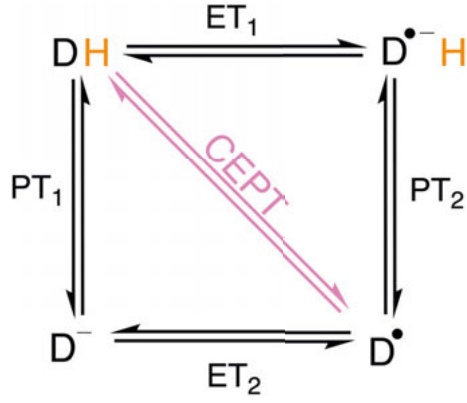

Figure 2.1. The possible PCET mechanisms available to a generic PCET donor molecule (DH) to form a neutral radical $D^{\bullet}$. Proton and electron acceptors are implied.

In this chapter, the theoretical background of ET, PT and CEPT will be briefly introduced. This is followed by a derivation of the stepwise mechanisms, which arise from two limiting cases. We will then introduce how the different mechanisms depend on driving forces for ET and PT. Finally, water as a proton acceptor and the possible pH dependence of PCET rate constants are introduced.

2.1 Theoretical Background to ET, PT and PCET

The rate constants for PT, ET and PCET are essentially all dependent on the same parameters: coupling between reactant and product state, reorganization energy and driving force.

2.1.1 Electron Transfer and Proton Transfer

The widely accepted semi-classical theory of ET was first developed by R. A. Marcus[63] for a classical system. The theory was then expanded to also include non-classical (quantum mechanical) descriptions of ET.[64–67] The semi-classical theory describes ET between a donor (D) and an acceptor (A). The electron transfer is typically described in three steps when D and A are freely diffusing species, moving from reactants (R) D and A to products (P) D^+ and A^-:

$$D + A \underset{k_{-d}}{\overset{k_d}{\rightleftharpoons}} D|A \tag{2.1}$$

$$D|A \underset{k_{-ET}}{\overset{k_{ET}}{\rightleftharpoons}} D^+|A^- \tag{2.2}$$

$$D^+|A^- \longrightarrow D^+ + A^- \tag{2.3}$$

D and A diffuse together to form an outer sphere precursor complex (D|A), reaction 2.1. Here D and A are in the ground state, at the bottom of the R parabola in Figure 2.2. Then the precursor complex undergoes nuclear reorganization towards a transition state in which ET can take place, forming the successor complex ($D^+|A^-$), reaction 2.2. The transition state is where the R and P parabolas intersect in Figure 2.2. Note that the nuclear configuration must be the same for the precursor and successor complex at the transition state. If D and A are not diffusing, and instead held rigid such as in linked donor-acceptor molecules, a frozen matrix, or in a protein, then only reaction 2.2 happens. Finally, the successor complex dissociates to form the products D^+ and A^-, reaction 2.3, represented by the relaxation of the products down to the bottom of the P parabola. In Figure 2.2, the parabolas represent the Gibbs energy surface along the reaction coordinate.

The rate of ET is dependent on the Gibbs energy for activation ($\Delta G^\ddagger$), the Gibbs energy for the reaction (ΔG°), and the reorganization energy (λ). $\Delta G^\ddagger$ is defined by the reactant ground state and the intersection of the parabolas in Figure 2.2. ΔG° can be seen as the difference in height between the bottom of each parabola. The energy needed for the precursor complex to reorganize itself into the successor complex is represented by λ. Note that λ includes both inner reorganization, such as changing bond angles and lengths, and the outer reorganization necessary from the solvent. The rate for ET is given by Eq. 2.4.

$$k_{ET} = V_{el}^2 \sqrt{\frac{\pi}{\lambda k_B T}} \times \exp\left(-\frac{\Delta G^\ddagger}{k_B T}\right) \tag{2.4}$$

$$\Delta G^\ddagger = \left(\frac{(\Delta G^\circ + \lambda)^2}{4\lambda}\right) \tag{2.5}$$

where V_{el} is the electronic coupling, k_B is the Boltzmann constant, and T is the temperature. The theory describes two limits depending on the magnitude

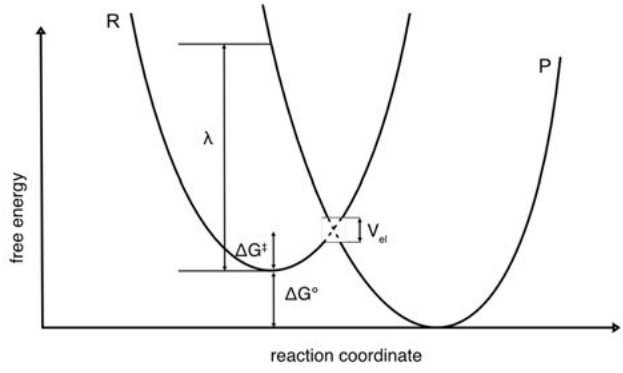

Figure 2.2. Schematic parabolas representing the free energy surface of the reactants (R) and products (P). The driving force for the reaction (ΔG°), the activation energy ($\Delta G^{\ddagger}$) and the reorganization energy (λ) are marked.

of the electronic coupling known as the adiabatic limit and the non-adiabatic limit. In the adiabatic limit, the probability of ET between donor and acceptor is large (close to 1). This leads to a mixing of the reactant (R) and product (P) energy surfaces, creating a different surface that smoothly takes the electron from R to P. In this limit, the electron only needs to have sufficient activation energy for the reaction to occur. The opposite limit is when the probability approaches 0. In this non-adiabatic limit, the electron cannot pass over the barrier, the electron instead must tunnel through the barrier. Note that this is not the same barrier as is seen in Figure 2.2, but is rather the barrier between the potential energy curves for the electron.[68,69]

When an increase in driving force gives faster rate constants, the reaction is said to be in the Marcus normal region where $|\Delta G^{\circ}_{\mathrm{ET}}| < \lambda$. However, one interesting feature of Eq. 2.4 is that when the driving force for ET is greater than the reorganization energy ($|\Delta G^{\circ}_{\mathrm{ET}}| > \lambda$), increasing the driving force further leads to slower rate constants. This is referred to as the Marcus inverted region.

PT can be described with a similar formalism as ET. For PT, proton coupling and PT distances between D and A govern if the reaction is adiabatic or non-adiabatic.[70,71] Since the proton is a much heavier particle compared to the electron, its transfer is limited to much shorter distances, and the transfer is slower.[72]

The stepwise PCET reactions can be described by individual PT and ET steps. These can be a mix of adiabatic and non-adiabatic depending on each specific system.[73]

2.1.2 Concerted PCET

A theory for CEPT has been developed over the last decades.[74–76] The generally accepted model used today, Eq. 2.8, is related to Marcus theory for ET, Eq. 2.4. In CEPT, proton and electron are transferred in one step from the donor, D, (electron and proton acceptors not included):

$$\mathrm{D} \xrightarrow{\mathrm{CEPT}} \mathrm{D}^{\bullet} + \mathrm{e}^{-} + \mathrm{H}^{+} \tag{2.6}$$

For most CEPT reactions, both electron and proton transfer are non-adiabatic, meaning that both particles tunnel.

The derivation is beyond the scope of this thesis, but there are a few important conclusions to draw from the results. The rate constant for CEPT depends on the Boltzmann probability of observing the quantum proton vibrational states μ in the reactant state (P_μ), the electronic coupling constant (V_{el}), the distance-dependent Franck-Condon overlap between proton vibrational wavefunctions ($S_{\mu\nu}r_{\mathrm{PT}}$), the reorganization energy of the system (λ), the temperature (T), and the driving force for the PCET reaction ($\Delta G^{\circ}_{\mathrm{CEPT}}$), yielding a similar expression to that for ET:

$$k_{\mathrm{CEPT}}(r_{\mathrm{PT}}) = \sum_{\mu} P_\mu \sum_{\nu} \frac{|V_{\mathrm{el}}|^2 |S_{\mu\nu}(r_{\mathrm{PT}})|^2}{\hbar} \sqrt{\frac{\pi}{\lambda k_{\mathrm{B}} T}} \times \exp\left(-\frac{(\Delta G^{\ddagger}_{\mu\nu}}{k_{\mathrm{B}} T}\right) \tag{2.7}$$

$$\Delta G^{\ddagger}_{\mu\nu} = \left(\frac{(\Delta G^{\circ}_{\mu\nu} + \lambda)^2}{4\lambda}\right) \tag{2.8}$$

where $\hbar$ is the reduced Planck constant and k_{B} is the Boltzmann constant. For CEPT, the driving force depends on both the ET and the PT driving force ($\Delta G^{\circ}_{\mu\nu} = \Delta G^{\circ}_{\mathrm{CEPT}} = \Delta G^{\circ}_{\mathrm{PT}} + \Delta G^{\circ}_{\mathrm{ET}}$).

In the electronically non-adiabatic limit, electrons are unable to rearrange fast enough for the proton to stay in the ground vibronic state. The vibronic coupling is then given by the product of the electronic coupling and the vibrational overlap.

Eq. 2.8 is only valid for non-adiabatic PCET where the rate constant for CEPT depends on both the electronic coupling and vibrational wavefunction overlap between the R and P. Since both proton and electron tunnel in one kinetic step, the probability of this reaction is lower than for the initial step in the stepwise mechanisms. We can also notice that the rate constant for CEPT depends on the reorganization energy. Just as in Marcus theory, λ is the sum of the outer and inner reorganization energies. Since the driving force for CEPT (ΔG_{CEPT}) is the sum of the driving force for each individual electron and proton transfer step, the driving force for CEPT is always more favorable than the driving force for each charge transfer step.

The competition between stepwise and concerted PCET mechanisms is discussed in all papers that make up this thesis.

2.2 Stepwise PCET

The proton and electron become coupled in stepwise PCET reactions because the initial step can alter the driving force for the follow-up step. For example, an initial ET shifts the pK_a of the proton being transferred to a lower value resulting in a larger driving force for the follow-up PT reaction than it would have had if it was the initial step. The same case is observed for PTET reactions where an initial PT will lower the reduction potential of the follow-up ET.

Stepwise PCET reactions can be written as a two-step reaction going from reactant A via a typically short-lived intermediate B, to product C:

$$\mathrm{A} \underset{k_{-1}}{\overset{k_1}{\rightleftharpoons}} \mathrm{B} \xrightarrow{k_2} \mathrm{C}$$

For example, for an ETPT reaction from W, A includes W$-$NH, B includes W$-$NH$^{\bullet+}$, and C includes W$-$N$^{\bullet}$. For a PTET reaction from Y, A includes Y$-$OH, B includes Y$-$OH$^-$, and C includes Y$-$O$^{\bullet}$. For both of these examples, the electron and proton acceptors that balance the reactions are implied. Below, the rate of consumption or formation for each species is described:

$$\frac{d[\mathrm{A}]}{dt} = -k_1[\mathrm{A}] + k_{-1}[\mathrm{B}] \tag{2.9}$$

$$\frac{d[\mathrm{B}]}{dt} = k_1[\mathrm{A}] - k_{-1}[\mathrm{B}] - k_2[\mathrm{B}] \tag{2.10}$$

$$\frac{d[\mathrm{C}]}{dt} = k_2[\mathrm{B}] \tag{2.11}$$

When the steady state is reached for the intermediate, the rate of formation is equal to the rate of decay, Eq. 2.10 ≈ 0. Using this so-called steady-state approximation, we can rewrite Eq. 2.11 as a function of [A]:

$$\frac{d[\mathrm{C}]}{dt} = \frac{k_1 k_2}{k_{-1} + k_2}[\mathrm{A}] = k_{\mathrm{obs}}[\mathrm{A}] \tag{2.12}$$

This reaction leads to two limiting cases: $k_{-1} \gg k_2$ and $k_{-1} \ll k_2$. If we consider the case where $k_{-1} \gg k_2$, the observed rate constant, k_{obs}, depends on the rate constant of both the initial and the follow-up step. This is what we refer to as a pre-equilibrium reaction (PTET$_{\text{pre-eq}}$ or ETPT$_{\text{pre-eq}}$). k_{obs} can then be written as the equilibrium constant for the initial step multiplied by the rate constant for the follow-up reaction step:

$$k_{\mathrm{obs}} \approx \frac{k_1}{k_{-1}} k_2 = K_1 k_2 \tag{2.13}$$

In the case of $k_{-1} \ll k_2$, the observed rate constant is approximately equal to the rate constant of the initial step. This is what we refer to as the PT or ET

limited reaction ($\mathrm{PTET_{lim}}$ or $\mathrm{ETPT_{lim}}$):

$$k_{\mathrm{obs}} = k_1 \tag{2.14}$$

A visual representation of how the rate constants for the different PCET mechanisms are affected by changes in PT and ET driving forces is seen in Figure 2.3. A partial derivative of Eq. 2.4, where k can be the rate constant for ET or PT, gives the following expression for how the rate constant depends on the free energy:

$$-\frac{\partial \ln k}{\partial \Delta G_1^\circ} = \frac{1}{2RT}\left(1 + \frac{\Delta G_1^\circ}{\lambda}\right) \tag{2.15}$$

For the mechanisms rate-limited by the initial transfer step, the rate constants depend on the driving force for that step (assuming we are in the Marcus normal region $|\Delta G_1^\circ| \ll \lambda_1$ such that $|\Delta G_1^\circ|/\lambda_1 \approx 0$):

$$-\frac{\partial \ln k}{\partial \Delta G_1^\circ} = \frac{1}{2RT} \approx \frac{1}{51\ \mathrm{meV}}\ \text{(at room temperature)} \tag{2.16}$$

The rate constants for the pre-equilibrium reactions depend on the equilibrium constant:

$$\Delta G_1^\circ = -RT\ln(K_{\mathrm{eq1}}) \tag{2.17}$$

resulting in the following relation between rate constant and driving force (again assuming $|\Delta G_1^\circ| \ll \lambda_1$):

$$-\frac{\partial \ln k}{\partial \Delta G_1^\circ} = \frac{1}{RT} \approx \frac{1}{26\ \mathrm{meV}}\ \text{(at room temperature)} \tag{2.18}$$

The influence that the driving force has on both rate constants and the PCET mechanism is explored in Paper II.

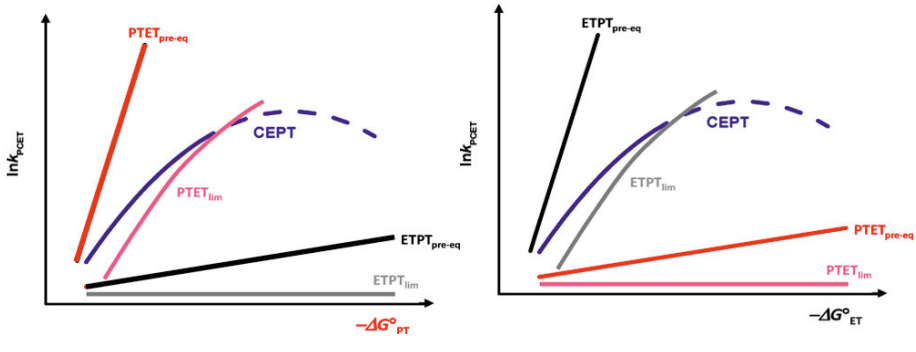

Figure 2.3. A graph illustrating the qualitative effect of altering the driving force for ET and PT on the rate constants for different PCET mechanisms. Reprinted with permission from J. Am. Chem. Soc. 2021, 143, 2, 560–576. Copyright 2021 American Chemical Society. Published by American Chemical Society.

2.3 Water as Proton Acceptor

The proton acceptor influences the driving force for PT just as the oxidant strength influences the driving force for ET. For PT the driving force depends on the ΔpK_a:

$$\Delta G^\circ = -RT\ln(K) = -\ln(10)RT\left(pK_a(\text{acceptor}) - pK_a(\text{donor})\right) \qquad (2.19)$$

In order for a PT reaction to have a negative ΔG° (i.e., be spontaneous) the proton acceptor must have a larger pK_a than the donor. Water is a very poor proton acceptor with $pK_a(H_3O^+) \equiv 0$. Nevertheless, many PCET reactions in Nature involve PT to bulk water, a water cluster, or a single water molecule (typically followed by rapid PT to the bulk).[11] A model for how PT to water can proceed despite its low pK_a value has been developed by Eigen and Weller[77,78] for photoacids, Reaction 2.20. Photoacids are species whose pK_a drops significantly (often to < 0) when excited.

$$H_2O\cdots HA \rightleftharpoons H_3O^+\cdots A^- \longrightarrow {H_3O_{aq}}^+ + A^- \qquad (2.20)$$

where HA represents the electronically excited photoacid. This reaction is similar to how we view ET, but here we have omitted reaction 2.1 where the species diffuse together, and instead assume that the acid has formed an encounter complex with water prior to excitation. The acid is then excited leading to proton transfer. The equilibrium seen in the first step depends on the acid dissociation constant, in other words, the pK_a of the acid. Only after subsequent solvent cage escape is the reaction finished. For this type of reaction with water, the rate constants increase by a factor of 10 per decrease in pK_a unit of the acid.

A similar reaction scheme can be set up for pre-equilibrium PCET reactions from reactant HX to water (electron acceptor not shown) for an $\text{ETPT}_{\text{pre-eq}}$ (2.21) and a $\text{PTET}_{\text{pre-eq}}$ (2.22) reaction:

$$H_2O\cdots HX \overset{-e^-}{\rightleftharpoons} H_2O\cdots HX^+ \rightleftharpoons H_3O^+\cdots X^\bullet \longrightarrow {H_3O_{aq}}^+ + X^\bullet \qquad (2.21)$$

$$H_2O\cdots HX \rightleftharpoons H_3O^+\cdots X^- \overset{-e^-}{\rightleftharpoons} H_3O^+\cdots X^\bullet \longrightarrow {H_3O_{aq}}^+ + X^\bullet \qquad (2.22)$$

Similar to acid deprotonation, the reaction is driven by cage escape. Subsequent dilution of the proton in the solution provides mixing entropy, which can shift the equilibrium towards dissociation.

For a CEPT reaction, both ET and PT happen in one kinetic step, we can still set up a similar reaction mechanism, but in this case, the neutral radical is formed directly in the intermediate:

$$H_2O\cdots HX \overset{-e^-}{\rightleftharpoons} H_3O^+\cdots X^\bullet \longrightarrow {H_3O_{aq}}^+ + X^\bullet \qquad (2.23)$$

The reaction schemes presented in this section show how PT to water can be driven by dissociation and solvent cage escape due to the mixing entropy of the product which is one possible explanation for how water can act as a proton acceptor despite its low pK_a value.

2.4 pH dependence of PCET Rate Constants

Determining PCET rate constants as a function of pH can be done as a step in determining the proton acceptor, and the PCET mechanism. The pH can affect, e.g., nearby hydrogen bonds, the electrostatics of a protein, the concentration of a proton-accepting species in solution, or shift the pre-equilibrium for a stepwise reaction. For PTET_{lim} or CEPT with PT to a species whose concentration depends on the pH, and for a $\text{PTET}_{\text{pre-eq}}$ reaction, the rate constants depend on pH following the Henderson-Hasselbalch Equation below:

$$\text{pH} = \text{pK}_\text{a} + \log_{10}\left(\frac{[\text{Base}]}{[\text{Acid}]}\right) \tag{2.24}$$

This equation gives a pH dependence that changes the rate constants by 10 per increase in pH. For a $\text{PTET}_{\text{pre-eq}}$ the rate constants are dependent on the pK_a of the donor, or the pK_a of the acceptor, or both, shifting the rate constants by a factor of ten per increase in pK_a.

In electrochemical determinations of reduction potentials, molecules that undergo PCET exhibit apparent potentials that change with pH, which is often plotted in Pourbaix diagrams. For a one proton/one electron transfer the reduction potentials are expected to change by 59 mV/pH unit.[79,80] This might appear to describe pH-dependent potentials, but that is not the case. The formal potentials are not pH-dependent. During an electrochemical determination of reduction potentials, all species involved (such as HA, HA^+, A^- and $\text{A}^\bullet$ for a general acid HA), exist at the same time in concentrations that depend on the pH. The current measured is the net current for the equilibrium of current out/in. The pH dependence subsequently arises from the Nernst equation.

pH-dependent PCET rate constants are only expected to originate as described above. Nevertheless, in Chapter 6, pH-dependent rate constants for tryptophan radical formation, published in Paper III, where the origin of the pH dependence is unknown, are discussed.

3. Transient Absorption Spectroscopy

Transient absorption (TA) spectroscopy is the study of light absorption as a function of time. Different molecules absorb different wavelengths of light. By monitoring which wavelengths are absorbed in a sample, we can often identify the molecules contained in the sample. The wavelengths and amount of light that is absorbed depend on the identity and concentration of the absorbing molecules. Absorption follows the Beer-Lambert law, Eq. 3.1 below, where I is the intensity of the light passed through the sample, I_0 is the intensity of the light without interacting with the sample, A is the absorption, ε is the extinction coefficient and is a parameter specific to the molecule that depends on the wavelength of irradiation, c is the concentration, and l is the length of the path which the light travels through the sample.

$$-\log_{10}\left(\frac{I}{I_0}\right) = A = \varepsilon \times \mathrm{c} \times l \tag{3.1}$$

Note that A has no unit, and can be related to the concentration of the sample via the Beer-Lambert law when the extinction coefficient is known.

When absorption of a sample is measured as a function of time (TA spectroscopy) the disappearance of starting material may be monitored, as well as the appearance of new species. In this way, we can follow the rate of chemical reactions and determine values such as the rate constant for a specific reaction.

3.1 Laser Flash-Photolysis Setup

The experimental setup for a typical nanosecond TA experiment is shown in Figure 3.1. The laser light is first passed through a frequency doubling and a frequency tripling crystal that transforms the 1064 nm laser light into 355 nm laser light. More excitation wavelengths can be obtained if the laser light is passed into an OPO which allows for tuning over a wide range of the visible spectrum. The laser pulse is thereafter directed into the sample chamber. Absorption changes upon laser excitation are monitored using a Xe-arc lamp positioned perpendicular to the incident laser light. After the sample, a monochromator is used to select which wavelength the detector, a photomultiplier tube (PMT), should pick up. An output signal from the PMT, proportional to the number of photons passing through the sample, is digitized in the oscilloscope and finally sent to the computer. In Paper I–III, an Nd:YAG laser was used to excite the sample.

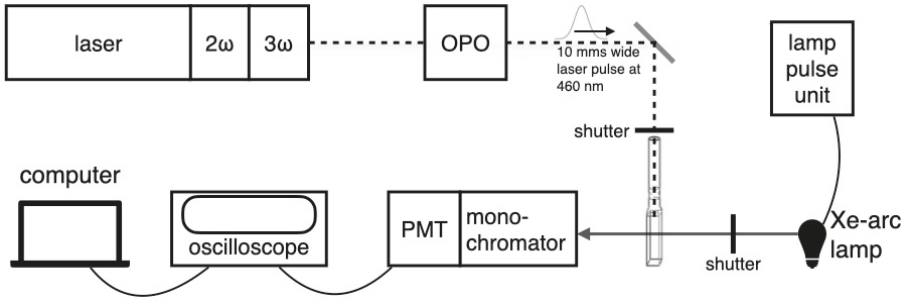

Figure 3.1. The ns transient absorption setup that was used to collect kinetic traces.

3.1.1 Using Laser Flash-Photolysis on Long Timescales

The above-described setup for ns laser flash-photolysis has been used for reactions up to seconds in Paper I–III. While there exist other setups for such slow reactions, such as stopped-flow, there are advantages to using flash-photolysis.

Flash-photolysis allows for the generation of the oxidant *in situ* via the flash-quench method described in Section 3.2. This is especially advantageous for most semi-stable oxidants that can then react instead of degrading. The laser flash provided to the sample makes a few micromolar of the oxidized photosensitizer. The low concentration of oxidant compared to reactant (protein or amino acid being studied) ensures that we have pseudo-first-order kinetics. This also allows us to collect several laser flashes per sample before we run out of reactant, even in non-reversible flash-quench mixtures. The drawback of using ns flash-photolysis to study slow reactions on the ms–s timescale are issues with probe-light stability and dealing with significant probe-light photochemistry. The former can often be accounted for if a new baseline is corrected for each sample, and the latter is discussed in the next section.

3.1.2 Dealing With Probe-Light Photochemistry

Probe-light photochemistry is always present in TA experiments. This becomes especially problematic when using irreversible quenchers, as was done in Paper I–III of this thesis. This problem is especially large for slower reactions where more probe light has time to reach the sample. In order to minimize this effect, a second monochromator can be introduced to the setup shown in Figure 3.1 between the Xe-arc lamp and the sample chamber. This provides two advantages; first, it filters off a majority of unwanted wavelengths that can start unwanted photochemistry in the sample. Second, passing the light through the monochromator's mirrors and grating lowers the light intensity, which means less light to do unwanted photochemistry in the sample.

To ensure that probe-light photochemistry is sufficiently minimized, TA traces can be monitored to ensure that they do not change with laser flash number, as was done in Paper I–III.

3.2 Flash-Quench Method

The flash-quench method is used to form the oxidant from a photosensitizer *in situ*. Figure 3.2 shows the flash-quench method for an oxidative quencher (Qox).

$$\mathrm{PS} \xrightarrow{h\nu} {}^{*}\mathrm{PS} \tag{3.2}$$

$${}^{*}\mathrm{PS} + \mathrm{Qox} \xrightarrow{\mathrm{ET}} \mathrm{PS}^{+} + \mathrm{Qox}^{-} \tag{3.3}$$

$$\mathrm{PS}^{+} + \mathrm{DH} \xrightarrow{\mathrm{ET}} \mathrm{PS} + \mathrm{D}^{\bullet} + \mathrm{H}^{+} \tag{3.4}$$

First, the photosensitizer (PS) is excited (1), it then diffuses together with the quencher (Qox), which takes an electron (2). PS+ can then react with whatever reactant is present (DH) (3). The quencher can be reversible, meaning that ET back to the photosensitizer is possible. If a reversible quencher is used, then the reaction with the reactant must be faster than the PS/Qox recombination. When an irreversible Q is used, the reaction with reactant can be much slower. Note that the oxidized PS will not stay oxidized forever, its stability depends on other species in the solution and possible degradation pathways.

Forming the reactant *in situ* has a few advantages over mixing the reactive species. First, the reactive species can be reformed many times. Second, for fast (ns–µs) reactions, you do not have to wait for the two species to mix, allowing us to follow these fast reactions.

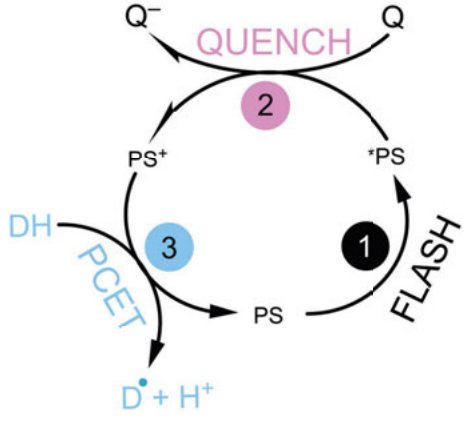

Figure 3.2. The mechanism of *in situ* oxidant formation from a photosensitizer via laser flash-quench photolysis and subsequent PCET reaction with DH.

3.3 Studying PCET Reactions using TA Spectroscopy

The PCET reactions studied in Paper I–III are all between an amino acid, the oxidized photosensitizer, and a proton acceptor. In all cases studied, we could follow the electron transfer between the oxidized photosensitizer and the amino acid. This was done by either monitoring the photosensitizer recovery to its ground state or monitoring the disappearance of the oxidized photosensitizer. In Paper I and II, as well as for some experiments in Paper III we could also follow the formation of the amino acid radicals via their spectroscopic signals.

4. Characterization of X_{32} and the Radicals Formed Upon PCET in α_3Y and MP$-\alpha_3$C (Paper I and II)

The environment surrounding the redox active amino acid can have a great influence on its reactivity: the availability of nearby proton acceptors can modulate the PCET mechanism and, depending on the mechanism, also its rate. In this chapter, we discuss the X_{32} site in α_3X, its effect on pK_a values, and its effect on radical lifetime. We will also discuss the differences and similarities between the radicals formed for α_3Y, 2MP$-\alpha_3$C, and 4MP$-\alpha_3$C.

4.1 The α_3X Family of Model Proteins

α_3X contains a primary sequence of 65 amino acid residues that fold into three α-helices. The α_3 scaffold is shown in Figure 4.1. The amino acid targeted for redox chemistry (amino acid X, identified by its one-letter abbreviation) is in position 32. The first α_3X proteins were designed to obtain formal reduction potentials for redox-active amino acids sequestered in a protein. In the design of the protein scaffold, three criteria were used: (i) The protein should behave as a natural protein. This means that it must form well-defined secondary and tertiary structures in solution. (ii) It should contain a single amino acid residue that could be studied over a wide range of pH values in order to obtain reduction potentials as a function of pH. The protein must therefore be well folded in a wide pH range. (iii) The rest of the α_3-scaffold should be redox inert such that the X_{32} radical state can be stabilized and characterized. In the years since the first two model proteins were prepared, α_3Y and α_3W, it has been shown that these criteria have been fulfilled.[13] Solution nuclear magnetic resonance (NMR) and circular dichroism studies have shown that the proteins exhibit a high degree of helicity, which is retained over a wide pH range (4 to 10).[13,37,81] Importantly, voltammetry studies have demonstrated that X_{32} can be oxidized and reduced in a fully reversible manner.[82] A wide variety of natural and unnatural amino acids have been incorporated into the α_3-scaffold such as tyrosine, fluorotyrosines, tryptophan, aminotyrosine and mercaptophenols, Figure 4.1.

Two of the proteins studied in this thesis: α_3Y and 2MP$-\alpha_3$C have previously been structurally characterized using solution NMR spectroscopy.[39,83] NMR characterization of 4MP$-\alpha_3$C is presented in Paper II. These proteins

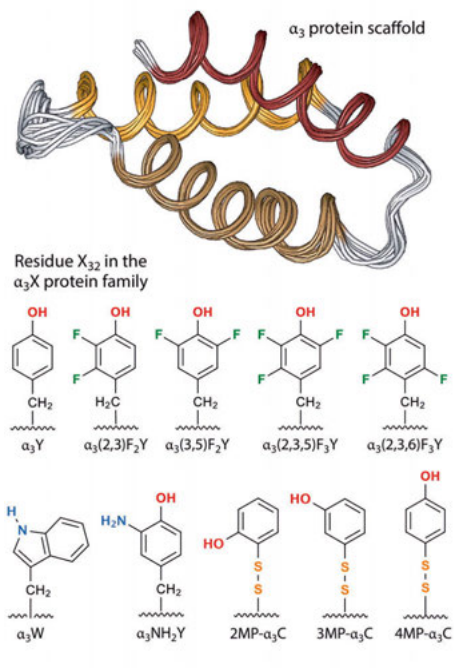

Figure 4.1. The α_3 protein scaffold containing the following residues: GSR(1)-VKALEEKVKALEEKVKA-LGGGGR-IEELKKKX(32)EELKKKIEE-LGGGGE-VKKVEEEVKKLEEEIKK-L(65), shown with the different natural and unnatural amino acids that have been incorporated into the protein scaffold. Reprinted with permission from Annual Review of Biophysics 2022 51:1, 453–471. Copyright 2022 Annual Reviews.

have all been characterized using protein-film square wave voltammetry. The voltammograms were fully reversible and reproducible, yielding formal reduction potentials.[39,82–85]

The α_3X proteins exhibit another important characteristic: they are optically uncomplicated in the visible spectral region and can withstand laser flashes such that time-resolved laser flash-photolysis can be used to study the formation and decay of the radicals formed within.[39,40]

4.2 Structure and Characteristics of X_{32} for α_3Y, 2MP – α_3C and 4MP – α_3C

The α_3X model system allows for studies of Y or phenol reactivity as a function of solvent exposure. The NMR structure of α_3Y is shown in Figure 4.2 A, and is described in detail in ref. 39. α_3Y is described as an ensemble of 32 structures that represent the protein in solution. α_3Y was designed to bury Y_{32} inside the hydrophobic core of the protein and the structural analysis con-

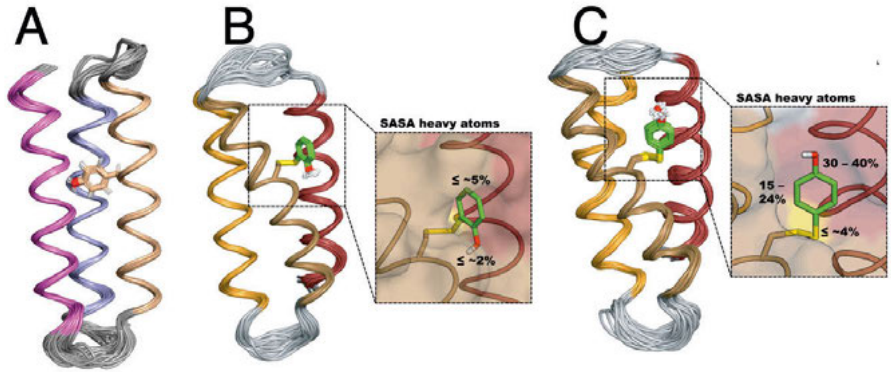

Figure 4.2. Ensemble structures determined by NMR of (A) α_3Y, protein data bank entry (PDB): 2MI7, (B) 2MP–α_3C, PDB: 2LXY and (C) 4MP–α_3C (PDB deposition in process). Panels (B) and (C) also show SASAs for the side chains and the phenol group and the phenol OH atoms. In all figures, hydrogen atoms are shown in white, oxygen atoms in red, and sulfur atoms are shown in yellow. (A) Reprinted with permission from J. Am. Chem. Soc. 2020, 142, 11550–11559. Copyright 2020 American Chemical Society.

firmed this design.[39] Y_{32} has effectively no solvent accessible surface area (SASA; $0.2 \pm 0.2\%$) and the phenol OH is buried > 6Å from the surface.[39]

The proteins 2–mercaptophenol–α_3C (2MP–α_3C) and 4–mercaptophenol–α_3C (4MP–α_3C) were constructed to probe if or how altering the solvent exposure of the phenolic OH group may affect the redox characteristics.[84] The MP–α_3C proteins have a cysteine (C) at position 32, which is linked to either a 2–mercaptophenol or 4–mercaptophenol via a disulfide bond, shown in Figures 4.2 B and C. Placing the phenol OH at different positions on the aromatic ring was predicted to result in different degrees of solvent exposure.[83] This approach to fine-tune the SASA was used instead of the more conventional way of putting Y at different positions in the protein by using site-directed mutagenesis because the latter method may introduce unwanted structural changes in the small α_3-bundle. Full structural analyses of 2MP–α_3C[83] and 4MP–α_3C (Paper II) by solution NMR spectroscopy confirmed the protein design. 2MP–C_{32} exhibits a residue SASA of $\leq 5\%$ and a phenol OH SASA of $\leq 2\%$ (Figure 4.2 B). 4MP–C_{32} displays a residue SASA of 15 to 24% and phenol OH SASA of 30 to 40% (Figure 4.2 C).

The structural analysis of 2MP–α_3C also revealed that 2MP–C_{32} is found within hydrogen bonding distance from E_{13}. The distance between these two residues is ≥ 2.5 Å (O–O distance) with the average distance being 3.2 ± 0.5 Å in the NMR ensemble, suggesting a weak hydrogen bond. The optimal hydrogen tunneling distance is about 0.48 Å.[72] If we assume that the O-H distance is ~ 1 Å, this gives an optimal O–O distance of ~ 2.5 Å for PT. This means that purely based on the distance between 2MP–C_{32} and E_{13}, the latter

Table 4.1. *Apparent* pK_a *values, SASAs, and average residue depth for* Y_{32}*,* $2MP-C_{32}$*, and* $4MP-C_{32}$

protein	pK_a	X_{32}–OH SASA (%)
α_3Y	11.3 ± 0.1 [81]	$0.2(\pm 0.2)$ [39]
2MP–α_3C	9.7 ± 0.2*	≤ 2
4MP–α_3C	9.5 ± 0.1 [84]	30–40

* Determined in Paper II.

is a very probable proton acceptor in this system. However, proton tunneling depends not only on distance but also on wavefunction overlap between the donor and acceptor. The effect of the hydrogen bond on rate constants for PCET and investigations into E_{13} as a possible proton acceptor are explored in Chapter 5.

pK_a values determined for the residues at position 32 are consistently higher than for the amino acid in solution. A correlation can be made between the amount of SASA and the shift in pK_a for Y_{32}, 2MP–C_{32}, and 4MP–C_{32}. Y_{32} exhibits the smallest SASA, and the largest shift in pK_a: from ~ 10 in solution to 11.3 in α_3Y.[81] 2MP–C_{32} exhibits a slightly larger SASA and its pK_a shifts from 9.0 (for 2MP linked to a C) in solution to 9.7 in 2MP–α_3C.[84] Finally, the pK_a of 4MP–C_{32} shifts from 9.2 (for 4MP linked to a C) in solution to 9.5 in 4MP–α_3C.[84] It is also possible that interactions between 2MP–C_{32} and E_{13} results in a higher pK_a for 2MP–C_{32} compared to 4MP–C_{32}. pK_a values and SASA are presented in Table 4.1. For a large SASA, species in the solution such as buffer are more likely to act as the proton acceptor, than for a deeply buried residue that exhibits no SASA.

4.2.1 Protein Molecular Dynamics Simulations on α_3Y

Radical formation via PCET from Y_{32}, with ET to an external oxidant, has been studied previously.[39] Given the residue depth, absence of SASA, and the fact that Y_{32} was surrounded by aliphatic amino acids, it was unclear what the primary proton acceptor could be for the PCET reaction. To learn more about the protein conformational motions, and if water could enter the hydrophobic cavity near site Y_{32}, molecular dynamics (MD) simulations were performed.

Results obtained using two different force fields showed that fluctuations in the side chain rotameric states of amino acids L_{12}, V_{55}, E_{59} and I_{62}, which are found near site 32 allow transient water access to Y_{32}, Figure 4.3. Following these local structural fluctuations, MD simulations showed how one or two water molecules at a time could diffuse into the hydrophobic cavity and interact with the Y_{32}–OH. Two trajectories calculated with one of the force fields used in the MD simulations showed that Y_{32}–OH also interacted with

aliphatic amino acids V_9, L_{58} and L_{12} (the last seen only for one trajectory), and with carboxylic amino acid E_{13}. All hydrogen-bonding interactions involving Y_{32} are presented in Table 4.2 for two trajectories. While the aliphatic amino acids cannot facilitate PT, E_{13} can. The interaction between E_{13} was unexpected because in the ensemble of NMR structures for α_3Y, the O–O distance between E_{13} and Y_{32} is ≥ 6.7 Å. It should be noted that the interaction between Y_{32} and E_{13} was only seen for one of the force fields used.

It had previously been determined that $\alpha_3 Y^{\bullet}$ decays via dimerization, as evidenced by a di-tyrosine emission following radical formation.[39] The MD simulations published in Paper I are for the ground state (unreacted) α_3Y, a larger degree of protein conformational changes likely follows radical formation. Larger conformational changes than those observed in the MD simulations are likely needed for dimerization.

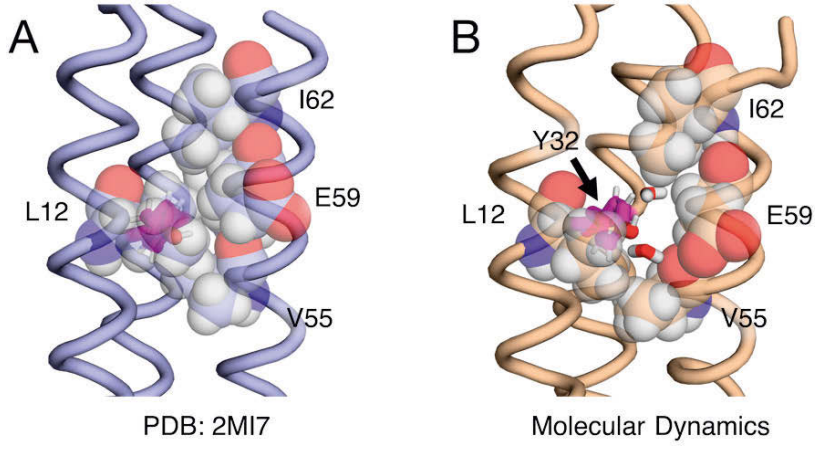

Figure 4.3. Illustration of side chain motions observed in an MD trajectory propagated with the AMBER ff14SB force field. (A) The starting structure from the α_3Y solution NMR structure.citeGlover2014 (B) A configuration from the MD trajectory in which two water molecules transiently reside within hydrogen-bonding distance to Y32. The backbone is depicted as tubes, and the residues occluding water access in panel A or bordering the water channel in panel B are depicted as spheres. Reprinted with permission from J. Am. Chem. Soc. 2020, 142, 11550–11559. Copyright 2020 American Chemical Society.

4.3 Characterization of Radicals formed in α_3X

The radicals formed upon PCET were characterized in terms of their optical (UV-vis) spectra, electron paramagnetic resonance (EPR) spectra, and spin density distribution over the phenol ring calculated using density functional

Table 4.2. *Hydrogen-Bonding Interactions Involving Y_{32} for MD Trajectories of α_3Y Propagated with the AMBER ff14SB Force Field.*

	V_9:O	E_{13}:Oε_1,ε_2	L_{58}:O	L_{12}:O	WAT:O*
Traj. 1	54.1 %	24.0 %	5.12 %	-	38.2 %
Traj. 2	39.38 %	21.56 %	3.98 %	3.32 %	27.7 %

* The numbers reported reflect the sum of the hydrogen-bonding interactions with Y_{32} acting as an H-bond acceptor or donor and can include contributions from multiple water molecules.

theory (DFT). Radicals were generated by use of $[Ru(bpy)_3]^{2+}$ ($E^\circ = 1260$ mV) as photosensitizer. Using a photosensitizer, the oxidant was formed *in situ* using the flash-quench method, see Chapter 3. Rates of radical formation and determination of PCET mechanisms are presented and discussed in Chapter 5.

Optical Spectroscopy of the Radicals Formed Following PCET

Y_{32} has previously been shown to form a neutral radical upon oxidation. The radical state exhibited a half-life of 2 to 10 s, radical spectra as a function of time are seen in Figure 4.4. Radical decay was shown to proceed via dimerization.[39] In Paper II, absorption spectra were recorded for $2\,MP-C_{32}$ and $4\,MP-C_{32}$ radicals, at pH $6.5(\pm 0.1)$, Figure 4.5. $2\,MP-C_{32}$ exhibited similar spectral features to Y_{32}, while $4\,MP-C_{32}$ was more similar to 4-hydroxythiophenol radical.[86]

From the time-resolved spectra in Figure 4.4, the half-lives of the radicals were calculated using $t_{1/2} = 1/k_2 \times \mathrm{Abs}_0(MP^\bullet - C_{32})$. The half-lives are 230s for $2\,MP^\bullet - C_{32}$, 130s for $4\,MP^\bullet - C_{32}$, and 24s for $2\,MP^\bullet - C_{32} - E_{13}A$. $2\,MP^\bullet - C_{32} - E_{13}A$ is the radical formed inside a mutant of $2\,MP-\alpha_3C$ where E_{13} has been mutated to an alanine (A), see Chapter 5. For $2\,MP-C_{32}$ and $4\,MP-C_{32}$, similar concentrations of radicals were formed which means that their half-lives can be compared. $2\,MP^\bullet - C_{32}$ and $4\,MP^\bullet - C_{32}$ exhibit similar half-lives, which suggests that the increased solvent exposure exhibited by $4\,MP-C_{32}$ compared to $2\,MP-C_{32}$ does not significantly facilitate dimerization.

In order to verify the primary nature of the species observed in the TA spectra, and also to understand more about why the $2\,MP^\bullet - C_{32}$ exhibited such different UV-vis spectra compared to the $4\,MP^\bullet - C_{32}$, EPR spectra were recorded for $2\,MP^\bullet - C_{32}$ and $4\,MP^\bullet - C_{32}$.

Magnetic Spectroscopy of the Radicals Formed Following PCET

EPR spectra were recorded at room temperature under continuous illumination for $2\,MP-\alpha_3C$ and $4\,MP-\alpha_3C$ (Figure 4.6). The spectra exhibit different hyperfine splitting patterns between the two proteins since $4\,MP^\bullet - C_{32}$ has $2+2$ equivalent protons on the ring, while $2\,MP^\bullet - C_{32}$ has no chemically equivalent

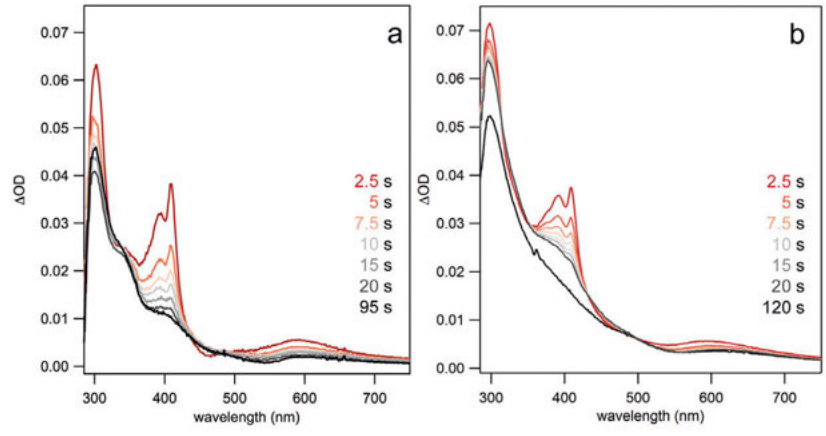

Figure 4.4. Radical absorption spectra for α_3Y at pH 5.5 (a) and 8.5 (b). Reprinted with permission from J. Am. Chem. Soc. 2014, 136, 40, 14039–14051. Copyright 2014 American Chemical Society.

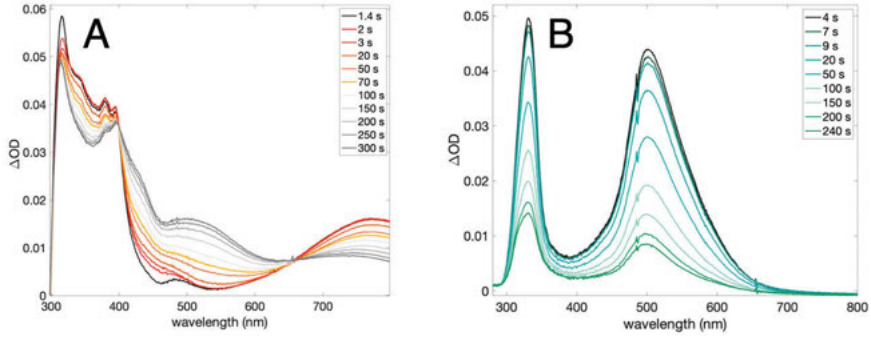

Figure 4.5. Radical absorption spectra for (A) 2MP – α_3C and (B) 2MP – α_3C recorded at pH 6.5($\pm$0.1).

protons on the phenol ring. The spectra are consistent with the formation of the primary radicals $2MP^{\bullet} - C_{32}$ and $4MP^{\bullet} - C_{32}$.

To investigate the difference between the radicals further, DFT calculations on small molecule mimics were performed.

DFT Calculations on Small Molecule Mimics

To better understand the differences and similarities of the radical spin populations between α_3Y, 2MP – α_3C and 4MP – α_3C, DFT calculations were performed on model molecules, shown in Figure 4.7. The DFT calculations yielded Mulliken spin populations, shown in Table 4.3. Calculations were made for both the neutral and positively charged radicals, with the neutral radicals exhibiting an overall larger spin population on the O. Furthermore, $4MP^{\bullet} - C_{32}$ exhibited a slightly larger population on the first S (closest to the

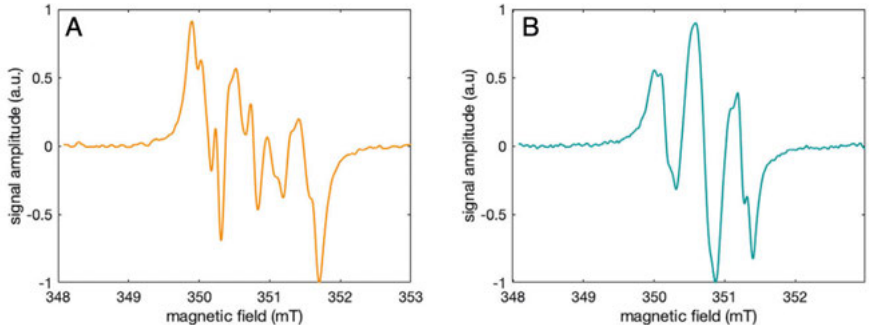

Figure 4.6. EPR spectra recorded under constant illumination on a sample containing protein, $[Ru(bpy)_3]^{2+}$, and $[Co(NH_3)_5]^{2+}$ in 100 mM KP_i and 40 mM KCl pH 6.5 buffer. (A) 2MP$-\alpha_3$C. (B) 4MP$-\alpha_3$C.

phenol ring) than the other molecules. Notably, 2MP$^\bullet-C_{32}$ was the most similar to $Y_{32}^\bullet$. The results from the DFT calculations show that neither of the MP$-C_{32}$ radicals exhibits the same spin population as a Y radical, however, they are not too different, with 2MP$-C_{32}$ being the most similar.

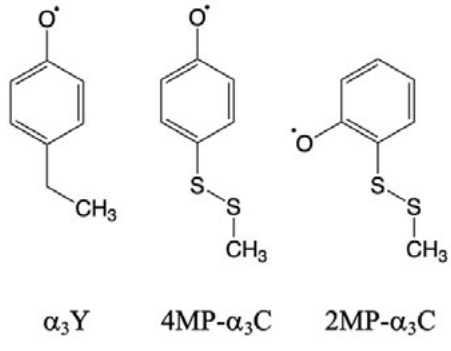

Figure 4.7. Radicals of the molecule mimics of the proteins used for DFT calculations.

4.4 Summary and Conclusions

The environment surrounding X_{32} can affect the primary proton acceptor and thereby the rates of radical formation, as well as the lifetime of the radicals formed. In this chapter, the solution NMR structures of α_3Y, 2MP$-\alpha_3$C, and 4MP$-\alpha_3$C have been presented. They show that α_3Y and 2MP$-\alpha_3$C both exhibit small SASAs, while 4MP$-\alpha_3$C is much more solvent exposed. The protein scaffold affects the pK_a of the residue positioned at site 32 resulting in larger pK_a values than for that amino acid in solution.

Table 4.3. *Mulliken spin populations on key atoms of side chain analogs of the redox active side chain in 2MP–α_3C and 4MP–α_3C. Here, O refers to the hydroxyl oxygen of the side chain, S refers to the sulfur atom closest to the phenol ring, and S2 refers to the sulfur atom most distal from the phenol ring, i.e., closest to the backbone. "Total S" refers to the total spin population on the sulfur atoms in the molecule.*

System	Atom			Total S	Level of theory
	O	S	S2		
4MP–O$^{\bullet}$	0.319098	0.048405	0.002208	0.050613	CASSCF/aug-cc-pvtz
2MP–O$^{\bullet}$	0.310252	0.012860	0.006378	0.019238	CASSCF/aug-cc-pvtz
Y–O$^{\bullet}$	0.337425	–	–	–	CASSCF/aug-cc-pvtz
4MP–OH$^{+\bullet}$	0.041210	0.470241	0.078072	0.548313	CASSCF/aug-cc-pvtz
2MP–OH$^{+\bullet}$	0.120380	0.104978	0.003320	0.108298	CASSCF/aug-cc-pvtz
Y–OH$^{+\bullet}$	0.106288	–	–	–	CASSCF/aug-cc-pvtz

Given the very small SASA for α_3Y and the lack of viable proton acceptors at the Y_{32} site, it was unclear what the primary proton acceptor could be. In Paper I MD simulations were performed on α_3Y that showed that water could access site 32 following local protein conformational changes. These simulations also suggested that E_{13} could come within hydrogen bonding distance to Y_{32}, despite the distance of $\geq$ 6.7 Å observed in the NMR ensemble. In 2MP–α_3C, E_{13} is found $\geq$ 2.5 Å from 2MP–C_{32} (O–O distance) which suggests an internal hydrogen bond.

The α_3-bundle provides an environment wherein long-lived radicals can be generated and then studied. The radicals of 2MP–C_{32}, and 4MP–C_{32} have been characterized using time-resolved UV-vis spectroscopy, EPR spectroscopy, and DFT calculations in Paper II and compared to previously published results for Y_{32}. The UV-vis spectroscopy show that 2MP$^{\bullet}$–C_{32} exhibits characteristics most similar to $Y_{32}{}^{\bullet}$, while 4MP$^{\bullet}$–C_{32} is more similar to a 4-hydroxy-thiophenoxyl. The EPR spectra recorded confirms that the primary 2MP$^{\bullet}$–C_{32} and 4MP$^{\bullet}$–C_{32} radicals are formed. DFT calculations of model molecules suggest that both 2MP$^{\bullet}$–C_{32} and 4MP$^{\bullet}$–C_{32} exhibit slight spin density on the sulfur, with 4MP$^{\bullet}$–C_{32} showing the largest sulfur spin density.

The results discussed in this chapter highlight the effect of fluctuations in the side chain rotamers on the redox reactivity of Y by showing that such changes near the site where Y_{32} sits can promote solvent access. The half-lives of the MP–C_{32} and Y_{32} radicals formed are very long, and the radicals are stabilized by the protein environment. This is the same effect as is seen in natural proteins where radicals can be stabilized compared to radicals in solution.

5. Determining Primary Proton Acceptors and Exploring the Effect of Altering the PT and ET Driving Forces for Tyrosine Radical Formation via PCET in a Protein (Paper I and II)

PCET from tyrosine-derivatives has been shown to proceed via either PTET or CEPT in molecular model systems depending on the bulk pH and the driving force for PT and ET.[41,55] Studies on Y in natural enzymes have often not been able to experimentally show by which PCET pathway the reaction proceeds, because performing such detailed studies on proteins can be difficult. It is known that pK_a and pH values can shift inside enzymes, therefore it is of great importance to understand how these parameters can affect the PCET reactions of Y buried in a protein.

In this chapter, the primary proton acceptor and mechanism of the PCET reaction from Y_{32}, $2MP-C_{32}$, and $4MP-C_{32}$ are discussed. We also discuss the effect of altering the driving force for ET and PT on the PCET mechanism.

5.1 The effect of the α_3-scaffold on PCET reactivity

While the electron can tunnel over several Å through the α_3 protein backbone, the proton is limited to a distance < 1Å. MD simulations on α_3Y (discussed in Chapter 4) had suggested that both water and E_{13} could form transient H-bonds with $Y_{32}-OH$, and thereby act as proton acceptors. However, in the solution NMR ensemble, Y32 is surrounded by aliphatic amino acids (Figure 5.1 A), and the distance to E_{13} is ≥ 6.7 Å. For $2MP-\alpha_3C$, E_{13} was expected to act as the primary proton acceptor. The average distance between $2MP-C_{32}$ and E_{13} was 3.2 ± 0.5 Å, which is a weak hydrogen bond (Figure 5.1 B). Furthermore, the large SASA exhibited by $4MP-C_{32}$ was thought to make deprotonation to the solution facile (Figure 5.1 C).

The α_3-scaffold not only affects the pK_a values, as discussed in Chapter 4, it also affects the reduction potentials, Table 5.1. The reduction potentials for the X_{32} sites investigated are fully reversible in protein-film square wave voltammograms and typically shifted to larger values compared to X in solution by about 45 to 65 mV.[85]

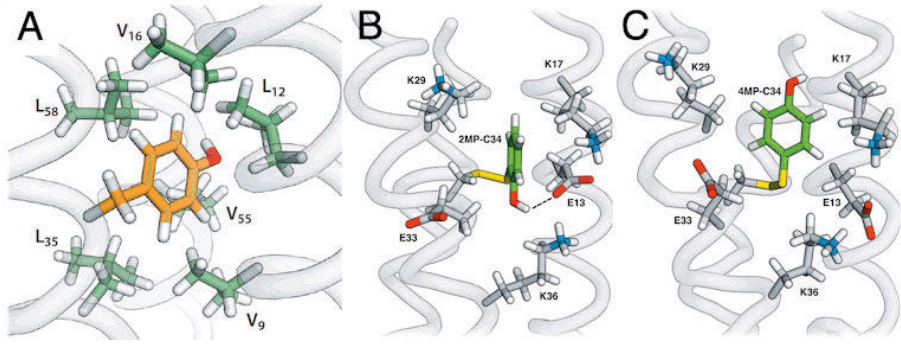

Figure 5.1. The surrounding of site 32 for (A) Y_{32}, (B) $2MP-C_{32}$, (C) $4MP-C_{32}$. In (A-C), hydrogens are shown in white, oxygens in red, and (B-C) sulfur in bright yellow. (A) Reprinted with permission from Annual Review of Biophysics 2022 51:1, 453–471. Copyright 2022 Annual Reviews.

Table 5.1. *Apparent* pK_a *values and reduction potentials for the proteins discussed in this chapter.*

protein	pK_a	$E^{\circ\prime}$ ($X_{32}{}^{\bullet/0}$) at pH 5.5 (V)	$E^{\circ\prime}$ ($X_{32}{}^{\bullet/0}$) at pH 8.5 (V)
α_3Y	11.3 ± 0.1 [81]	1.065 ± 2 [82]	0.909 ± 3 [82]
$\alpha_3Y-E_{13}A$	11.1 ± 0.3 *	-	-
$2MP-\alpha_3C$	9.7 ± 0.2 **	1.011 ± 3 [83]	0.847 ± 2 [83]
$2MP-\alpha_3C-E_{13}A$	9.2 ± 0.2 **	-	-
$4MP-\alpha_3C$	9.5 ± 0.1 [84]	0.890 ± 1 [84]	-

* Determined in Appendix I.
** Determined in Paper II.

5.1.1 α_3Y and $2MP-\alpha_3C$ $E_{13}A$ Variants

To investigate if E_{13} acts as the proton acceptor for α_3Y and $2MP-\alpha_3C$, a variant was prepared for both proteins where E_{13} was mutated to an A ($\alpha_3Y-E_{13}A$ and $2MP-\alpha_3C-E_{13}A$), the chemical structure of E and A are found in Figure 5.2. The mutation gave a small shift in pK_a value from 11.3 ± 0.1 to 11.1 ± 0.3 for $\alpha_3Y-E_{13}A$ and as slightly larger shift from 9.7 ± 0.2 to 9.2 ± 0.2 for $2MP-\alpha_3C-E_{13}A$. If E_{13} is the primary proton acceptor, then a mutation to A is expected to result in slower rate constants since A cannot act as a proton acceptor.

Rate constants as a function of pH were determined for $\alpha_3Y-E_{13}A$ and $2MP-\alpha_3C-E_{13}A$ and compared to α_3Y and $2MP-\alpha_3C$, respectively, Figure 5.3. For both E_{13}A-variants, the rate constants are similar to α_3Y or $2MP-\alpha_3C$, respectively, but faster. Since the rate constants did not get slower for the variant, E_{13} can be excluded as proton acceptor in both α_3Y and $2MP-\alpha_3C$. The faster rate constants could be due to the lower pK_a value

for both variants compared to α_3Y and 2MP–α_3C. Alternatively, the E_{13}A mutation could lead to changes in the α_3-scaffold that somehow promotes faster PT, such as increased solvent exposure.

These results suggest that for 2MP–α_3C, the H-bond between the phenol-OH and E_{13} is too weak to facilitate PT. While the O–O distance between 2MP–C_{32} and E_{13} is $\geq$ 2.5 Å in the solution NMR, the two residues are not pointing towards each other in any of the structures in the NMR ensemble. Consequently, there appears to be a lack of wavefunction overlap between 2MP–C_{32} and E_{13} that can facilitate PT.

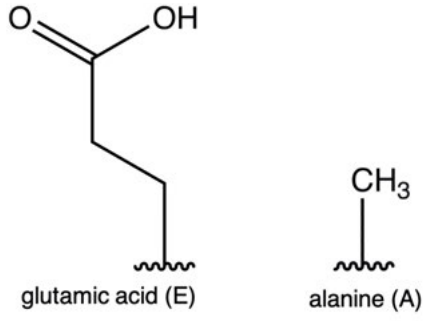

Figure 5.2. The chemical structure of glutamic acid (E) and alanine (A).

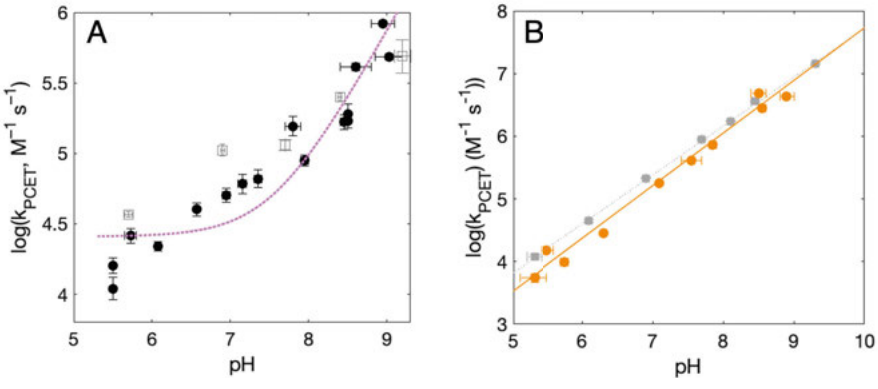

Figure 5.3. Rate constants for radical formation as a function of pH for (A) α_3Y (black round filled markers with a purple fit) and α_3Y–E_{13}A (gray open squares), and (B) 2MP–α_3C (orange round markers with an orange solid line fit) and 2MP–α_3C–E_{13}A (gray square markers with a gray dotted fit).

5.1.2 Excluding Buffer as the Proton Acceptor

Species present in the solution that could act as proton acceptors are phosphate buffer, OH^-, and H_2O. The rate constant for radical formation was measured

as a function of phosphate buffer concentration ([KP_i]) for all proteins to determine if the buffer species were acting as the proton acceptor, Figure 5.4. If the buffer was acting as the proton acceptor, a larger concentration of buffer should lead to faster rate constants. None of the proteins showed rate constants that changed with the concentration of buffer, indicating that buffer was not the primary proton acceptor. It was surprising that rate constants for 4MP–α_3C were unaffected by buffer concentration given that 4MP–C_{32} exhibits 30 to 40% solvent exposure of the phenol-OH group. These results suggest that either the buffer species are too large to enter into the protein cavity, and/or local electrostatics surrounding site 32 did not facilitate negatively charged species to come sufficiently close.

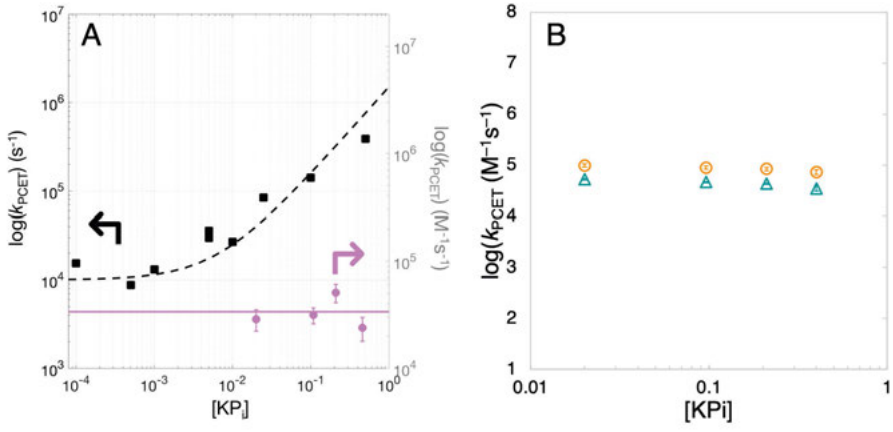

Figure 5.4. PCET rate constants measured as a function of [KP_i]. Error bars are shown when the error is larger than the marker. (A) Data for α_3Y compared to a linked ruthenium photosensitizer-tyrosine model complex (Ru-Y). The left y-axis represents first-order rate constants for Ru–Y,[48] and the right y-axis, second-order rate constants for α_3Y. Black squares show data collected for Ru–Y in pH 7 phosphate buffer with a fit to the data using $k_{obs} = f_b[\text{buffer}]k_b$ (dashed black line). Purple circles show data for α_3Y collected in pH 6.5 phosphate buffer with a linear, constant value fit to the data (solid purple line). (B) Second order PCET rate constants for 2MP–α_3C (orange circles) and 4MP–α_3C (green triangles) determined at pH 6.5. (A) Reprinted with permission from J. Am. Chem. Soc. 2020, 142, 11550–11559. Copyright 2020 American Chemical Society.

5.1.3 Effect of Increased Solvent Exposure on PCET Rate Constants and Primary Proton Acceptor

Given how deeply buried Y_{32} is in α_3Y, we wanted to see if increased solvent exposure (larger SASA), would lead to faster rate constants by making depro-

tonation more facile. To investigate this, PCET rate constants for 4MP–α_3C were compared to rate constants for 2MP–α_3C and 2MP–α_3C–E_{13}A.

PCET rate constants for radical formation were determined as a function of pH for 4MP–α_3C, 2MP–α_3C and 2MP–α_3C–E_{13}A using $[Ru(bpy)_3]^{3+}$ as oxidant, Figure 5.5. The rate constants are very similar for all proteins, with 4MP–α_3C exhibiting slightly larger rate constants throughout the pH range investigated. A difference in p$K_a$values and E°' between 4MP–α_3C and 2MP–α_3C can explain why the former exhibits faster rate constants. It is therefore not clear from this experiment if the faster rate constants for 4MP–α_3C are in part also due to greater solvent access. The small difference in rate constants between the three proteins indicates that if the increased solvent exposure affects the rate constants, then this effect is minor.

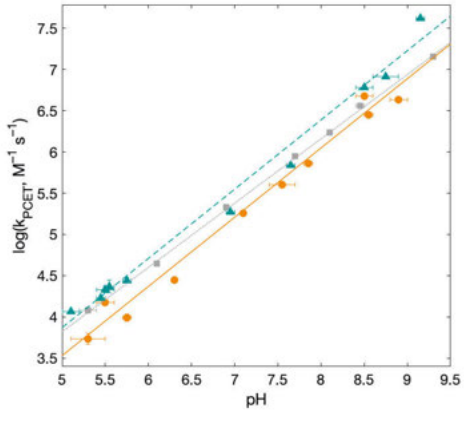

Figure 5.5. log(k_{PCET}) as a function of pH for 2MP–α_3C (orange round markers with a solid line fit), 2MP–α_3C (green round markers with a dashed line fit), and 2MP–α_3C–E_{13}A (gray round markers with a dotted line fit) using $[Ru(bpy)_3]^{3+}$ as oxidant.

5.2 PCET from Y in α_3Y

PCET rate constants for radical formation were determined for α_3Y as a function of pH in order to determine the PCET mechanism in Paper I with $[Ru(bpy)_3]^{2+}$ (Table 5.3.2) as photosensitizer (Figure 5.6 (A), note that this is the same data as shown in Figure 5.3 (A)). The rate constants were observed to increase with increasing pH and mostly level out at low pH.

5.2.1 Mechanistic Assignment and Primary Proton Acceptor for PCET from α_3Y

Significant kinetic isotope effects (KIEs) have previously been determined, indicating that PT was part of the rate-limiting step.[39] This meant that the reaction was either PTET or CEPT. The pH-dependent rate constants observed suggested either a PTET_{lim} or CEPT mechanism with OH^- as proton acceptor (buffer species has been excluded as proton acceptor), or a $\text{PTET}_{\text{pre-eq}}$ mechanism. OH^- was excluded as the primary proton acceptor for a CEPT and PTET_{lim} reaction based on the fact that the pH dependence observed for the rate constants was much weaker than one decade per pH unit. Furthermore, OH^- was excluded for CEPT and PTET_{lim} reactions based on the magnitude of the rate constants compared to the concentrations of OH^- present at the pH values investigated.

The pH dependence observed was instead suggested to represent PCET from the fraction of Y_{32} that is protonated, and the fraction of Y_{32} that is deprotonated in a rapid pre-equilibrium, f_{YOH} and f_{YO^-}, respectively. Both of these species react with a different rate constant, giving the following expression for the PCET rate constant:

$$k_{\text{PCET}} = k_{\text{YOH}} f_{\text{YOH}} + k_{\text{YO}^-} f_{\text{YO}^-} \tag{5.1}$$

At the lower pH-values, the fraction of protonated Y_{32} is approximately one, and because the fraction of deprotonated Y_{32} can be estimated from the pH and pK_a, we get the following equation:

$$k_{\text{PCET}} = k_{\text{YOH}} + k_{\text{YO}^-} \times 10^{\text{pH}-\text{p}K_a} \tag{5.2}$$

where k_{YOH} is independent of pH, and f_{YO^-} depends on the pH of the solution. Fitting the rate constants to Eq. 5.2 gives $k_{\text{YOH}} = 2.6 \times 10^4\ \text{M}^{-1}\,\text{s}^{-1}$ and $k_{\text{YO}^-} = 1.4 \times 10^8\ \text{M}^{-1}\,\text{s}^{-1}$. In Figure 5.6 (A), each component of the fit is shown as a dashed line.

Since PTET_{lim} had been excluded, we attributed the pH-dependent rate constants to $\text{PTET}_{\text{pre-eq}}$. The pH-independent rate constant was instead assigned to a CEPT mechanism based on previously determined KIEs, with water as the primary proton acceptor.

5.2.2 Proton Transfer from Y_{32}

The MD-simulations presented in Chapter 4 suggested that water is readily available on the timescale of the transient absorption experiment. If deprotonation from Y_{32} is compared to deprotonation from phenol (PhOH) in solution, the reaction from deprotonated Y_{32} or PhOH ($Y_{32}-O^-$ or PhO$-$) is similarly accelerated compared to the reaction from protonated Y_{32} or PhOH: $k_{Y_{32}-\text{OH}}/k_{Y_{32}-O^-} \approx 5000$ for Y_{32} and $k_{\text{PhOH}}/k_{\text{PhO}^-} \approx 9000$ for phenol. These

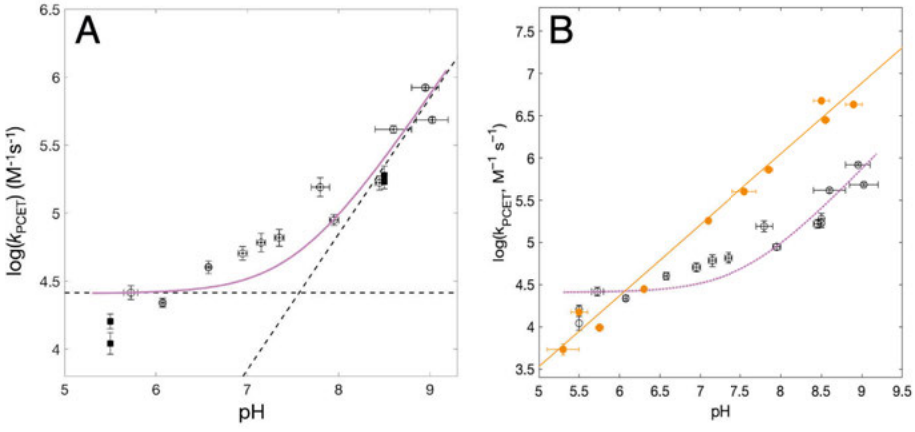

Figure 5.6. (A) Rate constants for PCET from α_3Y by $[Ru(bpy)_3]^{3+}$ as a function of pH. Purple solid line shows a fit to Eq. 5.2, where $k_{YOH} = 2.6 \times 10^4$ $M^{-1}\,s^{-1}$ and $k_{YO^-} = 1.4 \times 10^8$ $M^{-1}\,s^{-1}$ The dashed lines show the pH-independent and pH-dependent terms of the fit. Vertical error bars correspond to $\pm$ one standard deviation. Horizontal error bars correspond to the change in pH during the flash photolysis experiment. (B) Rate constants for PCET as a function of pH for 2MP–α_3C (orange circles) shown together with data from (A). Lines show linear fits to pH data with a slope of 0.84. (A) Reprinted with permission from J. Am. Chem. Soc. 2020, 142, 11550–11559. Copyright 2020 American Chemical Society.

results suggest that despite Y_{32} being buried on average 7.7 ± 0.3 Å from the protein surface, and exhibiting $0.2 \pm 0.2\%$ SASA, deprotonation to water is facile. Initial deprotonation likely happens to one or two water molecules that have diffused into the protein, and the proton is then transferred to bulk water.

5.3 Altering PCET Driving Forces for Y Sequestered in a Protein

Y linked to a photosensitizer has been shown to participate in PTET, ETPT, and CEPT mechanisms when the driving force for ET and PT as well as the pH was altered.[55] A visual representation of which PCET mechanism dominates and how the mechanism changes with different ΔG°_{ET} and ΔG°_{PT} is found in the zone diagram in Figure 5.7.[12] These zone diagrams are constructed such that the contributions to ΔG°_{PT} and ΔG°_{ET}: ΔpK_a and ΔE°, are on the x- and y-axis, respectively. This means that larger driving forces for ET and PT are presented by moving up and to the right in the diagram. Figure 5.7 (A) shows a zone diagram for a system with relatively large vibronic coupling for the CEPT reaction, while (B) shows a zone diagram with 10 times smaller vibronic coupling. The effect that the change in vibronic coupling has on the size and shape of the CEPT region can be gauged by comparing these two figures.

The zone diagram does not predict the rate constant for any of the mechanisms, it only shows how altering the driving force for PT or ET can affect the PCET mechanism. The rate constant for each mechanism depends differently on the driving force for PT and ET, as shown in Figure 2.3 in Chapter 2, which is the basis for the construction of the zone diagrams.

In this section, rate constants for α_3Y, determined in Paper I, are presented first together with an assignment of the PCET mechanisms. The effect of altering the PT driving force is investigated by comparing rate constants for α_3Y to rate constants for 2MP–α_3C from Paper II. Finally, the effect of altering the ET driving force is explored for 2MP–α_3C and 4MP–α_3C (Paper II).

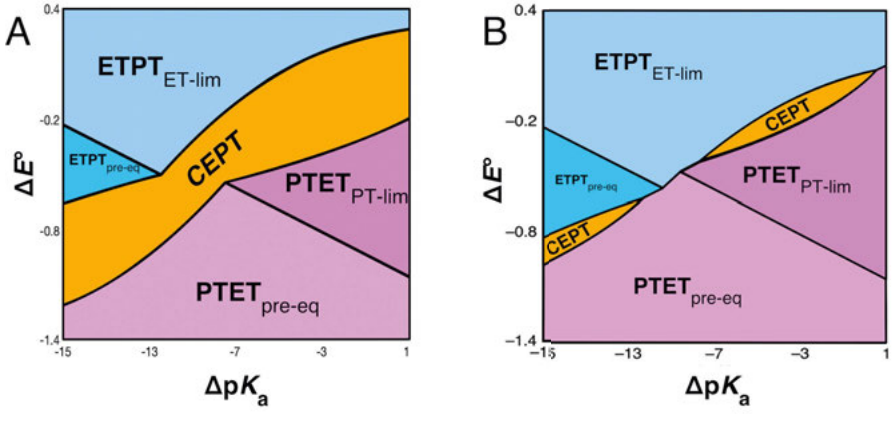

Figure 5.7. (A) A zone diagram for a PCET reaction that exhibits a relatively large vibronic coupling for the CEPT reaction. (B) A zone diagram for a PCET reaction where the vibronic coupling is 10 times smaller than in (A). Modified with permission from J. Am. Chem. Soc. 2021, 143, 2, 560–576 Copyright 2020 American Chemical Society.

5.3.1 Effect of Altering the PT Driving Force

The driving force for PT depends on the ΔpK_a between reactants and products. This means that the driving force can be altered by either changing the pK_a of the donor or the acceptor. For α_3Y, 2MP–α_3C and 4MP–α_3C phosphate buffer is unable to come sufficiently close to act as a proton acceptor. This makes altering the proton acceptor by the introduction of different bases, as is often done for small molecules, very difficult. Instead, we can investigate the effect of altering the PT driving force by comparing results obtained for α_3Y and 2MP–α_3C using the same oxidant. 2MP–C_{32} exhibits a lower pK_a value by 1.6 units compared to Y_{32}, which corresponds to a change in PT driving force of 95 meV. The rate constants for 2MP–C_{32} radical formation exhibited a very different pH dependence compared to what had previously been

observed for α_3Y in Paper I, using the same photosensitizer ($[Ru(bpy)_3]^{2+}$), Figure 5.6 (B). At high pH, the rate constants for both proteins increase with pH, but at low pH the rate constants for $Y_{32}^{\bullet}$ formation mostly level out, while the rate constants for $2MP^{\bullet}-C_{32}$ formation continue to decrease. This means that (at least) in the low pH region, the two proteins exhibit different PCET mechanisms, which suggests that increasing the PT driving force alters the PCET mechanism from CEPT (for α_3Y) at low pH. Mechanistic assignments are discussed *vide infra*.

5.3.2 Effect of Altering the ET Driving Force

In studying the effect of altering the ET driving force, three different photosensitizers were used, Table 5.3.2.

Table 5.2. *Photosensitizers used, their abbreviation and reduction potential.*

photosensitizer	abbreviation	E°(3+/2+) (mV vs. NHE)
Ruthenium 4,4'-dimethyl-2,2'-bipyridine	$[Ru(dmb)_3]^{2+}$	1100
Ruthenium 2,2'-bipyridine	$[Ru(bpy)_3]^{2+}$	1260
Ruthenium 4,4'-ethyl-ester-2,2'-bipyridine	$[Ru(deeb)_3]^{2+}$	1450*

* Converted to value in water vs. NHE, see Paper II.

Rate constants using $[Ru(bpy)_3]^{3+}$ for $MP-\alpha_3C$ as oxidant have been presented in the previous sections, Figure 5.5. Using these values as a starting point, a weaker oxidant ($[Ru(dmb)_3]^{3+}$) was used, and rate constants were determined at pH 5.5 and 8.5 using 3 to 4 different concentrations of protein, shown in Table 5.3.2 together with rate constants for two stronger oxidants. The rate constants are slower with the weaker oxidant at both pH values investigated. This result excludes a PCET mechanism that is rate-limited by PT (i.e., $PTET_{pre\text{-}eq}$) for the rate constants in Figure 5.5.

The strongest oxidant ($[Ru(deeb)_3]^{3+}$), provided about 300 meV more driving force for ET compared to $[Ru(bpy)_3]^{3+}$, used for α_3Y. Rate constants were determined for $2MP-\alpha_3C$ and $4MP-\alpha_3C$ as a function of pH, Figure 5.8. The data show that with the strongest oxidant, the rate constants for radical formation in $2MP-\alpha_3C$ and $4MP-\alpha_3C$ exhibit a similar trend with pH as α_3Y, but that they are overall faster. The data was fit with Eq. 5.2 giving $k_{YOH} = 8.4\times10^5\ M^{-1}\,s^{-1}$, and $k_{YO^-} = 2.7\times10^8\ M^{-1}\,s^{-1}$ for $2MP-\alpha_3C$, and $k_{YOH} = 2.3\times10^6\ M^{-1}\,s^{-1}$, $k_{YO^-} = 4.0\times10^8\ M^{-1}\,s^{-1}$ for $4MP-\alpha_3C$. This is consistent with a larger driving force for both ET from the stronger oxidant and for PT from the smaller pK_a values exhibited by the $MP-\alpha_3C$ proteins compared to α_3Y, discussed *vide infra*.

Table 5.3. *Rate constants for radical formation determined using 3 to 4 concentrations of protein at each pH.*

system	k_{PCET} ($M^{-1}\,s^{-1}$) at pH 5.5	k_{PCET} ($M^{-1}\,s^{-1}$) at pH 8.5
$2MP-\alpha_3C/[Ru(dmb)_3]^{3+}$	2.75×10^3	7.66×10^5
$4MP-\alpha_3C/[Ru(dmb)_3]^{3+}$	4.44×10^3	1.52×10^6
$2MP-\alpha_3C/[Ru(bpy)_3]^{3+}$	1.50×10^4	4.78×10^6
$4MP-\alpha_3C/[Ru(bpy)_3]^{3+}$	2.14×10^4	6.09×10^6
$2MP-\alpha_3C/[Ru(deeb)_3]^{3+}$	–*	3.18×10^7
$4MP-\alpha_3C/[Ru(deeb)_3]^{3+}$	–*	5.40×10^7

* Due to increased probe-light photochemistry when persulfate was used as the quencher, reliable TA traces could not be obtained using small concentrations of protein at pH 5.5.

5.3.3 Mechanistic Assignments for $2MP-\alpha_3C$ and $4MP-\alpha_3C$

α_3Y reacting with $[Ru(bpy)_3]^{3+}$ exhibited a mix of two mechanisms with CEPT dominating at low pH, and $PTET_{pre\text{-}eq}$ dominating at high pH.

The rate constants obtained with $[Ru(bpy)_3]^{3+}$ as oxidant as a function of pH for $MP-\alpha_3C$ showed a linear slope of 0.84 for both $2MP-\alpha_3C$ and $4MP-\alpha_3C$ in a $\log(k_{PCET})$ versus pH plot, Figure 5.5. A slope of 1 can originate from a $PTET_{pre\text{-}eq}$ mechanism, or from reacting with a species whose concentration depends on the pH (such as OH^-) in a $PTET_{lim}$ or CEPT mechanism, see Chapter 2. The deviation of the slope from 1 observed for $2MP-\alpha_3C$ and $4MP-\alpha_3C$ can be due to interactions from the protein. For example, none of the α_3X proteins exhibit the typical Nernstian slope of 59 mV/pH unit in the Pourbaix diagram as expected for a 1 electron/1 proton reaction.[40,85] In Paper II, CEPT with OH^- as the primary proton acceptor was excluded based on the magnitude of the rate constants compared to the low concentration of OH^- present in the pH region studied. This left $PTET_{pre\text{-}eq}$ or $PTET_{lim}$ as possible reaction mechanisms. For a $PTET_{pre\text{-}eq}$, the rate constants depend weakly on the oxidant strength, while for a $PTET_{lim}$ the rate constants are independent of the oxidation strength (Figure 2.3 in Chapter 2). Results obtained with the weakest oxidant ($[Ru(dmb)_3]^{3+}$) were used to exclude $PTET_{lim}$ as the PCET mechanism. The rate constants determined at pH 5.5 and 8.5 for $2MP-\alpha_3C$ and $4MP-\alpha_3C$ were slower using $[Ru(dmb)_3]^{3+}$ compared to rate constants using $[Ru(bpy)_3]^{3+}$, suggesting a $PTET_{pre\text{-}eq}$ mechanism for both proteins using these oxidants.

When the strongest oxidant ($[Ru(deeb)_3]^{3+}$) was used, the rate constants for PCET from $MP-C_{32}$ could be fitted with Eq. 5.2. This suggests that a pH-dependent mechanism at high pH ($PTET_{pre\text{-}eq}$ or $PTET_{lim}$/CEPT with a pH-dependent proton acceptor), and a pH-independent mechanism at low pH (CEPT with H_2O as proton acceptor or ETPT). CEPT in the high pH region was excluded based on the magnitude of the rate constants compared to the

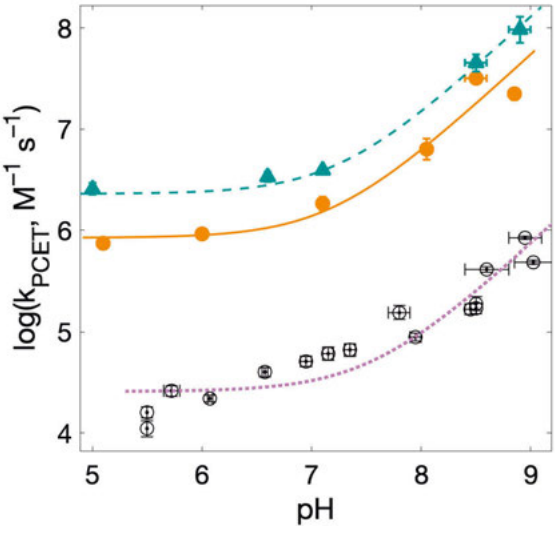

Figure 5.8. Rate constants for radical formation as a function of pH for 2MP–α_3C (orange markers with an orange solid line fit), 4MP–α_3C (teal markers with a teal dashed line fit), with $[Ru(deeb)_3]^{3+}$ as oxidant, and α_3Y (black markers with a purple dotted line fit) with $[Ru(bpy)_3]^{3+}$ as oxidant. The solid orange fit has the function: $f(x) = 8.4 \times 10^5 + 2.7 \times 10^8 \times 10^{(x-9.7)}$. The dashed teal fit has the function: $f(x) = 2.3 \times 10^6 + 4.0 \times 10^8 \times 10^{(x-9.5)}$.

[OH–] present in the solution which is too low to account for the rate constants. $PTET_{lim}$ mechanism was excluded based on the fact that the rate constants were observed to increase with the stronger oxidant which would not be the case for a $PTET_{lim}$ reaction. This leaves $PTET_{pre\text{-}eq}$ as the most probable PCET mechanism in the high pH region. At low pH, the mechanism could be either CEPT or ETPT based on the pH-independent rate constants. Significant KIEs of about 3 were reported for both 2MP–α_3C and 4MP–α_3C using $[Ru(deeb)_3]^{3+}$ as oxidant at pH 5.6 in Paper II. This excludes ETPT and leaves CEPT as the most likely PCET mechanism in the low pH region. We also predict that the primary proton acceptor is H_2O because $[OH^-]$ is too low to account for the observed rate constants, and PT to H_2O explains the pH-independent rate constants.

5.3.4 Marcus Behavior of the MP–α_3C and α_3Y Rate Constants

The Marcus equation for ET predicts that the ET rate constants will increase with increasing driving force for ET (ΔG°_{ET}) until a maximum rate is achieved, following which the rate constants will decrease with increasing driving force. When $\ln(k_{ET})$ is plotted as a function of ΔG°_{ET} the result is a bell-shaped curve.[12]

To confirm that the rate constants determined using the different oxidants and MP–α_3C or α_3Y followed the Marcus equation, $\ln(k_{YO^-})$ was plotted as a function of ΔG°_{ET} (filled pink circles in Figure 5.9). Given that only two pH values were measured using $[Ru(dmb)_3]^{3+}$ as oxidant, a fit to Eq. 5.2 is unreliable. Therefore, the rate constants at pH 8.5 were used instead of k_{YO^-} in Figure 5.9. Simulated rate constants are also shown in Figure 5.9 (unfilled black circles). They were calculated using $\lambda = 1.1$ eV and using the same driving forces as for the experimental data. Measured and simulated rate constants show good overlap, which indicates (i) that the assignment of the pH-dependent k_{YO^-} term is appropriate, and (ii) that the MP–α_3C and α_3Y proteins can be used together to investigate the effect of altering the driving force for the PCET reaction.

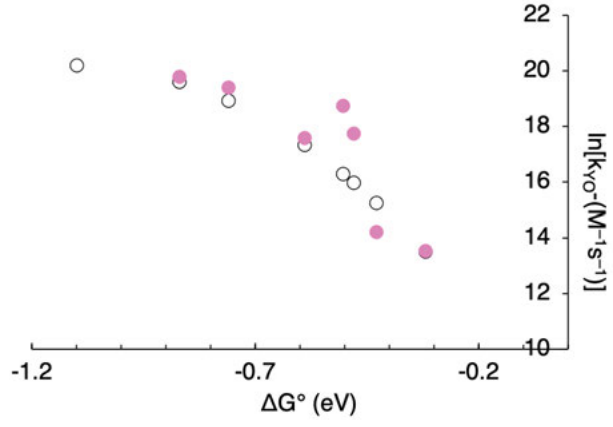

Figure 5.9. Natural logarithm (ln) of k_{YO^-} rate constants (filled pink cirlces) and simulated values (unfilled black circles) plotted as a function of driving force for 2MP–α_3C and 4MP–α_3C using $[[Ru(dmb)_3]^{3+}$, $[Ru(bpy)_3]^{3+}$, and $[Ru(deeb)_3]^{3+}$ as oxidants and α_3Y with $[Ru(bpy)_3]^{3+}$ as oxidant (filled pink circles). The simulated values were obtained using $\lambda = 1.1$ eV. k_{YO^-} rate constants for oxidation by $[Ru(bpy)_3]^{3+}$ and $[Ru(deeb)_3]^{3+}$ were obtained from fitting the rate constants as a function of pH with one pH-independent term and one pH-dependent term.

5.3.5 Moving Along the Zone Diagram for a Tyrosine Radical Formation in α_3X

Switching from α_3Y/$[Ru(bpy)_3]^{3+}$ to 2MP–α_3C/$[Ru(bpy)_3]^{3+}$ allows us to alter the driving force for PT by 95 meV from the change in pK_a. The switch is accompanied by a change in $E^\circ(X_{32}{}^\bullet/X_{32}{}^-)$ of about 20 meV towards a lower ET driving force. In other words, this change means moving to the right and down in the zone diagram. This results in a change in the mechanism from $PTET_{pre\text{-}eq}$/CEPT for α_3Y to only $PTET_{pre\text{-}eq}$ for 2MP–α_3C.

When we then change the driving force for ET by using a stronger oxidant, switching from 2MP–α_3C/$[Ru(bpy)_3]^{3+}$ to 2MP–α_3C/$[Ru(deeb)_3]^{3+}$, we provide the system with 280 meV more driving force for ET. This means moving up in the zone diagram. The result is that we go from $PTET_{pre\text{-}eq}$ to a mix of $PTET_{pre\text{-}eq}$/CEPT, the same mechanisms that we started out with when using α_3Y/$[Ru(bpy)_3]^{3+}$. For the CEPT mechanism (observed at low pH values), the change in the driving force between α_3Y/$[Ru(bpy)_3]^{3+}$ and 2MP–α_3C/$[Ru(deeb)_3]^{3+}$ is about 335 meV. This is accompanied by a change in rate constants for the CEPT mechanism from $k_{YOH} = k_{CEPT} = 2.6 \times 10^4$ $mol^{-1}\,s^{-1}$ to $k_{YOH} = k_{CEPT} = 8.4 \times 10^5$ $mol^{-1}\,s^{-1}$, which corresponds to a change of 1.5 orders of magnitude. This change in the rate constant with increased CEPT driving force corresponds to a change of one $\ln(k_{CEPT})$ per 96 meV, which is consistent with a CEPT reaction in the Marcus normal region.

5.4 Implications For Natural Systems

Y pK_a values can shift in proteins depending on the immediate environment such as nearby proton acceptors.[87] The pH inside a protein can also be different from the bulk pH. The results presented in Paper I and II show that the Y PCET mechanism is affected by the pH and the driving force for ET and PT. These results also indicate that when water is the proton acceptor, a lower pH value is more likely to result in concerted PCET compared to a high pH value.

For Y_{32}, water is the most likely proton acceptor. The fact that CEPT from Y_{32} could proceed with water as the proton acceptor is interesting for understanding the radical transfer pathway in class 1a Ribonucleotide Reductase, Figure 1.3 A in Chapter 1. It had previously been suggested that the ET between the subunits was coupled to deprotonation to water, however, no mechanism was suggested.[88] Following the publication of Paper I, MD simulations were carried out that supported PCET over the subunits with PT to water situated between the subunits.[24] The results from Paper I suggests that this PCET reaction could proceed via CEPT or $PTET_{pre\text{-}eq}$.

5.5 Summary and Conclusions

In this chapter, PCET in the α_3-bundle has been discussed. PT to E_{13} in α_3Y and 2MP–α_3C has been excluded, as well as PT to phosphate buffer for α_3Y, 2MP–α_3C, and 4MP–α_3C leaving OH^- and H_2O as the possible primary proton acceptors. The exclusion of PT to E_{13} from 2MP–α_3C was unexpected given the weak hydrogen bond observed in the ensemble of NMR structures. The fact that phosphate buffer was found to not accept the proton suggests that it is either too large or too charged to come close enough to site 32. Rate constants for 2MP–α_3C compared to 4MP–α_3C show that the

increased solvent exposure exhibited by 4MP–α_3C has no effect, or only a minor effect, on the rate constants. Rate constants for 4MP–α_3C were faster than for 2MP–α_3C, but this is likely mainly due to the difference in pK_a values and reduction potentials.

The effect of altering ΔG°_{PT} and ΔG°_{ET} has also been discussed. Our results show that a difference in 95 meV for ΔG°_{PT} was sufficient to shift the mechanism from a mixture of CEPT at low pH and $PTET_{pre\text{-}eq}$ at high pH, to only $PTET_{pre\text{-}eq}$ in the entire pH range investigated. When we then altered ΔG°_{ET} by 280 meV, the mechanism shifted at low pH to CEPT. When the proteins exhibited a CEPT mechanism, H_2O is the most likely primary proton acceptor.

6. PCET from Freely Solvated Tryptophan Derivatives (Paper III)

It has long been questioned whether W can undergo CEPT with water as the primary proton acceptor. Nevertheless, previous mechanistic studies on small molecule W-analogs in aqueous solution have exhibited CEPT rate constants that are weakly dependent on the pH.[60,62] While this weak (< 1) pH dependence appears to phenomenologically correlate with a CEPT reaction with water as the primary proton acceptor,[48,60–62,89,90] its existence has been questioned, and in the case of W-analogs alternatively explained.[43] In this chapter, we discuss results from Paper III where we study PCET rate constants and mechanisms for two W-analogs. Small molecule analogs are studied because it is with these that the weak pH dependence has been primarily observed, furthermore, the results can aid our understanding of solvent-exposed Ws in biological systems.

6.1 Previous Mechanistic Studies

W exhibits a very large pK_a value in its reduced state (~ 17) which drops to 4.3 once the molecule has been oxidized.[20,21] As a result of these pK_a values, W often undergoes ETPT or ET (without PT) in biological systems. In Paper III, PCET from two W analogs was studied, namely WEE and NAWEE, Figure 6.1. The analogs in Figure 6.1 are designed to block one or both of the functional groups that make the peptide bond, ensuring that the indole proton (marked in pink in Figure 1.1, Chapter 1) is the proton donor in the PCET reaction.

The tryptophan analog WEE has previously been studied and exhibited weakly pH-dependent PCET rate constants with an unknown origin, black data in Figure 6.6 (A).[43,60] Zhang et al.[60] first published a study on WEE where they showed that WEE exhibits pH-dependent rate constants assigned to a CEPT mechanism with water as the primary proton acceptor when an appropriately weak oxidant was used. As discussed in Chapter 2, there is currently no theoretical explanation for pH-dependent rate constants with water (H_2O) as the primary proton acceptor. The mechanistic assignment by Zhang et al.[60] was thus based on two things.

1. Switching between a stronger and a weaker oxidant resulted in rate constants independent of pH (with the stronger oxidant) and rate constants exhibiting a weak pH dependence (with the weaker oxidant), suggesting different PCET mechanisms.

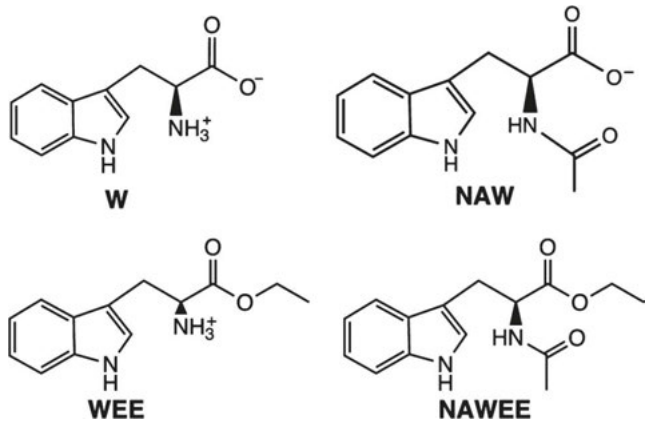

Figure 6.1. Chemical Structures of tryptophan and its three analogs discussed in this Chapter shown at pH = 7. W: tryptophan, NAW: n-acetyl tryptophan, WEE: tryptophan ethyl-ester, NAWEE: n-acetyl tryptophan ethyl-ester. Reprinted with permission from J. Am. Chem. Soc. 2022, 144, 16, 7308–7319. Copyright 2022 The Authors. Published by American Chemical Society.

2. The pH-dependent rate constants exhibited a significant KIE of 2 to 5 depending on the pH using the weak oxidant, indicating that PT was a part of the rate-limiting step. A PT-limited reaction was excluded based on the very large pK_a of W ($\sim$ 17), and an ET-limited reaction was excluded based on the pH dependence of the rate constants and the KIE.

Weakly pH-dependent CEPT rate constants had previously been observed in linked tyrosine-photosensitizer and tryptophan-photosensitizer systems when H_2O was acting as the primary proton acceptor.[48,55,61,89]

The work and conclusions drawn by Zhang et al.[60] was questioned by Bonin et al.[43]. The basis for their alternative conclusions can be summarized in three points as follows.

1. Bonin et al.[43] showed that the quencher used in the flash-quench formation of the oxidant *in situ* by Zhang et al.[60], methylviologen (MV^{2+}), forms an adduct with WEE at high concentrations and pH. Switching to another quencher gave rate constants that appeared to level out at high and low pH, i.e., that looked like a titration curve (gray open squares, Figure 6.6 (A)).

2. The rate constants reported by Bonin et al.[43] appeared to follow a titration behavior around pH 7.5. This is the pK_a of the unprotected amine group present on WEE. Consequently, Bonin et al.[43] concluded that this amine group was responsible for the observed pH-dependent rate constants due to the change in electrostatic interaction between WEE and the tri-cationic photosensitizer. This conclusion was further evidenced by the (erroneous, *vide infra*) thermodynamic cycle presented

for electron transfer between WEE and the used oxidized photosensitizer ($Ru(dmb)_3]^{3+}$). These results suggested that the driving force for ET was larger at high pH because of the electrostatics for the encounter–successor complex.

3. Bonin et al.[43] also studied the W analog NAWEE (Figure 6.1) where both the amine and carboxylic groups are protected. When using the same photosensitizer, NAWEE did not exhibit pH-dependent rate constants. This indicated that the reaction between NAWEE and oxidant was likely limited by ET (ETPT or pure ET). Using two ill-defined irreversible cyclic voltammograms (CV) scans, it was suggested that NAWEE was more difficult to oxidize. This meant that when the same oxidant was used, NAWEE had a lower driving force for ET compared to WEE, which placed WEE further into the ETPT zone ($ETPT_{pre\text{-}eq}$ or $ETPT_{lim}$) compared to NAWEE, Figure 5.7, Chapter 5. Therefore, if NAWEE exhibited ETPT rate constants, so much WEE. This led to the conclusion that both WEE and NAWEE oxidation was limited by ET, and proceeded either via pure ET or ETPT.

The motivation for studying the system again in Paper III rose from three parts: First, a later study by Dongare et al.[62] on covalently linked tryptophan-photosensitizer gave direct spectroscopic-kinetic evidence for a CEPT mechanism from W where the rate constants exhibited the same weak pH dependence. Second, an error had been made by Bonin et al.[43] when the thermodynamic cycle was calculated. Without this error, the driving force for ET was higher at low pH rather than at high pH, which does not correlate with the observed rate constants. Third, it had been shown that functionalizing the amine group on W led to lower reduction potentials rather than higher for NAW compared to W.[59] If this was true also for WEE and NAWEE, then WEE and NAWEE need not be in the same mechanistic region of the zone diagram, meaning that the pH-independent rate constants for NAWEE could be explained by a shift in mechanism compared to WEE to an ETPT mechanism, rather than a proof that the amine group of WEE was involved in creating the pH dependence.

6.2 Encounter/Successor Complex Electrostatics

Bonin et al.[43] proposed a pure ET or ETPT reaction. This means that the driving force for the rate-limiting step would be ΔG°_{ET}. The Coulombic work for reactant and product states contributes to ΔG°_{ET}:[68]

$$\Delta G^{\circ}_{E}T = -F(E^{\circ}(Ru^{III/II}) - E^{\circ}(\mathrm{W}^{\bullet+}/\mathrm{W})) + w_{\mathrm{P}} - w_{\mathrm{R}} \qquad (6.1)$$

In the ET reaction between WEE and the oxidant $[Ru(dmb)_3]^{3+}$, WEE goes from (+1) charge to (+2) charge at acidic pH, and from (0) to (+1) charge at

basic pH. The difference in charge between low and high pH is due to the amine group that is not protected on WEE, which exhibits a pK_a of 7.5.[43] During the PCET reaction, the oxidant goes from (+3) to (+2). The reactions for only ET are:

$$^{+}\text{WEE} + \text{Ru}^{\text{III}} \xrightarrow{\text{ET}} {}^{+}\text{WEE}^{+} + \text{Ru}^{\text{II}} \text{ (at low pH)} \tag{6.2}$$

$$\text{WEE} + \text{Ru}^{\text{III}} \xrightarrow{\text{ET}} \text{WEE}^{+} + \text{Ru}^{\text{II}} \text{ (at high pH)} \tag{6.3}$$

where the positive charge on the amine group is shown as $^{+}$WEE. The work terms for the thermodynamic cycle were erroneously calculated as the sum between product and reactant when the correct terms should be the difference:

$$w_{\text{P,A}} - w_{\text{R,A}} = (2 \times 2 - 3 \times 1)w_0 = 1w_0 \text{ (at low pH)} \tag{6.4}$$

$$w_{\text{P,B}} - w_{\text{R,B}} = (2 \times 1 - 3 \times 0)w_0 = 2w_0 \text{ (at high pH)} \tag{6.5}$$

where A = acid, B = base, and $w_0 = e_0^2/4\pi\varepsilon_0\varepsilon_S d$. Bonin et al.[43] estimated w_0 as 26 meV, which means that the work term contribution to $\Delta G^{\circ}_{\text{ET}}$ is +26 meV at low pH, and +52 meV at high pH. This is very different from the $7w_0 = +180$ meV calculated by Bonin et al.[43] at low pH and +52 meV at high pH. Not only do our results give a smaller difference between the acidic form and the base form, but it also shows that the work term contribution is more positive at high pH, meaning $\Delta G^{\circ}_{\text{ET}}$ is less negative.

As shown in Paper III, the pH-dependent data presented in Figure 6.6 cannot be explained by an ET-limited reaction with a driving force that is modulated by the protonation state of the amine group on WEE.

6.3 Determining the Reduction Potentials of WEE and NAWEE

The reduction potentials for the W-analogs determine the driving force for ET. When determining PCET mechanisms it is, therefore, a very important property to establish for any PCET reactant. Bonin et al.[43] used two ill-defined, irreversible CV scans to claim that NAWEE was more difficult to oxidize than WEE, Figure 6.2 (A). Since NAWEE exhibited pH-independent rate constants when the same oxidant was used, this was taken as proof that WEE would also exhibit pH-independent rate constants as long as it had the unprotected amine group. Previous work from Gagliardi et al.[59] had shown that functionalizing the amine group leads to lower reduction potentials, the opposite of what was suggested by Bonin et al.[43]. This motivated us to do a more rigorous characterization of the reduction potentials of WEE and NAWEE.

CVs of tryptophan are generally very irreversible due to the very fast dimerization that follows upon oxidation. This means that typically no peak is seen when reductive current is applied. In order to determine apparent reduction

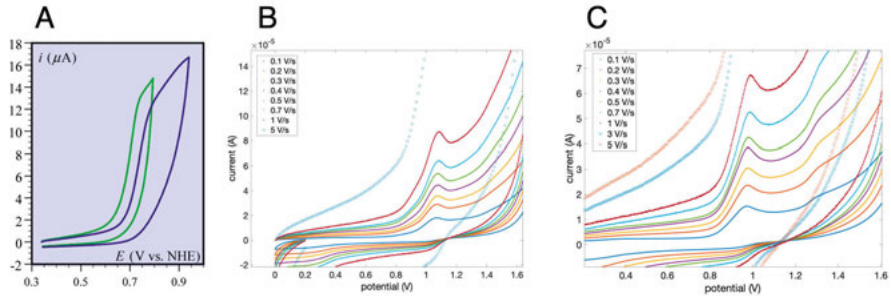

Figure 6.2. Cyclic voltammogram (CV) scans collected for WEE and NAWEE in 0.1 M KNO_3 aqueous solution. (A) 1 mM NAWEE (blue) and WEE (green) at pH 10, potentials shown vs. NHE. (B) 0.2 mM WEE at different scan rates at pH 5.2, potentials shown vs. Ag/AgCl. (C) 0.2 mM NAWEE at different scan rates at pH 5.2, potentials shown vs. Ag/AgCl. (A) Reprinted with permission from J. Am. Chem. Soc. 2013, 135, 38, 14359–14366. Copyright 2013 American Chemical Society. Published by American Chemical Society. (B-C) Reprinted with permission from J. Am. Chem. Soc. 2022, 144, 16, 7308–7319. Copyright 2022 The Authors. Published by American Chemical Society.

potentials for irreversible reactions, the peak potentials can be measured as a function of scan rate (v). When this is done, a linear relationship with a slope of 19.7 mV is expected.[42] The apparent reduction potentials (E°') for the W$^{\bullet}$/W couple were determined by measuring peak potentials (E_p) as a function of v for WEE and NAWEE, Figure 6.2 (B) and (C), respectively. At pH 5.2 the CVs were still rather ill-defined but with a clear E_{peak} around 1V, which made determining the reduction potential possible. The peak potentials were plotted vs. scan rate and the reduction potential was extracted from the y-intercept, Figure 6.3. The results show that NAWEE has a lower reduction potential than WEE. This means that when the same oxidant strength was used for reaction with WEE and NAWEE, the latter exhibited an overall larger driving force for ET. Since a larger ET driving force can alter the PCET mechanism from CEPT to ETPT,[12] this explains the pH-independent rate constants observed for NAWEE.

6.4 PCET Rate Constants for WEE and NAWEE as a Function of pH

Rate constants for radical formation were determined by observing the formation of the W$^{\bullet}$ (WEE$^{\bullet}$ or NAWEE$^{\bullet}$) radical or the recovery of the photosensitizer. When other species absorbed in the same wavelength region as the radicals, the recovery of the photosensitizer to the ground state was instead monitored. Neutral and cationic tryptophan radicals absorb in a similar region, however, the cationic species exhibits a larger absorption coefficient with a

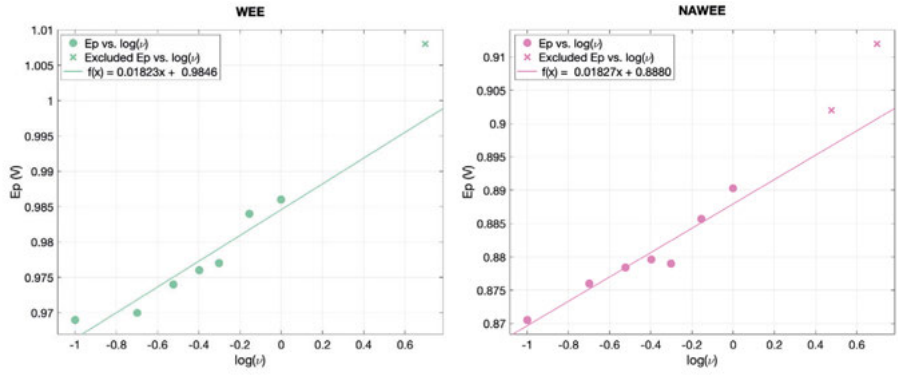

Figure 6.3. Peak potentials plotted as a function of log(ν) for WEE (left) and NAWEE (right). The lines represent linear fits to points having scan rates between 0.1 and 1 V/s (filled circles). The data points represented by crosses were not included in the fits. Potentials are referenced to NHE. Reprinted with permission from J. Am. Chem. Soc. 2022, 144, 16, 7308–7319. Copyright 2022 The Authors. Published by American Chemical Society.

peak at 560 nm, while the neutral radical exhibits a peak at 510 nm.[62,91] This allows for distinction between the two radicals by comparing the magnitude of the absorption at their respective maxima. As seen in Figure 6.5, the absorption at 510 is larger than at 560 at pH 6.0 (A) indicating a neutral radical, while the opposite is seen at pH 2.2 (B) indicating a cationic radical.

The flash-quench method, introduced in Chapter 3, was used to form the oxidized photosensitizer. At pH $>$ 7.5 for WEE, $[Co(NH_3)_5Cl]^{2+}$ was found to be too slow of a quencher. At these pH values, the oxidized photosensitizer was instead formed via two-photon ionization, right side of Figure 6.4.[92–95]

6.4.1 Determination of PCET Rate Constants for WEE Radical Formation

The rate constants for WEE radical formation were determined using the photosensitizer $[Ru(dmb)_3]^{2+}$, Figure 6.6. The results will be discussed in the following regions (marked by dashed lines in Figure 6.6 (A)); pH $<$ 4, 5 $<$ pH $<$ 8 and pH $>$ 8.

pH $<$ 4

The pK_a for oxidized tryptophan is about 4.3,[20] therefore WEE is not expected to deprotonate upon oxidation at these pH values. Monitoring the radical formation at 510 and 560 nm showed that indeed, only the protonated radical was formed during the timescale of the experiment. An example of this at pH 2.2 is seen in Figure 6.5 (B). In this pH region, the rate constants (pink filled triangles in Figure 6.6 (A)) appear to level out. To ascertain that pseudo-first-

Table 6.1. *Names, abbreviations, formal (where applicable) and apparent reduction potentials for tryptophan, three analogs and the photosensitizers used.*

name	abbreviation and redox couple	E° or $E^{\circ\prime}$ (V vs. NHE)
tryptophan	$W^\bullet/W$	1.15 (pH 5.2)*
n-acetyl tryptophan	$NAW^\bullet/NAW$	1.0 (pH 5.2)*
tryptophan ethyl ester	$WEE^\bullet/WEE$	1.00 (pH 5.2)**
n-acetyl tryptophan ethyl ester	$NAWEE^\bullet/NAWEE$	0.908 (pH 5.2)**
ruthenium 4,4'-dimethyl-2,2'-bipyridine	$[Ru(dmb)_3]^{3+/2+}$	1.10
zinc(II) tetra(4-sulphonatophenyl) porphyrin	$[Zn(TPPS)]^{3-/4-}$	0.87

* Calculated from E° using $pK_a(W^\bullet H^+) = 4.3$.[20,21]
** Measured in Paper III.

order kinetics dominated, the rate constants were determined as a function of [WEE] at pH 3. The TA traces that were obtained when [WEE] < 80 mM did not exhibit pseudo-first-order kinetics. Instead, more complicated kinetics was observed that likely represents an uphill pre-equilibrium ET ($\Delta E^\circ > 0$), followed by follow-up reactions of the radical cation (e.g., deprotonation or dimerization). At larger concentrations of WEE, the equilibrium shifts (see Section 2.2 in Chapter 2), and the forward rate constant dominates, allowing us to determine k_{ET}.

$5 <$ pH < 8

In this pH region, the previously published data exhibited different slopes (both < 1) depending on which quencher was used. Rate constants obtained with the irreversible $[Co(NH_3)_5Cl]^{2+}$ quencher agreed somewhat with data recorded by Bonin et al.[43]. In this region, the formation of the neutral WEE radical could be observed because of the optical transparency of the reduced quencher.

pH > 8

In this pH region, Bonin et al.[43] published data that appeared to level out, while the data from[60] continued to increase with increasing pH. The rate constants at pH > 8 in Paper III were measured using two-photon ionization of $[Ru(bpy)_3]^{2+}$ to form the Ru(III) oxidant. The results, orange-filled diamonds in Figure 6.6 (A), show that the WEE rate constants indeed continue to increase with increasing pH. This is a strong argument against a titration of the amine side-group on WEE being responsible for the observed pH dependence.

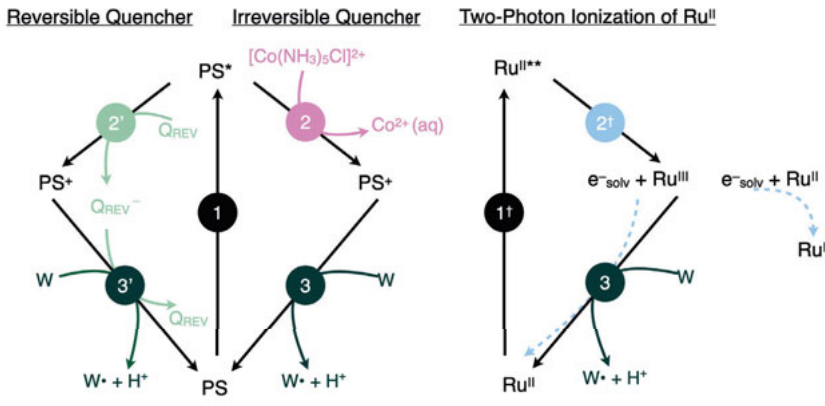

Figure 6.4. Generation of W$^\bullet$ by flash-quench photolysis using a reversible quencher (left), an irreversible quencher (middle), or two-photon ionization (right). (1) represents laser excitation of the photosensitizer (PS = $[Ru(dmb)_3]^{2+}$ or $[ZnTPPS]^{4-}$), which is followed by oxidative quenching by an irreversible quencher (2), a reversible quencher (2'), or ionization ($2^{\ddagger}$). Recovery of the photosensitizer to the ground state (3) either via reaction with a W analog or via a combination of reaction with W and recombining with the electron lost in the oxidation process. Reprinted with permission from J. Am. Chem. Soc. 2022, 144, 16, 7308–7319. Copyright 2022 The Authors. Published by American Chemical Society.

6.4.2 Determination of PCET Rate Constants for NAWEE Oxidation

Previous rate constants determined for NAWEE using $[Ru(dmb)_3]^{3+}$ as oxidant were replicated with the $[Co(NH_3)_5Cl]^{2+}$ quencher to confirm that they exhibited the same pH-independence as previously published using another quencher, Figure 6.7. Rate constants for NAWEE oxidation by $[Ru(dmb)_3]^{3+}$ using $[Co(NH_3)_5Cl]^{2+}$ quencher exhibited no pH dependence, and we concluded, like the previous publication,[43] that the rate constants were limited by ET. A weaker oxidant was then used to attempt to alter the PCET mechanism to CEPT, following the same logic discussed in Chapter 5.3.2. The oxidant used was zinc(II) tetra(4-sulphonatophenyl) porphyrin ($[Zn(TPPS)]^{4-}$, $E^\circ = 0.87$ V).[96]

The rate constants determined as a function of pH for NAWEE were slower with the weaker oxidant, as expected, and exhibited rate constants that increased with pH, Figure 6.7. The slope obtained from fitting $\log(k_2)$ vs. pH to a straight line was the same for the data collected with NAWEE as for the data collected with WEE in the same pH-region using different oxidants, Figure 6.6 (B). Unfortunately, KIEs could not be determined due to the very slow rate constants exhibited by NAWEE, which makes following the reaction with laser-flash photolysis very difficult.

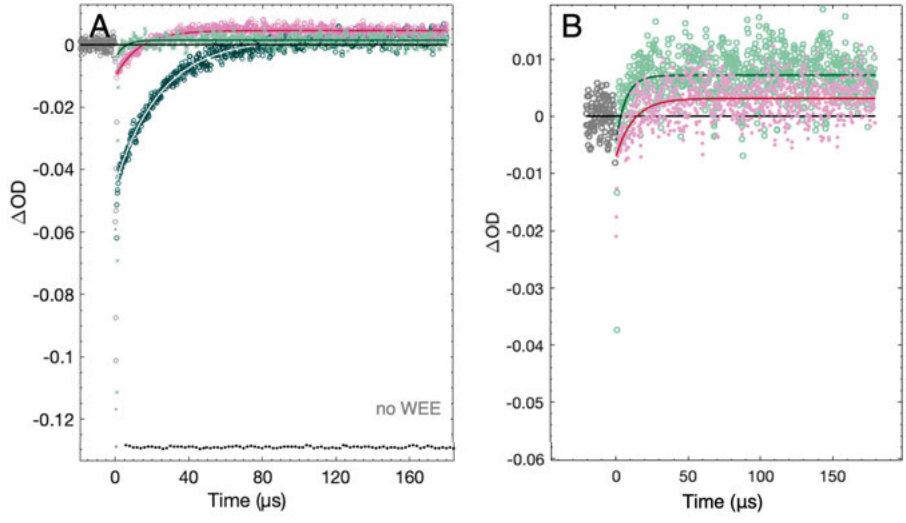

Figure 6.5. TA kinetic traces (markers) and single-exponential fits (lines) after laser pulse excitation at 460 nm of a solution containing $[Ru(dmb)_3]^{2+}$, WEE, and $[Co(NH_3)_5Cl]^{2+}$ in 0.5 mM KP_i . (A) Traces recorded at pH $6.0(\pm 0.1)$ at 510 nm (pink circles; magenta line), 560 nm (light-green crosses; dark-green line), and 450 nm (dark green circles; white line). Black dots indicate the control experiment obtained at 450 nm without WEE and normalized to the 450 nm bleach. At this pH, the neutral radical dominates. (B) Traces recorded at pH 2.2, at 560 nm (light green circles; solid dark green line) and 510 nm (pink circles; red line). At this pH, the cationic W radical dominates. (A) Reprinted with permission from J. Am. Chem. Soc. 2022, 144, 16, 7308–7319. Copyright 2022 The Authors. Published by American Chemical Society.

6.5 Mechanistic Assignment of the PCET reaction in WEE and NAWEE

Following the publication of Paper III, we learned that the pK_a of oxidized W can change with functionalizations to the amine and carboxylic side groups.[97] Functionalizing either the amino or the carboxylic side group gave a higher pK_a value of 4.7 to 4.8. Note that the W analogs studied were NAW and n-acetyl tryptophan methyl ether, not WEE nor NAWEE. Nevertheless, this corresponds well with the results observed in Figure 6.6 (A) where the pink data exhibit a leveling out of the rate constants at pH ≈ 4.8. This does not change the interpretation published in Paper III.

Below the mechanistic assignments for WEE and NAWEE are presented followed by a discussion about water as the primary proton acceptor.

WEE

At pH $<$ pK_a of oxidized tryptophan, WEE oxidation is not coupled to proton transfer, as evidenced by the formation of the cationic radical. At these pH

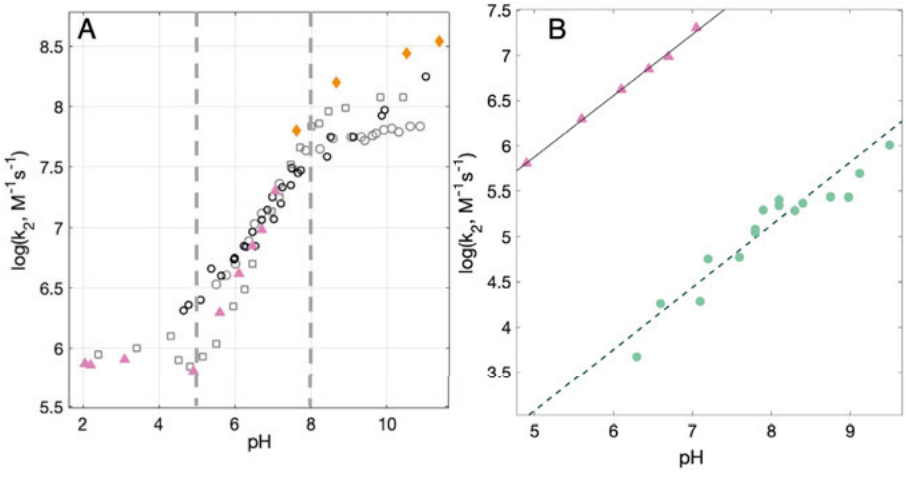

Figure 6.6. (A) PCET rate constants for WEE oxidation by $[Ru(dmb)_3]^{3+}$ as a function of pH. Filled pink triangles represent data collected using $[Co(NH_3)_5Cl]^{2+}$ as a quencher. Filled orange diamonds represent data where the oxidant was formed via two-photon ionization. Data in gray from ref. 43, black data from ref. 60. Circles represent data collected using MV^{2+} as a quencher. Squares represent data collected using $[Ru(NH_3)_6]^{3+}$ as a quencher. The dashed vertical lines mark pH regions defined in the text. (B) Experimental second-order PCET rate constants for NAWEE oxidation by $[ZnTPPS]^{3-}$ (green dots). The dashed black line represents a linear fit corresponding to $f(x) = 0.69x - 0.39$. Also shown are PCET rate constants for WEE obtained using $[Ru(dmb)_3]^{3+}$ as the oxidant and $[Co(NH_3)_5Cl]^{2+}$ as the quencher (pink triangles), reproduced from (A) fit to $f(x) = 0.68x + 2.5$ is shown as a solid black line. Both figures: Reprinted with permission from J. Am. Chem. Soc. 2022, 144, 16, 7308–7319. Copyright 2022 The Authors. Published by American Chemical Society.

values, the driving force for ET is $\Delta G^{\circ}_{ET} \geq 0$ (i.e., the reaction is uphill). The reaction can still proceed if sufficient [WEE] is present in the solution such that $[WEE] \gg [[Ru(dmb)_3]^{2+}]$. With these conditions met, we could determine k_{ET}, seen in Figure 6.6 (A) as pink triangles in the lower pH region of the plot.

At larger pH values, the rate constants increase with increasing pH, suggesting a different mechanism. Since the rate constants increase beyond k_{ET}, they cannot be ET limited. We, therefore, exclude ETPT as the reaction mechanism in this pH region. Previous publications reported a KIE for WEE between 2 and 5, indicating that PT is part of the rate-limiting step.[60] PTET can also be excluded as follows. $PTET_{pre\text{-}eq}$ should exhibit a slope of 1 in a $\log(k_2)$ vs. pH plot. Furthermore, because of the large pK_a value of W (≈ 17), the fraction of deprotonated W would be too small at the pH values measured to account for the observed rate constants. $PTET_{lim}$ can only proceed if OH^- is the primary proton acceptor since H_2O would give a much too small driving force for PT. OH^- is excluded *vide infra* based on the magnitude of the rate constants. This leaves CEPT as the only viable PCET mechanism at pH > $pK_a(W^{\bullet+})$.

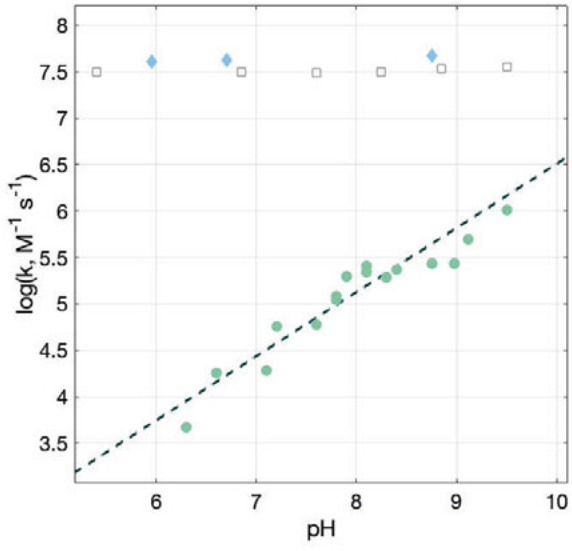

Figure 6.7. Rate constants for NAWEE oxidation as a function of pH using different photosensitizers and quenchers. Green filled circles: $[ZnTPPS]^{3-}$ as photosensitizer and $[Co(NH_3)_5Cl]^{2+}$ as quencher. Filled blue diamonds: $[Ru(dmb)_3]^{2+}$ as photosensitizer and $[Co(NH_3)_5Cl]^{2+}$ as quencher. Unfilled gray squares: $[Ru(dmb)_3]^{2+}$ as photosensitizer and $[Ru(NH_3)_6]^{3+}$ as quencher, from ref. 43.

NAWEE

Rate constants for NAWEE with $[Zn(TPPS)]^{4-}$ as oxidant were too slow to allow determination at very low pH values, therefore k_{ET} could not be estimated. For the same reason, KIEs could not be determined either. We can still exclude the ETPT mechanism with this weaker oxidant on the basis that it should not exhibit any pH dependence. PTET can be excluded analogously as to WEE. This again leaves CEPT as the PCET mechanism.

Water as the Primary Proton Acceptor

Previous studies have shown that 0.5 mM KP_i is a sufficiently low concentration of buffer so that buffer species do not act as the proton acceptor.[48,60] Furthermore, a reaction with buffer as proton acceptor would exhibit a slope of 1 on a $\log(k_2)$ versus pH plot as the concentration of proton accepting buffer-species increases with pH below the pK_a of the buffer, which is unlike the slope observed. A final piece of evidence that buffer species do not partake in the PCET reaction is that the study by Bonin et al.[43] did not add any buffer species to their samples, which exhibit the same pH dependence at pH < 8 that was observed in Paper III.

Having excluded buffer, H_2O or OH^- are the only available proton acceptors in the solution. Reaction with OH^- would give the following expression

for the measured (second-order) rate constant:

$$k'_{\text{obs}} = \frac{k_d}{k_{-d}} \times k_{\text{OH}^-}[\text{OH}^-] \tag{6.6}$$

where k_d/k_{-d} is on the order of 1 M^{-1}, and k_{OH^-} is a pseudo-first-order rate constant see the SI of Paper III for a derivation. Only at pH > 12 for WEE and pH > 9 for NAWEE does OH^- exist in sufficient concentration to account for the observed rate constants. This means that in the entire pH range studied, OH^- can be excluded as a proton acceptor. Furthermore, if OH^- was acting as the primary proton acceptor, then the rate constants are expected to exhibit a slope equal to 1 in a $\log(k_2)$ vs. pH plot. However, since the slope in Figure 6.6 is less than 1, OH^- is not the proton acceptor.

CEPT from W with water as the primary proton acceptor can be described as similar to proton transfer for photoacids, see Chapter 2, where the reaction is in part driven by dissociation and mixing entropy of the product. This may explain how the reaction can be concerted given the large pK_a value of W.

6.6 Summary and Conclusion

Given the large pK_a of $\text{W}^{\bullet+}$ (4.3), it has been questioned if W can undergo CEPT with H_2O as the primary proton acceptor. In this chapter, we have presented results from Paper III that show that two W analogs (WEE and NAWEE) can undergo CEPT, as is evidenced by the rate constants that are faster than ET-limited rate constants. All proton acceptors apart from H_2O have been excluded leaving it as the most likely proton acceptor. The PCET rate constants for WEE and NAWEE exhibit a pH dependence that is less than 1 in a plot of $\log(k_2)$ vs. pH. While this type of pH dependence has been observed previously, it still lacks a theoretical explanation.[43,60,62] The results presented herein have interesting implications for W in natural proteins and enzymes, suggesting that solvent-exposed Ws in proteins can undergo CEPT reactions even with water as the proton acceptor.

7. Summary and Outlook

Without Y and W, life on Earth as we know it would not exist. These two amino acids are fundamental to a wide variety of redox reactions in Nature, where they can act as radical scavengers or partake in catalytic reactions. Both Y and W can partake in $1e^-/\,1H^+$ PCET reactions. Studying which PCET reactions they can partake in and which factors govern their PCET mechanisms is important for expanding our fundamental knowledge about the world around us, and for designing better catalysts inspired by Nature.

In a sense, Y and W complement each other. Their pK_a values differ by about 7 units relative to each other, with W exhibiting the largest values. Upon oxidation, these values shift down by 12 to 13 pK_a units, resulting in PCET. Y exhibits a higher reduction potential of $E^\circ(Y^{\bullet+}/Y) = 1.510$ V compared to $E^\circ(Y^{\bullet+}/Y) = 1.293$ V determined in a protein environment. This results in easier oxidation of W compared to Y. Together they span a wider range of redox potentials compared to on their own. Choosing between Y and W thus provides a way of finetuning redox potentials and the proton-coupling of the ET.

In Paper I and II, a protein model system is used to investigate Y PCET rate constants and mechanism as well as how these can shift with the driving force for ET and PT. The protein model system α_3X contains a single redox active amino acid X (X = one-letter abbreviation of the amino acid studied) at position 32, X_{32}. α_3X strikes a unique balance between small model systems and enzymes by providing a well-defined environment that exhibits stability over a wide pH range. many characteristics of an enzyme, while simultaneously being tunable by the introduction of external oxidants and different amino acids.

In Paper I, the PCET mechanism for Y_{32} (Y at position 32) oxidation by an external oxidant is investigated as a function of pH and concentration of buffer. Solution NMR studies show that Y_{32} exhibits almost no SASA and is surrounded by aliphatic amino acids. A previous publication had shown that a long-lived radical was formed inα_3Y upon PCET, however, given the low SASA it was unclear what the primary proton acceptor was. MD simulations published in Paper I showed that side chains surrounding Y_{32} rotate to allow H_2O access to site 32. Rate constants as a function of pH were determined in order to elucidate the PCET mechanism. Our results showed that the mechanism shifted with pH, from a CEPT mechanism at low pH to $PTET_{pre\text{-}eq}$ at high pH. This shows how pH can be a tool in shifting the PCET mechanism in proteins. While the negatively charged phosphate buffer ions do not enter into sufficiently close proximity to Y_{32}, a smaller base or a neutrally charged base might be able to. This can be investigated using different buffers.

In Paper II, two Y derivatives, 2-mercaptophenol and 4-mercaptophenol linked to C_{32} in α_3C via a disulfide bond (2MP$-\alpha_3$C and 4MP$-\alpha_3$C, respectively) are investigated in order to understand increased solvent exposure or a weak hydrogen bond affects the PCET rate constants and mechanism. Surprisingly, the results show that neither increased solvent, nor a weak hydrogen bond significantly perturbed the PCET rate constants for 2MP$-\alpha_3$C and 4MP$-\alpha_3$C. We then used these proteins to study the effect of altering the driving force for PT and ET on the rate constants and PCET mechanism. By comparing the PCET rate constants of α_3Y to the PCET rate constants of 2MP$-\alpha_3$C, which exhibit different pK_a values than α_3Y, we can simulate the effect of altering the PT driving force of α_3Y and 2MP$-\alpha_3$C. From our comparison, the effect of increasing the PT driving force is that the PCET rate constants go from a mix of CEPT at low pH and $PTET_{pre\text{-}eq}$ at high pH, to $PTET_{pre\text{-}eq}$ in the entire studied pH range. When we then altered the driving force for ET by changing the external oxidant, we could again observe the same mix for $PTET_{pre\text{-}eq}$ at high pH and CEPT at low pH that α_3Y exhibited. For the CEPT mechanism, we showed that H_2O is the most likely proton acceptor. These results confirm that PCET from Y in proteins is dependent on the same parameters as small molecules of Y and Y derivatives in solution; pH and PT and ET driving forces. Since these parameters can be altered in enzymes by changing the microenvironment surrounding an amino acid, different radical forming PCET mechanisms are likely in play depending on the enzyme environment.

The influence of pK_a versus reduction potential on PCET from Y could be further probed using 3MP$-\alpha_3$C. Its pK_a is not yet determined but should be > 10,[84] and is likely similar to the pK_a of 2MP$-\alpha_3$C. 3MP$-\alpha_3$C exhibits a more positive reduction potential than α_3Y, which could give some interesting insights into the dependence of reduction potential on the Y PCET mechanism. A weak hydrogen bond between 2MP$-C_{32}$ and E_{13} observed in the solution NMR is either too long or does not exhibit sufficient wavefunction overlap to facilitate PT. If a shorter hydrogen bond with a better wavefunction overlap could be designed in α_3Y, it would make a good model for Y and W oxidation with a hydrogen-bonded acceptor. The effect that the H-bond might have on pH dependence and PCET mechanisms could then be explored. Hopefully, the results could be used to predict by which PCET mechanism Y in enzymes react depending on the availability of proton acceptors.

In Paper III, two small molecule analogs of W were investigated. Previous publications disagreed on whether or not W molecular analogs could undergo CEPT with H_2O as the primary proton acceptor. Given the large pK_a value of oxidized W ($= 4.3$), it had been hypothesized that W PCET could only proceed via ETPT when H_2O was a proton acceptor. Our results show that when appropriate oxidation strengths are used both W analogs investigated can indeed undergo CEPT with H_2O as the primary proton acceptor. This suggests that solution-exposed Ws in enzymes are able to do the same. Fur-

thermore, the CEPT rate constants determined for the two analogs exhibit a weak pH dependence that lacks a theoretical explanation, but that has phenomenologically been associated with CEPT rate constants with H_2O as the primary proton acceptor. The next step is to identify a protein system where W PCET can proceed via CEPT with H_2O as the primary proton acceptor. The already designed α_3W system shows a hydrogen bond between the indole proton and a nearby amino acid in MD simulations which means that it can not be used to study PCET with water as the proton acceptor without mutations to the protein sequence. It is important that the protein gates buffer or other proton-accepting species in the solution from acting as proton acceptors since these would likely outcompete water.

Popular Science Summary

Radicals in biology have a bad reputation as harbingers of aging and cancer. While there are radical species that can harm our bodies and indeed cause cancer, radicals are also responsible for many vital processes in Nature and our bodies. For example, bird's navigation, making DNA building blocks, DNA repair, and photosynthesis, are all biological reactions that involve radicals.

A radical is typically formed when an electron is removed from, or added to, a stable molecule or atom, which produces a charged and less stable molecule or atom. The radical is less stable because it "wants" to get the electron back or to give the added electron away, which is what makes radicals so reactive. The fact that radicals are very reactive is why they are used in Nature, often for otherwise difficult reactions.

Out of the 20 common amino acids that are used to make the vast majority of proteins in Nature, only a handful participate in radical reactions. Two such amino acids are tyrosine and tryptophan, which are the focus of this thesis. When either tyrosine or tryptophan loses an electron, forming a charged radical, it can also lose a proton, in what is called a *proton-coupled electron transfer* (PCET) reaction, which results in a neutral (uncharged) radical. PCET can proceed via two different mechanisms: stepwise and concerted. In the former, the proton and electron are transferred one after the other, while in the latter mechanism, the proton and electron are transferred simultaneously. The concerted mechanism has the advantage of being more energy-efficient and is therefore thought to be the most common in biological systems. Regardless of the PCET mechanism, the proton and electron can transfer to either the same place or in different directions to different sites. In biological systems, the proton and electron are very often transferred in different directions.

In this thesis, we want to understand which factors regulate the PCET mechanism for *tyrosine* radical formation in a *model protein*, and which factors regulate the PCET mechanism for *tryptophan* radical formation in a *water solution*. Understanding what regulates the PCET mechanism increases our knowledge of PCET reactions in Nature, and helps chemists that want to mimic the energy-efficient biochemical reactions from Nature.

However, since radicals are such reactive species, they are inherently very short-lived, which often makes them difficult to study. The study of radical formation and decay can be further hampered by side reactions that can obscure the reactions one wants to study. Furthermore, proteins can contain several tyrosines and tryptophans, which makes it difficult to observe the tyrosine or tryptophan that actually formed a radical.

In order to study the PCET reactions of tyrosines and tryptophans, we use so-called model systems. Model systems are designed to study a specific part or function of a more complex system. For example, the model systems used in this thesis are designed to isolate the radicals formed from unwanted side reactions. There are different complexities to model systems that one can use when studying radical amino acids. In the most simple system used in this thesis, we took the amino acid out from the protein and put it in a water solution. While this is a very simple model system, it can nevertheless tell us about how amino acids positioned at the protein surface react. A more complex approach, also used in this thesis, is to study the amino acid in a small model protein. We used a protein designed to only include one radical amino acid, which is buried in the protein interior. This model system allowed us to study radical formation inside a protein. With both systems we investigated the PCET mechanism for radical formation, and which factors governed it, such as pH and the energy needed to remove an electron or proton.

In order to determine the PCET mechanism for radical formation, we study the rates for radical formation and decay by using a method called transient absorption spectroscopy. With this method, we determine concentrations of radicals formed over time by observing how much light they absorb. That is, we essentially study how fast the concentration of radical increases (in units of concentration of radical per second), and decreases. We can determine which PCET mechanism is primarily used by varying the pH and the energy needed to remove an electron or proton, and using transient absorption to observe how the rates of radical formation depend on the pH and the energy needed for electron transfer, proton transfer, or both.

The results presented in this thesis have thus far been used to show that PCET from tyrosine with water as the proton acceptor can proceed via the concerted mechanism. This deepens our understanding of one of the PCET steps in an enzyme, Class 1a Ribonucleotide Reductase, that makes the building blocks of DNA. This thesis also shows that tryptophan PCET can use the concerted mechanism when water is the primary proton acceptor, which has previously been debated in several studies, but we now believe this debate is settled. These results contribute to our fundamental understanding of tyrosine and tryptophan radical formation in biological systems.

Populärvetenskaplig Sammanfattning på Svenska

Radikaler inom biologi har ett dåligt rykte som bärare av åldrande och cancer. Även om det finns radikaler som kan skada våra kroppar och faktiskt orsaka cancer, är radikaler också ansvariga för många livsviktiga processer i naturen och våra kroppar. Fågelnavigering, tillverkning av DNA-byggstenar, DNA-reparation, och fotosyntes är alla exempel på biologiska reaktioner som är beroende av radikaler.

En radikal bildas vanligtvis när en elektron tas bort från eller läggs till i en stabil molekyl eller atom, vilket gör molekylen eller atomen laddad och mindre stabil. Radikalen är mindre stabil eftersom den "vill" få tillbaka elektronen eller ge bort den tillsatta elektronen, vilket är det som gör radikaler så reaktiva. Det faktum att radikaler är mycket reaktiva är varför de används i naturen, där de möjliggör för annars svåra reaktioner.

Av de 20 vanligaste aminosyrorna som används för att göra proteiner i naturen är det bara en handfull som deltar i radikalreaktioner. Två sådana aminosyror är tyrosin och tryptofan, vilka är fokus för denna avhandling. När antingen tyrosin eller tryptofan förlorar en elektron och bildar en laddad radikal kan den också förlora en proton, vilket resulterar i en neutral (oladdad) radikal. Detta kallas för en protonkopplad elektronöverföringsreaktion (PCET). PCET kan fortgå via två olika mekanismer: stegvis och samordnad. I den första av dessa mekanismer överförs protonen och elektronen i två steg efter varandra, medan i den senare mekanismen överförs protonen och elektronen samtidigt. Den samordnade mekanismen har fördelen av att den är mer energieffektiv och tros därför vara den vanligaste i biologiska system. Oavsett PCET-mekanismen kan protonen och elektronen överföras till antingen samma plats eller i olika riktningar till olika platser. I biologiska system överförs protonen och elektronen mycket ofta i olika riktningar.

I denna avhandling vill vi förstå vilka olika faktorer som reglerar PCET-mekanismen för bildning av tyrosinradikaler i ett modellprotein, och vilka faktorer som reglerar PCET-mekanismen för tryptofanradikalbildning i en vattenlösning. Att förstå vad som reglerar PCET-mekanismen ökar vår kunskap om PCET-reaktioner i naturen och hjälper kemister som vill efterlikna de energieffektiva biokemiska reaktionerna från naturen.

Men, eftersom radikaler är sådana reaktiva arter, är de till sin natur mycket kortlivade. Detta gör dem ofta svåra att studera. Att studera radikalbildning och radikalförfall är också svårt på grund av sidoreaktioner som kan skymma

de reaktioner man vill studera. Dessutom har proteiner vanligtvis flera tyrosiner och tryptofaner i sig, vilket gör det svårt att observera just det tyrosinet eller tryptofanet som faktiskt bildar en radikal.

För att studera PCET-reaktionerna av tyrosiner och tryptofaner använder vi så kallade modellsystem. Modellsystem är utformade för att studera en specifik del av ett mer komplext system. Till exempel är modellsystemen som används i denna avhandling designade för att isolera de radikaler som bildas från oönskade bakgrundssignaler. Det finns olika nivåer av komplexitet för att modellera system som man kan använda sig av när man studerar radikala aminosyror. I det enklaste systemet som används i denna avhandling tog vi ut aminosyran från proteinet och lade den i en vattenlösning. Även om detta är ett mycket enkelt modellsystem kan det faktiskt berätta för oss om hur aminosyror placerade på proteinytan, där proteinet är kommer i kontakt med sin omgivning, reagerar. Ett mer komplext tillvägagångssätt, som också används i denna avhandling, är att studera aminosyran i ett litet modellprotein. Vi använde ett protein designat av forskare så att det bara innehåller en radikal aminosyra, som är placerad i proteinets inre. Detta modellsystem gjorde det möjligt för oss att studera radikalbildning inuti ett protein. Med båda systemen undersökte vi PCET-mekanismen för radikalbildning, och vilka faktorer som styrde den, såsom pH och den så kallade drivkraften.

För att bestämma PCET-mekanismen för radikalbildning studerar vi hastigheterna för radikalbildning och radikalsönderfall genom att använda en metod som kallas transient absorption. Med denna metod bestämmer vi koncentrationer av radikaler som bildas över tid genom att observera hur mycket ljus de absorberar. Det vill säga, vi studerar i huvudsak hur snabbt koncentrationen av radikaler ökar och minskar, i enheter av koncentration av radikaler per sekund. Vi kan avgöra vilken PCET-mekanism som främst används genom att variera pH och reaktionens drivkraft, och använda transient absorption för att observera hur hastigheten för radikalbildning beror på pH och drivkraften för elektronöverföring, protonöverföring eller båda.

Resultaten som presenteras i denna avhandling har hittills använts för att visa att PCET från tyrosin med vatten som protonacceptor kan ske via den samordnade mekanismen. Detta fördjupar vår förståelse av ett av PCET-stegen i ett enzym, klass 1a ribonukleotidreduktas, som gör byggstenarna i DNA. Denna avhandling visar också att tryptofan PCET kan använda den samordnade mekanismen när vatten är den primära protonacceptorn, vilket tidigare har diskuterats i flera studier, men vi anser nu att denna debatt är avgjord. Dessa resultat bidrar till vår grundläggande förståelse av tyrosin- och tryptofanradikalbildning i biologiska system.

Acknowledgments

I am so incredibly grateful for all the people that have supported me through these years. Our department truly is a magical place for bringing incredible people together. I would like to name a few people especially, (and unfortunately forgetting some, forgive me).

To my supervisor **Leif Hammarström**, thank you for putting so much trust in me, for pushing me to always be better, and for being a good person.

To my co-supervisor **Starla Glover**, thank you for all the scientific discussions, and time you have spent reading and correcting my manuscripts. You truly have an attention to detail that I hope to one day learn.

To my amazing collaborator **Cecilia Tommos**, thank you for making my PhD possible by designing and providing the proteins I have studied. You have taught me so much about biochemistry, I only wish we could have had more time for discussions.

Thank you to my other two main collaborators **Sharon Hammes-Schiffer** and **Clorice Reinhardt**. Sharon, you are such an inspiration. Clorice, though we have never met in person, you have been incredibly supportive and I always look forward to opening your emails.

To the wonderful members of the PhysChem groups (past and present); **Kelly, Mariia, Martin, Alenka, Robin D, Sara, Min-Li, Dylan, Nora, Luca, Sina, Anđela, Sicong, Hongwei, Beri, Aijie, Catherine, Vitor, Samir, Mohammed, Andrew, Ludovico, Victor, Reiner, Jacinto and Haining**. I wish I could have had five more years with each and every one of you.

Thank you to **Ping** for scientific collaborations, spontaneous coffee breaks, and great chats.

Thank you to the PhD students that started at the same time as me: **Holly, João and Kate**. We are almost all there now!

A special thanks to my office mates. Seeing your happy faces every day truly makes my day better. I would also like to thank:

Belinda Pettersson Rimgard, you were one of the first people I met in Uppsala 10 (!) years ago. Since then I have truly walked in your footsteps, following you from bachelor's to PhD. Thank you for always showing the way, supporting me, and being a great friend.

Nidhi Kaul, you are an amazing person and scientist. Some of the discussions we have had still roll around in my head, and I thank you for that. My only wish is that we shared a more similar circadian rhythm so that I got to see you more often.

Andrea Rosicchini, my first (and only) student that I got to supervise. Thank you for sharing my love for PCET, and take good care of BB when I am gone.

Rima Charaf, thank you for sharing my enthusiasm for kinetics, PCET, and spritz. I am so happy that I got a chance to get to know you and be your friend.

Sigrid Berglund, thank you for always having a shoulder to cry on, a joke to laugh at, and for sharing my passion for knitting. I am so incredibly lucky that we did our PhDs at the same time, I do not think I could have finished without you.

Till Östgöta Nation och mina underbara vänner därifrån: **Astri**, **Karin**, **Amanda**, **Denise**, **Olof**, **Viktor**, **Björn**, **Hussam**, **Maria**, **Sanna**, och **Peder**. Ett särskilt tack till **Lowe**, **Adam**, och **Charlie**, det är alltid ett nöje att lämna Uppsala få komma hem till er över en helg.

Till DnD-gänget: **Malte**, **Viking**, **Per**, och **Falk**, DnD med er varje vecka är det enda som är heligt i min kalender.

Tack för allt stöd jag fått från **Lotte**, **Lars**, **Hanna**, **Andreas**. Tack **Anna** för att du korrekturläst, och ett extra stort tack till **Jacob** designat framsidan till min avhandling!

Till min familj. Tack **Mamma** för att du stöttat och pushat mig, och framförallt tack för att du introducerat mig till handarbete, något som har blivit en stor källa till återhämtning när jag är stressad.

Tack **Pappa** för att du alltid finns där, och att du alltid är redo att lyssna på och diskutera alla mina olika ideer.

Tack **Hans Kristian**, **Ingrid**, och **Olivia** för uppmuntran och välbehövda pauser i Norge.

Tack till mina finaste vänner, mina "beautys" **Linnea** och **Viktoria**.

Ett speciellt tack till **Gustav**, den här avhandlingen hade inte blivit av utan ditt konstanta stöd och uppmuntran.

References

[1] Apoorva M Ranjekar and Ganapati D Yadav. Steam reforming of methanol for hydrogen production: A critical analysis of catalysis, processes, and scope. *Ind. Eng. Chem. Res.*, 60(1):89–113, 2021.

[2] Feng Liu, Javier J Concepcion, Jonah W Jurss, Thomas Cardolaccia, Joseph L Templeton, and Thomas J Meyer. Mechanisms of water oxidation from the blue dimer to photosystem ii. *Inorg. Chemi.*, 47(6):1727–1752, 2008.

[3] Marcal Capdevila-Cortada. Electrifying the haber–bosch. *Nat. Cat.*, 2(12): 1055–1055, 2019.

[4] Jie Jack Li. *CH bond activation in organic synthesis*. CRC press, 2015.

[5] Wolfgang Lubitz, Hideaki Ogata, Olaf Rudiger, and Edward Reijerse. Hydrogenases. *Chem. Rev.*, 114(8):4081–4148, 2014.

[6] Nicholas Cox, Dimitrios A Pantazis, and Wolfgang Lubitz. Current understanding of the mechanism of water oxidation in photosystem ii and its relation to xfel data. *Annu. Rev. Biochem.*, 89:795–820, 2020.

[7] Lance C Seefeldt, Zhi-Yong Yang, Dmitriy A Lukoyanov, Derek F Harris, Dennis R Dean, Simone Raugei, and Brian M Hoffman. Reduction of substrates by nitrogenases. *Chem. Rev.*, 120(12):5082–5106, 2020.

[8] Joan B Broderick, Benjamin R Duffus, Kaitlin S Duschene, and Eric M Shepard. Radical s-adenosylmethionine enzymes. *Chem. Rev.*, 114(8):4229–4317, 2014.

[9] Sharon Hammes-Schiffer. Introduction: Proton-coupled electron transfer. *Chem. Rev.*, 110(12):6937–6938, 2010.

[10] Steven Y Reece and Daniel G Nocera. Direct tyrosine oxidation using the mlct excited states of rhenium polypyridyl complexes. *J. Am. Chem. Soc.*, 127(26): 9448–9458, 2005.

[11] Agostino Migliore, Nicholas F Polizzi, Michael J Therien, and David N Beratan. Biochemistry and theory of proton-coupled electron transfer. *Chem. Rev.*, 114(7): 3381–3465, 2014.

[12] Robin Tyburski, Tianfei Liu, Starla D Glover, and Leif Hammarström. Proton-coupled electron transfer guidelines, fair and square. *J. Am. Chem. Soc.*, 143(2):560–576, 2021.

[13] Cecilia Tommos. Insights into the thermodynamics and kinetics of amino-acid radicals in proteins. *Annu. Rev. Biophys.*, 51, 2022.

[14] Karl J Koebke, Tyler BJ Pinter, Winston C Pitts, and Vincent L Pecoraro. Catalysis and electron transfer in de novo designed metalloproteins. *Chem. Rev.*, 2022.

[15] Matthias Granold, Parvana Hajieva, Monica Ioana Toşa, Florin-Dan Irimie, and Bernd Moosmann. Modern diversification of the amino acid repertoire driven by oxygen. *PNAS*, 115(1):41–46, 2018.

[16] Harry B Gray and Jay R Winkler. Hole hopping through tyrosine/tryptophan chains protects proteins from oxidative damage. *Proc. Natl. Acad. Sci.*, 112(35): 10920–10925, 2015.

[17] Jeffrey J Warren, Jay R Winkler, and Harry B Gray. Redox properties of tyrosine and related molecules. *FEBS Lett.*, 586(5):596–602, 2012.
[18] Jing Liu, Saumen Chakraborty, Parisa Hosseinzadeh, Yang Yu, Shiliang Tian, Igor Petrik, Ambika Bhagi, and Yi Lu. Metalloproteins containing cytochrome, iron–sulfur, or copper redox centers. *Chem. Rev.*, 114(8):4366–4469, 2014.
[19] William T Dixon and David Murphy. Determination of the acidity constants of some phenol radical cations by means of electron spin resonance. *J. Chem. Soc., Faraday Trans. 2*, 72:1221–1230, 1976.
[20] Slobodan V. Jovanovic and Michael G. Simic. Repair of tryptophan radicals by antioxidants. *J. Free Radic. Biol. Med.*, 1(2):125–129, 1985. ISSN 07485514. doi: 10.1016/0748-5514(85)90016-9.
[21] David A Armstrong, Robert E Huie, Willem H Koppenol, Sergei V Lymar, Gábor Merényi, Pedatsur Neta, Branko Ruscic, David M Stanbury, Steen Steenken, and Peter Wardman. Standard electrode potentials involving radicals in aqueous solution: inorganic radicals (iupac technical report). *Pure Appl. Chem.*, 87 (11-12):1139–1150, 2015.
[22] Ellen C Minnihan, Daniel G Nocera, and JoAnne Stubbe. Reversible, long-range radical transfer in e. coli class ia ribonucleotide reductase. *Acc. Chem. Res.*, 46 (11):2524–2535, 2013.
[23] Gyunghoon Kang, Alexander T Taguchi, JoAnne Stubbe, and Catherine L Drennan. Structure of a trapped radical transfer pathway within a ribonucleotide reductase holocomplex. *Science*, 368(6489):424–427, 2020.
[24] Clorice R Reinhardt, Pengfei Li, Gyunghoon Kang, JoAnne Stubbe, Catherine L Drennan, and Sharon Hammes-Schiffer. Conformational motions and water networks at the α/β interface in e. coli ribonucleotide reductase. *J. Ame. Chem. Soc.*, 142(32):13768–13778, 2020.
[25] Aziz Sancar. Structure and function of dna photolyase and cryptochrome blue-light photoreceptors. *Chem. Rev.*, 103(6):2203–2238, 2003.
[26] Zheyun Liu, Chuang Tan, Xunmin Guo, Jiang Li, Lijuan Wang, Aziz Sancar, and Dongping Zhong. Determining complete electron flow in the cofactor photoreduction of oxidized photolyase. *Proc. Natl. Acad. Sci.*, 110(32): 12966–12971, 2013.
[27] Kristina Westerlund, Bruce W Berry, Heidi K Privett, and Cecilia Tommos. Exploring amino-acid radical chemistry: protein engineering and de novo design. *Biochimica et Biophysica Acta (BBA)-Bioenergetics*, 1707(1):103–116, 2005.
[28] Spencer A Kerns, Ankita Biswas, Natalie M Minnetian, and AS Borovik. Artificial metalloproteins: At the interface between biology and chemistry. *JACS Au*, 2022.
[29] Harry B Gray and Jay R Winkler. Electron tunneling through proteins. *Q. Rev. Biophys.*, 36(3):341–372, 2003.
[30] Harry B Gray and Jay R Winkler. Long-range electron transfer. *Proc. Natl. Acad. Sci.*, 102(10):3534–3539, 2005.
[31] Bethany C Larson, Jennifer R Pomponio, Hannah S Shafaat, Rachel H Kim, Brian S Leigh, Michael J Tauber, and Judy E Kim. Photogeneration and quenching of tryptophan radical in azurin. *TJ. Phys. Chem. B*, 119(29): 9438–9449, 2015.

[32] Hannah S Shafaat, Brian S Leigh, Michael J Tauber, and Judy E Kim. Resonance raman characterization of a stable tryptophan radical in an azurin mutant. *J. Phys. Chem. B*, 113(1):382–388, 2009.
[33] Jeffrey W Slater and Hannah S Shafaat. Nickel-substituted rubredoxin as a minimal enzyme model for hydrogenase. *The Journal of Physical Chemistry Letters*, 6(18):3731–3736, 2015.
[34] Bridgette A Barry. Reaction dynamics and proton coupled electron transfer: Studies of tyrosine-based charge transfer in natural and biomimetic systems. *Biochim. Biophys. Acta, Bioenerg.*, 1847(1):46–54, 2015.
[35] Tyler G McCaslin, Cynthia V Pagba, San-Hui Chi, Hyea J Hwang, James C Gumbart, Joseph W Perry, Cristina Olivieri, Fernando Porcelli, Gianluigi Veglia, Zhanjun Guo, et al. Structure and function of tryptophan–tyrosine dyads in biomimetic β hairpins. *J. Phys. Chem. B*, 123(13):2780–2791, 2019.
[36] Matteo Tegoni. De novo designed copper α-helical peptides: From design to function. *Eur. J. Inorg. Chem.*, 2014(13):2177–2193, 2014.
[37] Cecilia Tommos, Jack J Skalicky, Denis L Pilloud, A Joshua Wand, and P Leslie Dutton. De novo proteins as models of radical enzymes. *Biochemistry*, 38(29): 9495–9507, 1999.
[38] Qing-Hong Dai, Cecilia Tommos, Ernesto J Fuentes, Margareta RA Blomberg, P Leslie Dutton, and A Joshua Wand. Structure of a de novo designed protein model of radical enzymes. *J. Am. Chem. Soc.*, 124(37):10952–10953, 2002.
[39] Starla D Glover, Christine Jorge, Li Liang, Kathleen G Valentine, Leif Hammarström, and Cecilia Tommos. Photochemical tyrosine oxidation in the structurally well-defined α_3y protein: proton-coupled electron transfer and a long-lived tyrosine radical. *J. Am. Chem. Soc.*, 136(40):14039–14051, 2014.
[40] Starla D Glover, Robin Tyburski, Li Liang, Cecilia Tommos, and Leif Hammarström. Pourbaix diagram, proton-coupled electron transfer, and decay kinetics of a protein tryptophan radical: Comparing the redox properties of $W_{32}^{\bullet}$ and $Y_{32}^{\bullet}$ generated inside the structurally characterized α_3w and α_3y proteins. *J. Am. Chem. Soc.*, 140(1):185–192, 2017.
[41] Robin Tyburski and Leif Hammarström. Strategies for switching the mechanism of proton-coupled electron transfer reactions illustrated by mechanistic zone diagrams. *Chem. Sci.*, 13(1):290–301, 2022.
[42] Cyrille Costentin, Cyril Louault, Marc Robert, and Jean-Michel Savéant. The electrochemical approach to concerted proton-electron transfers in the oxidation of phenols in water. *Proc. Natl. Acad. Sci.*, 106(43):18143–18148, 2009.
[43] Julien Bonin, Cyrille Costentin, Marc Robert, Mathilde Routier, and Jean-Michel Savéant. Proton-coupled electron transfers: ph-dependent driving forces? fundamentals and artifacts. *J. Am. Chem. Soc.*, 135(38):14359–14366, 2013.
[44] Ian J Rhile and James M Mayer. One-electron oxidation of a hydrogen-bonded phenol occurs by concerted proton-coupled electron transfer. *J. Am. Chem. Soc.*, 126(40):12718–12719, 2004.
[45] Cyrille Costentin, Marc Robert, and Jean-Michel Saveant. Concerted proton–electron transfers in the oxidation of phenols. *Phys. Chem. Chem. Phys.*, 12(37):11179–11190, 2010.
[46] Na Song and David M Stanbury. Overoxidation of phenol by hexachloroiridate (iv). *Inorg. Chem.*, 50(24):12762–12773, 2011.

[47] Julien Bonin, Cyrille Costentin, Marc Robert, and Jean-Michel Savéant. Pyridine as proton acceptor in the concerted proton electron transfer oxidation of phenol. *Org. Biomol. Chem.*, 9(11):4064–4069, 2011.

[48] Tania Irebo, Steven Y Reece, Martin Sjödin, Daniel G Nocera, and Leif Hammarström. Proton-coupled electron transfer of tyrosine oxidation: Buffer dependence and parallel mechanisms. *J. Am. Chem. Soc.*, 129(50):15462–15464, 2007.

[49] Na Song, Christopher J Gagliardi, Robert A Binstead, Ming-Tian Zhang, Holden Thorp, and Thomas J Meyer. Role of proton-coupled electron transfer in the redox interconversion between benzoquinone and hydroquinone. *J. Am. Chem. Soc.*, 134(45):18538–18541, 2012.

[50] Ann Magnuson, Helena Berglund, Peter Korall, Leif Hammarström, Björn Åkermark, Stenbjörn Styring, and Licheng Sun. Mimicking electron transfer reactions in photosystem ii: Synthesis and photochemical characterization of a ruthenium (ii) tris (bipyridyl) complex with a covalently linked tyrosine. *J. Am. Chem. Soc.*, 119(44):10720–10725, 1997.

[51] Fabien Lachaud, Annamaria Quaranta, Yann Pellegrin, Pierre Dorlet, Marie-France Charlot, Sun Un, Winfried Leibl, and Ally Aukauloo. A biomimetic model of the electron transfer between p680 and the tyrz–his190 pair of psii. *Angew. Chem. Int. Ed.*, 44(10):1536–1540, 2005.

[52] Linus O Johannissen, Tania Irebo, Martin Sjodin, Olof Johansson, and Leif Hammarström. The kinetic effect of internal hydrogen bonds on proton-coupled electron transfer from phenols: A theoretical analysis with modeling of experimental data. *J. Phys. Chem. B*, 113(50):16214–16225, 2009.

[53] Jackson D Megiatto Jr, Dalvin D Méndez-Hernández, Marely E Tejeda-Ferrari, Anne-Lucie Teillout, Manuel J Llansola-Portolés, Gerdenis Kodis, Oleg G Poluektov, Tijana Rajh, Vladimiro Mujica, Thomas L Groy, et al. A bioinspired redox relay that mimics radical interactions of the tyr–his pairs of photosystem ii. *Nat. Chem.*, 6(5):423–428, 2014.

[54] Hiroshi Ishikita, Alexander V Soudackov, and Sharon Hammes-Schiffer. Buffer-assisted proton-coupled electron transfer in a model rhenium- tyrosine complex. *J. Am. Chem. Soc.*, 129(36):11146–11152, 2007.

[55] Tania Irebo, Ming-Tian Zhang, Todd F Markle, Amy M Scott, and Leif Hammarström. Spanning four mechanistic regions of intramolecular proton-coupled electron transfer in a $Ru(bpy)_3^{2+}$–tyrosine complex. *J. Am. Chem. Soc.*, 134(39):16247–16254, 2012.

[56] Jing Chen, Martin Kuss-Petermann, and Oliver S Wenger. Dependence of reaction rates for bidirectional pcet on the electron donor–electron acceptor distance in phenol–ru (2, 2'-bipyridine) 32+ dyads. *J. Phys. Chem. B*, 119(6): 2263–2273, 2015.

[57] Mioy T Huynh, S Jimena Mora, Matias Villalba, Marely E Tejeda-Ferrari, Paul A Liddell, Brian R Cherry, Anne-Lucie Teillout, Charles W Machan, Clifford P Kubiak, Devens Gust, et al. Concerted one-electron two-proton transfer processes in models inspired by the tyr-his couple of photosystem ii. *ACS Cent. Sci.*, 3(5): 372–380, 2017.

[58] Giovanny A Parada, Zachary K Goldsmith, Scott Kolmar, Belinda Pettersson Rimgard, Brandon Q Mercado, Leif Hammarström, Sharon

Hammes-Schiffer, and James M Mayer. Concerted proton-electron transfer reactions in the marcus inverted region. *Science*, 364(6439):471–475, 2019.
[59] Christopher J Gagliardi, Robert A Binstead, H Holden Thorp, and Thomas J Meyer. Concerted electron–proton transfer (ept) in the oxidation of tryptophan with hydroxide as a base. *J. Am. Chem. Soc.*, 133(49):19594–19597, 2011.
[60] Ming-Tian Zhang, Johan Nilsson, and Leif Hammarström. Bimolecular proton-coupled electron transfer from tryptophan with water as the proton acceptor. *Energy Environ. Sci*, 5(7):7732–7736, 2012.
[61] Ming-Tian Zhang and Leif Hammarström. Proton-coupled electron transfer from tryptophan: A concerted mechanism with water as proton acceptor. *J. Am. Chem. Soc.*, 133(23):8806–8809, 2011.
[62] Prateek Dongare, Somnath Maji, and Leif Hammarström. Direct evidence of a tryptophan analogue radical formed in a concerted electron- proton transfer reaction in water. *J. Am. Chem. Soc.*, 138(7):2194–2199, 2016.
[63] Rudolph A Marcus. On the theory of oxidation-reduction reactions involving electron transfer. i. *J. Chem. Phys.*, 24(5):966–978, 1956.
[64] Neil R Kestner, Jean Logan, and Joshua Jortner. Thermal electron transfer reactions in polar solvents. *J. Phys. Chem.*, 78(21):2148–2166, 1974.
[65] Jens Ulstrup and Joshua Jortner. The effect of intramolecular quantum modes on free energy relationships for electron transfer reactions. *J. Chem. Phys.*, 63(10): 4358–4368, 1975.
[66] Paul Siders and Rudolph A Marcus. Quantum effects for electron-transfer reactions in the" inverted region". *J. Am. Chem. Soc.*, 103(4):748–752, 1981.
[67] Mordechai Bixon and Joshua Jortner. Quantum effects on electron-transfer processes. *Faraday Discuss.*, 74:17–29, 1982.
[68] Rudolph A Marcus and Norman Sutin. Electron transfers in chemistry and biology. *Biochim. Biophys. Acta - Bioenerg.*, 811(3):265–322, 1985.
[69] James R Bolton and Mary D Archer. Basic electron-transfer theory. *Electron Transfer in Inorganic, Organic, and Biological Systems*, 228:7–23, 1991.
[70] Daniel Borgis and James T Hynes. Molecular-dynamics simulation for a model nonadiabatic proton transfer reaction in solution. *J. Chem. Phys.*, 94(5): 3619–3628, 1991.
[71] Daniel Borgis and James T Hynes. Curve crossing formulation for proton transfer reactions in solution. *J Chem. Phys.*, 100(4):1118–1128, 1996.
[72] Lev I Krishtalik. The mechanism of the proton transfer: an outline. *Biochim. Biophys. Acta - Bioenerg.*, 1458(1):6–27, 2000.
[73] Sharon Hammes-Schiffer. Proton-coupled electron transfer: classification scheme and guide to theoretical methods. *Energy Environ. Sci.*, 5(7):7696–7703, 2012.
[74] Alexander Soudackov and Sharon Hammes-Schiffer. Derivation of rate expressions for nonadiabatic proton-coupled electron transfer reactions in solution. *J. Chem. Phys.*, 113(6):2385–2396, 2000.
[75] Sharon Hammes-Schiffer and Alexander V Soudackov. Proton-coupled electron transfer in solution, proteins, and electrochemistry. *J. Phys. Chem. B*, 112(45): 14108–14123, 2008.
[76] Sharon Hammes-Schiffer. Theory of proton-coupled electron transfer in energy conversion processes. *Acc. Chem. Res.*, 42(12):1881–1889, 2009.

[77] Manfred Eigen. Proton transfer, acid-base catalysis, and enzymatic hydrolysis.part i: Elementary processes. *Angew. Chem. Int.*, 3(1):1–19, 1964. ISSN 0570-0833.

[78] Albert Weller. Fast reactions of excited molecules. *Prog. React. Kinet. Mech.*, 1: 187, 1961. ISSN 0079-6743.

[79] Lev I Krishtalik. ph-dependent redox potential: how to use it correctly in the activation energy analysis. *Biochim. Biophys. Acta - Bioenerg.*, 1604(1):13–21, 2003.

[80] Cyrille Costentin, Marc Robert, and Jean-Michel Savéant. Concerted proton-electron transfer reactions in water. are the driving force and rate constant depending on ph when water acts as proton donor or acceptor? *J. Am. Chem. Soc.*, 129(18):5870–5879, 2007.

[81] Melissa C Martínez-Rivera, Bruce W Berry, Kathleen G Valentine, Kristina Westerlund, Sam Hay, and Cecilia Tommos. Electrochemical and structural properties of a protein system designed to generate tyrosine pourbaix diagrams. *J. Am. Chem. Soc.*, 133(44):17786–17795, 2011.

[82] Bruce W Berry, Melissa C Martínez-Rivera, and Cecilia Tommos. Reversible voltammograms and a pourbaix diagram for a protein tyrosine radical. *Proc. Natl. Acad. Sci.*, 109(25):9739–9743, 2012.

[83] Cecilia Tommos, Kathleen G Valentine, Melissa C Martínez-Rivera, Li Liang, and Veronica R Moorman. Reversible phenol oxidation and reduction in the structurally well-defined 2-mercaptophenol-α_3c protein. *Biochemistry*, 52(8): 1409–1418, 2013.

[84] Sam Hay, Kristina Westerlund, and Cecilia Tommos. Moving a phenol hydroxyl group from the surface to the interior of a protein: Effects on the phenol potential and pk_a. *Biochemistry*, 44(35):11891–11902, 2005.

[85] Kanchana R Ravichandran, Allan B Zong, Alexander T Taguchi, Daniel G Nocera, JoAnne Stubbe, and Cecilia Tommos. Formal reduction potentials of difluorotyrosine and trifluorotyrosine protein residues: Defining the thermodynamics of multistep radical transfer. *J. Am. Chem. Soc.*, 139(8): 2994–3004, 2017.

[86] GR Dey, R Hermann, S Naumov, and O Brede. Encounter geometry determines product characteristics of electron transfer from 4-hydroxythiophenol to n-butyl chloride radical cations. *Chem. Phys. Lett.*, 310(1-2):137–144, 1999. ISSN 0009-2614.

[87] Jason P Schwans, Fanny Sunden, Ana Gonzalez, Yingssu Tsai, and Daniel Herschlag. Uncovering the determinants of a highly perturbed tyrosine pk_a in the active site of ketosteroid isomerase. *Biochemistry*, 52(44):7840–7855, 2013.

[88] Thomas U Nick, Kanchana R Ravichandran, JoAnne Stubbe, Müge Kasanmascheff, and Marina Bennati. Spectroscopic evidence for a h bond network at y356 located at the subunit interface of active e. coli ribonucleotide reductase. *Biochemistry*, 56(28):3647–3656, 2017.

[89] Martin Sjödin, Stenbjörn Styring, Björn Åkermark, Licheng Sun, and Leif Hammarström. Proton-coupled electron transfer from tyrosine in a tyrosine-ruthenium- tris-bipyridine complex: Comparison with tyrosinez oxidation in photosystem ii. *J. Am. Chem. Soc.*, 122(16):3932–3936, 2000.

[90] Tania Irebo, Olof Johansson, and Leif Hammarström. The rate ladder of proton-coupled tyrosine oxidation in water: A systematic dependence on hydrogen bonds and protonation state. *J. Am. Chem. Soc.*, 130(29):9194–9195, 2008.

[91] Martin Sjödin, Stenbjörn Styring, Henriette Wolpher, Yunhua Xu, Licheng Sun, and Leif Hammarström. Switching the redox mechanism: models for proton-coupled electron transfer from tyrosine and tryptophan. *J. Am. Chem. Soc.*, 127(11):3855–3863, 2005.

[92] Dan Meisel, Max S Matheson, WA Mulac, and Joseph Rabani. Transients in the flash photolysis of aqueous solutions of tris (2, 2'bipyridine) ruthenium (ii) ion. *J. Phys. Chem.*, 81(15):1449–1455, 1977. ISSN 0022-3654.

[93] Martin Goez, Daniel von Ramin-Marro, Mohammad Hussein Othman Musa, and Martin Schiewek. Photoionization of [ru(bpy)3]2+: A catalytic cycle with water as sacrificial donor. *J. Phys. Chem. A*, 108(6):1090–1100, 2004.

[94] A. N. Tarnovsky, W. Gawelda, M. Johnson, C. Bressler, and M. Chergui. Photexcitation of aqueous ruthenium(ii)-tris-(2,2'-bipyridine) with high-intensity femtosecond laser pulses. *J. Phys. Chem. B*, 110(51):26497–505, 2006.

[95] Marim K Alnaed and John F Endicott. Chemical scavenging yields for short-lived products from the visible light photoionization of the tris(bipyridine)ruthenium(ii) triplet metal-to-ligand charge-transfer excited state. *J. Phys. Chem. A*, 122(48):9251–9266, 2018.

[96] Kuppuswamy Kalyanasundaram and Michael Neumann-Spallart. Photophysical and redox properties of water-soluble porphyrins in aqueous media. *J. Phys. Chem.*, 86(26):5163–5169, 1982.

[97] Yuliya S Zhuravleva, Olga B Morozova, Yuri P Tsentalovich, and Peter S Sherin. Proton-coupled electron transfer as the mechanism of reaction between triplet state of kynurenic acid and tryptophan. *J. Photochem. Photobiol. A*, 396:112522, 2020.

Appendix A.
pK_a determination and PCET Rate Constants for α_3Y–E$_{13}$A

The α_3X family of model proteins are introduced in Chapter 4. α_3Y–E$_{13}$A is based on α_3Y, but with position 13 mutated from a glutamic acid (E) to an alanine (A).

pK_a determination

The pK_a was determined using equal volume titration. In short, the protein was dissolved in 20 mM KP$_i$ + 20 mM borate (PB) buffer. A portion of the solution was removed and diluted with low pH PB buffer, while the remaining solution was equally diluted with high pH PB buffer. Starting from the high pH solution a UV-vis spectrum was collected, then a small volume was removed and an equal volume of low pH protein solution was added and UV-vis was again collected. Following this procedure, UV-vis spectra were collected between pH 13.1 and 6.3. The absorption at 293 nm was abstracted and corrected for the baseline shift with pH with the absorption at 340 nm. Finally, the corrected absorption at 293 nm was plotted as a function of pH and a fit to a single pK_a was added. The results gave pK_a11.1 $\pm$ 0.3.

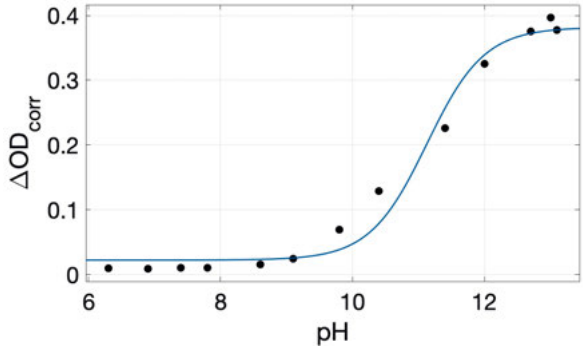

Figure A.1. Abs$_{298}$ − Abs$_{340}$ = ΔOD$_{corr}$ plotted as a function of pH for α_3Y–E$_{13}$A. Samples contained 150 µM protein in 20 mM phosphate and 20 mM borate buffer.

Kinetics for Radical Formation as a Function of Concentration of Buffer

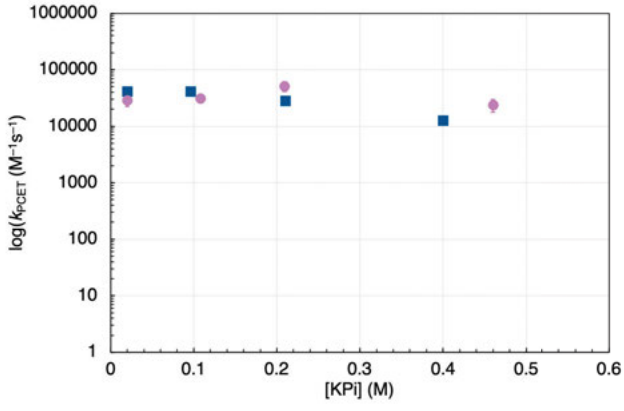

Figure A.2. Kinetics of radical formation as a function of buffer concentration for α_3Y–E_{13}A (blue squares) and α_3Y (purple circles) shown with respective standard deviations. Samples contained 390–860 μM protein, 25–40 μM $[Ru(bpy)_3]^{2+}$, and 4 mM $[Co(N_3]_5Cl]^{2+}$ in various concentration KPi and 40 mM KCl buffer.

Kinetics for radical formation were determined as a function of $[KP_i]$, Figure A.2, and exhibit no correlation. This was used to show that water or OH^- are the proton acceptors. Using the same reasoning as in the SI of Paper I, OH^- was excluded as the primary proton acceptor leaving H_2O.

Kinetics for Radical Formation as a Function of pH

The kinetics of radical formation was also determined as a function of pH. A similar pH dependence as for a3Y was observed, Figure A.3. This indicates that E_{13} is not the proton acceptor for α_3Y.

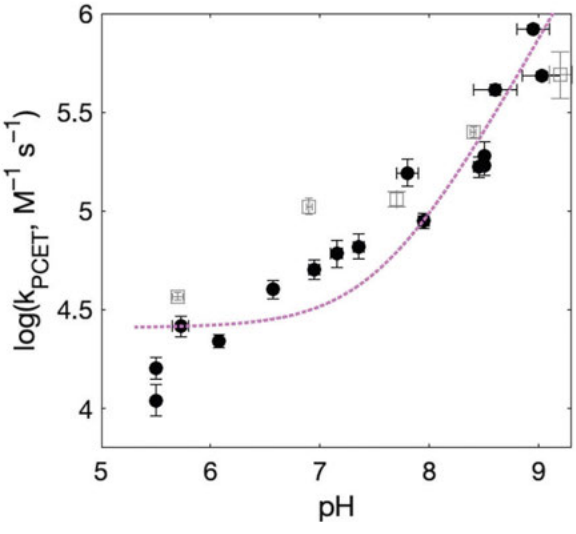

Figure A.3. Kinetics for radical formation shown as a function of pH for α_3Y–E_{13}A (blue squares) and α_3Y (purple circles) shown with respective standard deviations. Samples containing 410–1400 μM protein, 25–60 μM $[Ru(bpy)_3]^{2+}$, and 3–4 mM $[Co(N_3]_5Cl]^{2+}$ in 20–40 mM KPi and 40 mM KCl buffer.

Acta Universitatis Upsaliensis

Digital Comprehensive Summaries of Uppsala Dissertations from the Faculty of Science and Technology 2180

Editor: The Dean of the Faculty of Science and Technology

A doctoral dissertation from the Faculty of Science and Technology, Uppsala University, is usually a summary of a number of papers. A few copies of the complete dissertation are kept at major Swedish research libraries, while the summary alone is distributed internationally through the series Digital Comprehensive Summaries of Uppsala Dissertations from the Faculty of Science and Technology. (Prior to January, 2005, the series was published under the title "Comprehensive Summaries of Uppsala Dissertations from the Faculty of Science and Technology".)

Distribution: publications.uu.se
urn:nbn:se:uu:diva-482203

ACTA
UNIVERSITATIS
UPSALIENSIS
UPPSALA
2022